

**A COMPARISON OF TRADITIONAL AND UAV-SUPPLEMENTED APPROACHES  
FOR ASSESSING SALMONID HABITAT IN MOUNTAIN STREAMS**

by

Alexander Marcel MacDuff

B.Sc. Honours, EESC, University of British Columbia, 2017

A THESIS IN PARTIAL FULFILLMENT OF THE  
REQUIREMENTS FOR THE DEGREE OF

MASTER OF SCIENCE

in

THE COLLEGE OF GRADUATE STUDIES

(Earth & Environmental Sciences)

THE UNIVERSITY OF BRITISH COLUMBIA

(Okanagan)

May 2022

© Alexander M. MacDuff, 2022

The following individuals certify that they have read, and recommend to the College of Graduate Studies for acceptance, a thesis/dissertation entitled:

A Comparison of Traditional and UAV-Supplemented Approaches for Assessing Salmonid

Habitat in Mountain Streams

submitted by Alexander MacDuff in partial fulfillment of the requirements of  
the degree of Master of Science.

Dr. Bernard Bauer, Earth, Environmental & Geographic Sciences, I.K Barber Faculty of Science

---

**Supervisor**

Dr. Dwayne Tannant, Civil Engineering Program, School of Engineering

---

**Supervisory Committee Member**

Dr. Leif Burge, Earth, Environmental & Geographic Sciences, I.K. Barber Faculty of Science

---

**Supervisory Committee Member**

Dr. Brett Eaton, Department of Geography, Faculty of Arts, UBC Vancouver

---

**University Examiner**

## **Abstract**

Assessments of instream fish habitat in North America have been dominated by the Instream Flow Incremental Methodology (IFIM) used in conjunction with hydraulic modelling programs, such as the Physical Habitat Simulation (PHABSIM). While this methodology has repeatedly been described as invaluable for managing instream habitat, it has received significant criticism due to the intensive data demands and the logistical challenges that often limit data collection.

In the past decade, several studies have demonstrated a potential solution in the implementation of topographic surveys conducted with the use of Unmanned-Aerial-Vehicles (UAVs) to produce digital elevation models (DEMs) derived from aerial images using Structure-from-Motion (SfM) photogrammetric software. There remain significant concerns that this approach will not be applicable to mountainous streams. Therefore, this study aimed to evaluate the effectiveness of UAV-SfM surveys for supplementing an IFIM assessment for Upper Mission Creek in the Southern Interior of British Columbia.

Through an extensive field campaign, a total of 30 transects were surveyed multiple times with different methods, including the standard surveying convention using an engineer's level and stadia rod, recording depths on a wading rod while measuring discharge, an RTK-DGPS survey, and UAV flights. During the subsequent quality control exercises, variance in the UAV-SfM sourced DEM was found to be comparable to traditional surveying methods. Unexpectedly, transects derived from the photogrammetric DEM produced more accurate and precise hydraulic models for predicting mean flow velocities.

Habitat modelling demonstrated that reductions in the number of transects incorporated into the model, mimicking surveys with logistical constraints, led to highly variable and uncertain final estimates of wetted usable habitat. In contrast, supplementation of photogrammetric transects into the model was observed to compensate for reductions in the number of traditional transects in the model, thereby stabilizing habitat availability estimates.

Although mountainous streams are more challenging to survey, supplementation of UAV-SfM sourced topographic data into the IFIM offers significant improvements in accuracy, precision and scale while expediting assessments of instream habitat.

## **Lay Summary**

Historically, assessments of fish habitat have been hampered in mountainous environments due to logistical challenges associated with topographic surveying of channel geometry. A potential solution is to incorporate aerial surveys from Unmanned-Aerial-Vehicles (UAVs) in conjunction with photogrammetric software to produce detailed topographic information.

To test the effectiveness of this methodology, a traditional instream habitat assessment was conducted using standard surveying techniques (i.e., engineer's level and stadia rod) and the results were compared to estimates of habitat availability when UAV-based surveys were substituted and integrated into the modelling. Field measurements were conducted over eight, non-consecutive days on Upper Mission Creek, a mountain stream in the Southern Interior of British Columbia. The target fish species was Rainbow Trout.

Although mountainous regions are more challenging to survey and extra precautions are required in the field, incorporating aerial surveys from UAVs and the application of photogrammetry offers significant improvements to the accuracy, precision, and scale of the instream habitat assessments, as well as reducing the time and expense required to complete the field work.

## **Preface**

This research was conducted by Alexander MacDuff under the supervision of Dr. Bernard Bauer. As the primary researcher Alexander MacDuff, with assistance from Dr. Bauer was responsible for the study design, data analysis and interpretation and writing. Additional conceptual support was provided by Greg Courtice, with logistical and analytical support for the acquisition and processing of aerial images provided by David Scott and Dr. Dwayne Tannant.

Funding for this project was provided by the Natural Sciences and Engineering Research Council of Canada (NSERC). Additional financial and logistical support came from the University of British Columbia Okanagan.

# Table of Contents

<b>Abstract</b> .....	<b>ii</b>
<b>Preface</b> .....	<b>iv</b>
<b>Table of Contents</b> .....	<b>v</b>
<b>List of Figures</b> .....	<b>vii</b>
<b>List of Tables</b> .....	<b>xi</b>
<b>Abbreviations</b> .....	<b>xii</b>
<b>Acknowledgements</b> .....	<b>xiii</b>
<b>Chapter 1 . Introduction</b> .....	<b>1</b>
1.1 Project Overview .....	1
1.2 Research Objectives and Questions .....	4
<b>Chapter 2 . Literature Review</b> .....	<b>6</b>
2.1 Physical Habitat Conditions Required by Pacific Salmonids .....	6
2.1.1 "Fall" Migration and Spawning .....	7
2.1.2 Winter Incubation and Egg Survival.....	9
2.1.3 Spring Hatching .....	11
2.1.4 Summer Rearing and Feeding.....	12
2.2 Incremental Flow Instream Methodology.....	13
2.2.1 Introduction.....	13
2.2.2 Challenges with habitat suitability modelling.....	16
2.2.3 Recent Advancements – Hydraulic modelling.....	20
2.2.4 UAV-Supplementation of Channel Surveys .....	24
<b>Chapter 3 . Methods</b> .....	<b>29</b>
3.1 Study Site.....	29
3.2 Field Data Collection .....	31
3.2.1 Topographical Surveys .....	31
3.2.2 Georeferencing.....	33
3.2.3 Instream Flow Measurements .....	35
3.2.4 Drone Flights .....	36
3.3 Data quality control.....	38
3.3.1 Survey Data.....	38
3.3.2 Photogrammetric Data .....	39
3.3.3 Channel Hydraulics.....	40
3.3.4 HEC-RAS Modeling.....	41

3.4 Experimental Design.....	41
3.4.1 Hydraulic Modelling.....	42
3.4.2 Habitat Modelling.....	48
<b>Chapter 4 . Results.....</b>	<b>50</b>
4.1 Site Conditions.....	50
4.1.1 Hydrological conditions.....	50
4.1.2 Geomorphological character.....	53
4.1.3 Observations of Rainbow Trout.....	58
4.2 Data Quality Control.....	59
4.2.1 Evaluation of Field Data.....	59
4.2.2 Evaluation of Photogrammetric Data.....	63
4.3 Hydraulic Modelling.....	68
4.3.1 Calibration Efforts.....	68
4.3.2 Modelled Channel Hydraulics.....	72
4.3.3 Modelled Habitat Potential.....	76
<b>Chapter 5 . Discussion.....</b>	<b>88</b>
5.1 Field Data Collection Efforts.....	88
5.2 Photogrammetric Sampling.....	93
5.3 Hydraulic Modelling.....	96
5.4 Supplementing Transects.....	100
<b>Chapter 6 . Summary and Conclusions.....</b>	<b>109</b>
6.1 Key Findings.....	109
6.2 Future Recommendations.....	113
<b>References.....</b>	<b>119</b>
<b>Appendices.....</b>	<b>127</b>
Appendix A. Field Survey Discrepancies by Transect.....	127
Appendix B. GPS Survey Data.....	128
Appendix C. Photogrammetric Survey Error by Transect.....	129
Appendix D. Hydraulic Calibration Data.....	130
Appendix F. Transect Profiles.....	131

## List of Figures

Figure 2.1 Schematic of intergravel water flow through a salmonid redd. (from Pike et al., 2010). .....	11
Figure 2.2 Habitat suitability for adult Rainbow Trout according to flow velocity (m s <sup>-1</sup> ) (from Raleigh et al., 1984). The curve shows that flow velocities above about 0.75 m s <sup>-1</sup> are not suitable for Rainbow Trout. ....	15
Figure 2.3 A 3D representation of seven theoretical transects with six sampling points each. Dashed lines show the interpolation between transects, forming the lateral prisms of the 1.5 D hydraulic model. Whereas the red arrows show the pathway for interpolation in 1D hydraulic models for the same transects. ....	22
Figure 3.1 Location of study reach, within the Mission Creek (pink outline) and Okanagan Watersheds (black outline) of the Southern Interior of British Columbia. ....	29
Figure 3.2 Orthophoto of the study reach on Upper Mission Creek, taken Sept 30th, 2019.....	30
Figure 3.3 A juvenile Rainbow Trout ( <i>Oncorhynchus mykiss</i> ) observed within the study reach, July 13th, 2019.....	31
Figure 3.4 Transect A, looking downstream side-channel A as it separates from the main channel between transects 18-19 (Aug. 1st, 2019).....	32
Figure 3.5 A topographical survey following the standard surveying convention, transect 20, July 20th, 2019. ....	33
Figure 3.6 Location of the RTK -DPGS base-station and drone lunch pad (Green Cross), within the UMC study reach. ....	34
Figure 3.7 Ground level photo of the RTK -DPGS base station and drone lunch pad, at the gravel bar mid-reach, between transects 14-16 (August 13th , 2019). ....	35
Figure 3.8 Examples of ground control markers deployed in the field, including the initial test markers (left) used for the July 25h and Aug. 14th test flight, as well as the high contrast markers (right) employed on the final Sept. 30th flight. ....	37
Figure 3.9 A map showing the distribution of transects across the study reach for the ‘Best-Practices’ scenario’ (Scenario 0). ....	44
Figure 3.10 A map showing the distribution of transects for the reduced model, Model 3Ai with only 5 surveyed transects incorporated into the model.....	46
Figure 3.11 A map showing the distribution of transects for the supplemented model, Model 3Bi, with 5 traditional transects (red diamonds) and 22 photogrammetric transects (blue circles). ....	47

Figure 3.12 Habitat suitability for juvenile Rainbow Trout according to flow depth (m) (Raleigh et al. 1984). .....	48
Figure 3.13 Habitat suitability for juvenile Rainbow Trout according to flow velocity (m s <sup>-1</sup> ) (Raleigh et al. 1984). .....	48
Figure 4.1 The average annual hydrograph for Mission Creek recorded near East Kelowna, BC (Station 08NM116) by the Water Survey of Canada from 1967 to 2017. ....	50
Figure 4.2 Hydrograph for Mission Creek (Station 08NM116), between the June 23 <sup>rd</sup> to Nov 11 <sup>th</sup> , 2019, Study Period. Day 200 corresponds to July 19 whereas Day 300 corresponds to October 27 <sup>th</sup> , alternatively July 1 is Day 182 and Sept 1 is Day 244. ....	51
Figure 4.3 The log jam immediately downstream of transect 18, at the junction of side-channel A, with fresh additions of woody debris noted by the bright colouration at the base of the jam, Aug. 1 <sup>st</sup> , 2019. ....	52
Figure 4.4 The longitudinal slope profile of the Upper Mission Creek Study reach. ....	53
Figure 4.5 Upstream view from transect 2 showing cobble-boulder substrate materials (July 8 <sup>th</sup> , 2019). ....	55
Figure 4.6 The downstream view from transect 6 (July 8 <sup>th</sup> , 2019) showing the transition from rapids to pool-riffle sequences. ....	55
Figure 4.7 The view from transect 7, looking upstream towards transects 8, 9 and 10 (July 13, 2019). ....	56
Figure 4.8 Transect B, looking downstream on active side channel B (Aug. 1 <sup>st</sup> , 2019). ....	56
Figure 4.9 One of two inactive side channels behind the right (north) bank of transects 7-12. ....	57
Figure 4.10 Transects 18 and 19, with the flow moving from left to right and photographed from the outside bank of the mid-channel gravel bar (July 13 <sup>th</sup> , 2019). ....	57
Figure 4.11 Transect 20, looking upstream (Aug 1 <sup>st</sup> , 2019). ....	58
Figure 4.12 An example of turbulent ‘pocket’ water, July 13 <sup>th</sup> , 2019. ....	59
Figure 4.13 A regression plot comparing uncorrected photogrammetric transect points versus elevations from standard surveying techniques using an engineer’s level. ....	64
Figure 4.14 A regression plot comparing corrected photogrammetric transect points versus elevations from standard surveying convention. Problematic points have been deleted in this analysis. ....	65
Figure 4.15 Distribution of sub-reaches as defined by transect-specific discharges employed the calibration exercises (see text for explanation). ....	69

Figure 4.16 Deviation of the water surface elevation from the measured mean at each transect.	71
Figure 4.17 A graphical comparison of WUW estimates outputs from the ‘Best-Practices’ Scenario 0 (solid black line) against the upper and lower boundaries for Scenarios 1A (pink dashed line) and 1B (blue dashed line).	77
Figure 4.18 A graphical comparison of WUW estimates outputs from the ‘Best-Practice’ Scenario 0 (solid black line) against the upper and lower boundaries for Scenarios 2A (pink dashed line) and 2B (blue dashed line).	78
Figure 4.19 A graphical comparison of WUW estimates outputs from the ‘Best Practice’ Scenario 0 (solid black line) against the upper and lower boundaries for Scenarios 3A (pink dashed line) and 3B (blue dashed line).	78
Figure 4.20 A graphical comparison of WUW estimates outputs from the ‘Best-Practice’ Scenario 0 (solid black line) against those from the purely photogrammetric Scenario 4 (thick dashed green line).	79
Figure 4.21 A comparison of WUW estimates modelled in Scenario 1A (reduced, transect interval = 2 ) against WUW outputs from Scenario 0 (‘Best-Practice’) with the upper and lower bounds of the 90% confidence interval are represented by the two dashed lines above and below.	81
Figure 4.22 A comparison of WUW estimates modelled in Scenario 1B (supplemented, transect interval = 2 ) against WUW outputs from Scenario 0 (‘Best-Practice’) with the upper and lower bounds of the 90% confidence interval are represented by the two dashed lines above and below.	82
Figure 4.23 A comparison of WUW estimates modelled in Scenario 2A (supplemented, transect interval = 3 ) against WUW outputs from Scenario 0 (‘Best-Practice’) with the upper and lower bounds of the 90% confidence interval are represented by the two dashed lines above and below.	82
Figure 4.24 A comparison of WUW estimates for each transect modelled in Scenario 2B (supplemented, transect interval = 3) against WUW outputs from Scenario 0 (‘Best-Practice’) with the upper and lower bounds of the 90% confidence interval represented by the two dashed lines above and below.	83
Figure 4.25 A comparison of WUW estimates modelled in Scenario 3A (reduced, transect interval = 4 ) against WUW outputs from Scenario 0 (‘Best-Practices’) with the upper and lower bounds of the 90% confidence interval are represented by the two dashed lines above and below.	83
Figure 4.26 A comparison of WUW estimates modelled in Scenario 3B (supplemented, transect interval = 4 ) against WUW outputs from Scenario 0 (‘Best-Practice’) with the upper and lower bounds of the 90% confidence interval are represented by the two dashed lines above and below.	84

Figure 4.27 A comparison of WUW estimates for each transect modelled in Scenario 4 (photogrammetric only) against WUW outputs from Scenario 0 ('Best-Practice') with the upper and lower bounds of the 90% confidence interval represented by the two dashed lines above and below. .... 84

Figure 5.1 Transect 26 as viewed from the right bank of transect 25, Aug. 1st, 2019..... 89

Figure 5.2 Difference in engineers level and GPS survey measurements for pin-to-pin differences in elevation and horizontal distances across each transect. .... 92

Figure 5.3 Transect 6 as viewed from the left bank (July 7th, 2019) ..... 97

Figure 5.4 A graphical representation of the different slope energy gradients modelled for Upper Mission Creek, in Scenarios 0 (27 transects) and 3A (6 transects). Note, especially the rapid slope changes near transects 3, 14, 17, and 23 that are not reproduced in Scenario 3Ai. .... 101

Figure 5.5 Estimates of transect-specific WUW modelled in the 'Best-Practices' Scenario 0.... 102

## List of Tables

Table 2.1 Flow velocities and barrier heights prohibitive to the migration of Rainbow Trout, sorted by life stage (Slaney and Zaldokas, 1997). .....	9
Table 3.1 Summary of the number and combinations of surveyed and photogrammetric transects to be included in each scenario for the hydraulic models. ....	42
Table 4.1 A summary of morphological characteristics by transect. ....	54
Table 4.2 A summary of field trip dates, sorted by type and including estimates of discharges at the time, both at the Water Survey of Canada station in East Kelowna and measured in the field. ....	60
Table 4.3 A comparison of three topographical surveys (Eng. Lvl., Cal. and GPS) measurements for the elevation difference between left and right bank markers at each transect. ....	61
Table 4.4 Summary of discrepancies between the measurements from engineer’s level and GPS surveys for the horizontal distance of each transect, with error, reported as the difference from tape measurements, both in metres and as a percentage of transect length. ....	62
Table 4.5 A summary of error for photogrammetric measurements of elevation at survey points compared to measurements sampled following the standard surveying convention. ....	65
Table 4.6 A comparison of discrepancies between the corrected photogrammetric bathymetry and flow meter depth measurement, with residuals taken against measurements from the engineer’s level survey and summarized for the whole study reach with no statistical weighting. ....	67
Table 4.7 A comparison of discrepancies between the corrected photogrammetric bathymetry and flow meter depth measurement, with residuals taken against measurements from the engineer’s level survey, with transects assigned equal weight. ....	67
Table 4.8A summary of discharges, sorted by transect, used to calibrate the HEC-RAS model..	69
Table 4.9 A summary of calibration efforts, comparing the mean waterlines in HEC-RAS against the mean water line measured in the field on the calibration dates (Aug. 14th and 24th). Discrepancies between the measurements of at the left and right banks are also included. ....	71
Table 4.10 A summary comparison of modelled flow depth for each HEC-RAS Scenario against field measurement at the calibration discharges. ....	73
Table 4.11 A summary comparison of modelled velocity for each HEC-RAS scenario against field measurement at the calibration discharges. ....	75
Table 4.12 Regression result comparing the WUW estimates for each scenario against the ‘Best-Practices’ Scenario 0. ....	85

## Abbreviations

IFIM	Instream Flow Incremental Methodology
PHABSIM	Physical Habitat Simulation
HEC-RAS	Hydrological Engineering Centre – River Analysis System
SEFA	System for Environmental Flow Analysis
DEM	Digital Elevation Model
UAV	Unmanned Aerial Vehicle
SfM	Structure from Motion photogrammetric technique
RBT	Rainbow Trout
LWD	Large Woody Debris
MAE	Maximum Absolute Error
SDE	Standard Deviation of Error

## **Acknowledgements**

This thesis would not have been accomplished with the assistance of many people, for whom I will be forever grateful. First and foremost, I would like to thank my supervisor Dr. Bernard Bauer for all his guidance, patience, and support throughout this project. Thanks, Bernie, for believing in what once seemed like a crazy proposal and pushing me to put my best foot forward. I would also like to thank my committee members, Dr. Dwayne Tannant and Dr. Leif Burge for their guidance, support, and feedback.

I would also like to acknowledge everyone who helped out with data collection efforts: Anna MacDuff, David Scott, David MacDuff, Elizabeth Houghton, Madison Knodel, Marianni Nogare, Polina Orlov, Renee Larsen and Taylor McRae. Thank you so much, again!

I am especially grateful for the logistical support Dr. Tannant and David Scott provided. Without their assistance in providing the UAV imagery and photogrammetric software, this project wouldn't have succeeded.

A special thanks to Greg Courtice and Taylor McRae for all of our discussions, many of which ended up being formative in the final design of this project.

Big thanks go out to the fantastic staff and faculty of the Earth, Environmental and Geographic Sciences; Dr. Hornibrook, Dr. Scott, Dr. de Scally, Dr. Curtis, Stuart, Janet and Christina for all your support these past few years.

Most of all I need to thank my family for their constants support throughout this thesis. Especially my dad, David Macduff, who was always there to help me discuss ideas and improve my writing skills.

Finally, I am grateful for the funding from the Natural Sciences and Engineering Research Council of Canada (NSERC) through the NSERC Canada Graduate Scholarship Master's Award. Additional financial and logistical support came from the University of British Columbia Okanagan through the Work-Study program as well as the Graduate Entrance Scholarship and University Graduate Fellowship award.

# Chapter 1 . Introduction

## 1.1 Project Overview

The Incremental Flow Instream Methodology (IFIM) has been a dominant methodology for assessing stream habitat in North America since 1978 (Bovee and Milhous, 1978; Navarro et al., 1994; Lewis et al., 2004; Ahmadi-Nedushan et al., 2006; McParland, 2014; Booth et al., 2016). The basis of this approach is that the available instream habitat can be represented as the portion of the channel that matches the conditions (e.g., velocity, depth, gravel size, temperature) preferred by a particular fish species because these factors impose key limitations on biological productivity in streams (Bovee and Milhous, 1978; Navarro et al., 1994; Lewis et al., 2004; Slaney and Zaldokas, 1997; Kondolf, 2011; Booth et al., 2016).

The BC Instream Flow Incremental Methodology (BCIFIM) (Ahmadi-Nedushan et al., 2006; Winterhault, 2015; McParland et al., 2014) is a variant of the IFIM adapted for use in the province of British Columbia. The purpose of the BCIFIM “is to provide a standardized approach to the collection of instream flow information in relation to fish and fish habitat” (Lewis et al., 2004) and to identify the range of discharges required for ecological functions to be maintained throughout the year (McParland et al., 2014). Assessments of instream habitat are achieved by 1) characterizing the channel bathymetry at multiple transects using traditional surveying approaches; 2) sampling the flow velocity and depth across each transect; 3) sampling the sediment size distribution on the channel bed; and 4) documenting other relevant conditions using photos, sketches, and notes.

The field data are used in conjunction with hydraulic models to simulate the general flow conditions in a stream reach for a given discharge. From these representations of flow conditions, as well as in-field characterizations of the channel substrate and structure (e.g., LWD), the amount of useable habitat can be assigned for the species of interest in the study reach. Commonly employed modelling packages include Physical Habitat Simulation (PHABSIM 2019), Hydrologic Engineering Centre – River Analysis System (HEC-RAS, 2019), River 2D (River2D, 2019), and System for Environmental Flow Analysis (SEFA, 2019). Estimates of habitat availability for a given discharge are approximated as the Wetted Useable Area (WUA), which is the area of the stream channel having flow conditions matching the habitat criteria for

the species of interest. When these habitat criteria are applied to the hydraulic model results, they are collectively referred to as Habitat Association Models (HAMs) or Habitat Simulation Models (HSMs) (Lancaster and Downes, 2011). As fisheries productivity has continued to decline globally (Ahmadi-Nedushan *et al.*, 2006), salmonids in North America being a particularly well-documented example (Lichtowich, 1999), often as a response to habitat loss, HAMs have become an invaluable tool for managing watersheds to maintain their ecological function (Stalnaker *et al.* 2017, Reiser and Hilgert 2018, Nester *et al.* 2019). These models are important because they provide a standardized reproducible methodology that assesses change in habitat availability in response to shifts in discharge or morphology of the stream channel.

This approach based on habitat association modelling is not without limitations and has been subject to criticism, including: 1) considerable expense associated with fieldwork; 2) limited spatial scope due to accessibility; and 3) difficulties in accounting for habitat complexity and watershed-scale processes (Rumps *et al.*, 2017; Kondolf, 2011; Booth *et al.*, 2016; Wheaton *et al.*, 2017). For regions like the BC Interior, these issues are compounded because access to representative field sites is frequently limited by lack of roads, high density of forest cover, and rugged terrain. In the Thompson – Okanagan sub-region of the BC Southern Interior alone there are more than 1800 watersheds of third order or greater (BC Freshwater Atlas, 2019), the majority of which are salmon or trout-bearing streams often with limited access.

The key shortcoming of detailed channel assessments is that the surveys are limited to transects that are accessible by hiking and wading with surveying equipment in hand. Therefore, there remain questions regarding whether true habitat conditions have been sampled accurately and how representative the measured sites are of broader reach conditions, given a limited number of transects. In the case of small mountain streams, it is especially challenging to survey through and around dense riparian cover, large woody debris (LWD), boulder fields, and bedrock outcrops.

To understand the limitations of transect surveys faced with these kinds of logistical challenges, a great deal of effort has been put into quantifying the impact of transect numbers on the final IFIM results (Williams, 1997; Payne, 2004; Gard, 2005; Williams, 2010; Alleyon *et al.*, 2012; Inuo, 2019). The culmination of these efforts has yielded the following general

recommendations: 1) that no fewer than 15-20 transects be incorporated in the survey (Williams, 1996; Payne *et al.*, 2004); 2) that each habitat/morphological unit type be surveyed (Bovee, 1982); 3) that the length of the study reach should be at least fourteen times the average width of the channel so that at least two riffle-pool sequences are included (Bovee and Milhous 1978, Navarro *et al.* 1994, Lewis *et al.* 2004); and 4) that the spacing between transects should not exceed 1.5x the mean channel width (Inoue 2019). Practical application of these criteria remains a challenge, and in a meta-analysis of 600 IFIM assessments, Payne *et al.* (2004) found that the median density of transects surveyed was only 3.74 transects per kilometre.

As a potential solution to overcome the limitations imposed by access and safety, the integration of remote sensing techniques has been recommended to supplement transect surveys (Marcus and Fonstad, 2008; Fonstad *et al.*, 2013; Tamminga, 2016; Shintani and Fonstad, 2017; Wheaton *et al.*, 2017; Benjankar *et al.*, 2018; Lane *et al.*, 2020; Conesa-García *et al.*, 2020). In particular, the utilization of digital imagery from Unmanned Aerial Vehicles (UAVs) and photogrammetric techniques has been demonstrated to yield topographical and morphological information that is comparable to traditional detailed field assessments, but within a significantly shorter time frame (Carbonneau and Piégay, 2012; Biron *et al.*, 2013; Woodget *et al.*, 2014; Tamminga, 2016; Dietrich 2016; Shintani and Fonstad, 2017; Lane *et al.*, 2020). With regards to the standard IFIM assessments, the integration of UAV-based techniques offers the potential to increase the spatial coverage and accuracy of the assessments by increasing the density of transects and reducing the need for interpolation of habitat between measured transects.

However, while remote sensing techniques are increasingly looked to as a practical supplement to traditional surveys for assessing salmonid habitat, at this time there are two gaps in the existing literature with respect to mountainous streams. The first issue, highlighted by Shintani and Fonstad (2017), is that it remains unknown how well the UAV and photogrammetric approach performs for high-gradient streams with heterogeneous morphology and typically tannin-rich water. Secondly, while several studies have compared the accuracy and precision of photogrammetrically sourced topographic data against field measurements sampled with a Global Positioning System (GPS) instrument, there has yet to be a study that evaluates how uncertainty between photogrammetric and traditional surveying techniques propagates through habitat assessment models.

This thesis undertakes such a comparison on Upper Mission Creek (UMC), which is a Rainbow Trout (*Oncorhynchus mykiss*) bearing watershed that originates from the Graystones Plateau in South-Central British Columbia. A UAV-based methodology was deployed to generate a Digital Elevation Model (DEM) using recently developed photogrammetric techniques, from which photogrammetric transects were extracted to supplement a detailed BCIFIM assessment following standard procedures. The model estimates of habitat availability were evaluated for accuracy and reliability against those produced by both traditional field surveying techniques and direct instream measurements of channel hydraulics.

## **1.2 Research Objectives and Questions**

The primary objective of this thesis is to test if significant improvements can be made in the accuracy and spatial scope of stream habitat assessments, as defined in the BCIFIM procedures (Lewis *et al* 2004), by supplementing traditional surveys with UAV-based techniques. If such improvements are realized, there is the potential for assessing a large number of streams in the BC Interior that might not otherwise be assessed reliably. With stress on the ecological function of these watersheds increasing exponentially with the advance of climate change and human activities, the need for reliable assessments of environmental flows is becoming ever more critical in order to manage, conserve, and restore the health of BC's freshwater fisheries.

The focus of this study will be on the physical flow conditions traditionally used to quantify habitat availability for salmonids, specifically the flow depth and mean velocity. Therefore, improvements to accuracy will be assessed according to two criteria:

The accuracy and precision of hydraulic models at predicting in-channel flow conditions and salmonid habitat for a given discharge as validated against direct instream measurements sampled at the same discharge.

The magnitude of confidence intervals around estimates of salmonid habitat, and how these intervals vary with the removal of surveyed transects and supplementation or replacement by digitally derived transects.

### **Primary Research Question and Hypotheses:**

Does the use of UAVs to obtain photogrammetric data on reach-scale channel morphology and hydraulics lead to statistically significant improvements over traditional field surveying methods for assessing salmonid habitat in small mountain streams?

**H<sub>0</sub>:** There is no net improvement in the accuracy of habitat assessments based on traditional field methods following the BCIFM if photogrammetric data from UAVs are incorporated into the assessment.

**H<sub>1</sub>:** The inclusion of photogrammetric data from UAVs yields significant improvements to the accuracy of the habitat assessments above what can be attained using only BCIFM-based field-surveyed transects.

## **Chapter 2 . Literature Review**

The purpose of this chapter is to provide an essential background that informs the research objectives. The chapter is structured as follows: 1) a description of the general hydro-geomorphic conditions required by Salmonids that are native to the Pacific Northwest, with a specific focus on Rainbow Trout; 2) a summary of how Salmonid habitat criteria have traditionally been assessed; and 3) a discussion of recent developments leading to improved accuracy and efficiency of instream habitat assessments. With respect to the latter, particular attention is directed at the Instream Flow Incremental Methodology (IFIM), the dominant methodology for conducting detailed assessments in the BC. This leads to a summary of the software packages to model instream hydraulic habitat according to IFIM, such as Physical Habitat Simulation (PHABSIM) and its successors, as well as the utilization of remote sensing technologies to aid in IFIM type assessments.

### **2.1 Physical Habitat Conditions Required by Pacific Salmonids**

Pacific Salmonids are fishes belonging to the family Salmonidae, native to the North Pacific, and they include Pacific Salmon and Trout (*Oncorhynchus spp.*), Char (*Salvelinus spp.*), Grayling (*Thymallus spp.*), Whitefish and Cisco (*Coregonus spp.*), Inconnu (*Stenodus spp.*), and Round Whitefish (*Prosopium spp.*) (Pike *et al.* 2010). As a group, the native range of Salmonids is pan-Pacific, extending from Central California in the south to coastal rainforests of Alaska, along the north-western coast of North America, across to the Taiga of Siberia in north-eastern Russia and to the mountains of Southern Kyushu, Japan (Quinn, 2004). With a geographic range so large, Salmonids are an adaptable group with a great degree of genetic plasticity within species and with localized strains commonly bearing specific behavioural, and occasionally, physiological adaptations to watershed specific environments (Quinn, 2004).

Populations of Coho Salmon (*Oncorhynchus kisutch*) and Bull Char (*Salvelinus confluentus*), two distinct genera that are native to the Upper Fraser River in BC, can weigh in excess of 10 kg as adults. Despite their size, both species have adapted to utilize small headwater streams (3<sup>rd</sup> order or smaller) for spawning and rearing of juveniles due to reduced competition and predation that characterizes larger mainstem rivers (Quinn, 2004; Pike *et al.*, 2010). This genetic and behavioural plasticity in Salmonids has no better example than Rainbow Trout (RBT)

(*Oncorhynchus mykiss*), which span nearly the entire geographic range of Pacific Salmonids, with populations ranging from anadromous runs of steelhead in the Kamchatka Peninsula of eastern Russia to migratory but non-anadromous populations that dominate large oligotrophic lakes in southern BC and year-round residents of small alpine creeks in the Sierra Nevada of California.

Even within a relatively small region such as the Shuswap Watershed in the Southern Interior of BC, variations within Rainbow Trout can be extensive. The dominant population group resides principally in large lakes, adapted to feeding on salmon fry and reaching sizes greater than 60 cm in length and 10 kg in mass over lifespans that may extend up to 11 years. Other populations of Rainbow Trout are year-round residents of the 1<sup>st</sup> order tributaries to the Shuswap River, adapted to very small discharges and feeding on benthic and terrestrial invertebrates, reaching a maximum size of 20-30 cm in length and less than 0.5 kg in mass, with an average lifespan of fewer than four years.

The following literature review summarizes the key habitat conditions that are required by all Salmonids, with specific mention of RBT, in order to provide context for the criteria used to traditionally evaluate instream habitat. These in-stream conditions, including water temperature, hydraulic (flow) conditions, substrate characteristics, and general channel morphology will be broadly summarized based on life stage because habitat requirements are determined more by stage of development than by species (Quinn, 2004; Pike *et al.*, 2010).

### **2.1.1 "Fall" Migration and Spawning**

While the specific timing of the migration stage is quite variable and dependent on regional climate, discharge patterns, water temperature, and the evolutionary history of a specific Salmonid population, most Salmonids begin migrating to their natal spawning grounds during the late-summer or early fall (Pike *et al.*, 2010). Many anadromous populations of Steelhead migrate to their natal streams during fall, with similar run timings for Chinook and Coho Salmon, however, they forgo the spawning itself until the spring before the onset of freshet and reside nearby throughout the fall-winter months (Quinn, 2004). In contrast, Cutthroat Trout and non-anadromous populations of Rainbow Trout migrate and spawn during the spring preceding the onset of freshet.

In each case, the minimum environmental requirements at the migration stage are: 1) that flow depths are sufficient for unobstructed passage; 2) flow velocities are not prohibitively strong to swim against; and 3) water temperatures are below the metabolic threshold for stress when performing strenuous activities (e.g., swimming up a set of rapids) (Quin, 2004; Pike *et al.*, 2010). It should be noted that these constraints are not limited only to adults migrating to spawn, as all life stages of Salmonids face similar challenges. However, the concerns are most often associated with spawners because of the tendencies for these populations to migrate during the late summer – early fall when discharges are small and air temperatures are high.

The BC provincial guidelines prescribe a minimum depth requirement of 0.18 m for smaller, non-anadromous Rainbow Trout to allow passage. For larger specimens, often anadromous, the minimum depth prescribed is 0.25 m (Slaney and Zaldokas 1997). This estimate, however, is only applicable to short reach distances to allow passage through a riffle bar and into a deeper run. Without deeper water elsewhere in the reach, the fish become stressed due to exposure to predators and therefore may move back downstream to deeper flows that provide safety in cover and available space.

Slaney and Zaldokas (1997) also provide estimates of the maximum flow velocities that Rainbow Trout can manage over short bursts, such as a few minutes, compared to a prolonged period of travel for several hours (see Table 2.1). The maximum height that individuals can jump to pass a barrier is also referenced. These criteria can be used in hydraulic modelling exercises to determine safe discharge releases from dams (Winterhault, 2015) or for the construction of engineering infrastructure (e.g., bridges, weirs, levees, flow control structures) around the fish habitat of conservation concern.

Table 2.1 Flow velocities and barrier heights prohibitive to the migration of Rainbow Trout, sorted by life stage (Slaney and Zaldokas, 1997).

	Sustained (m s <sup>-1</sup> )	Prolonged (m s <sup>-1</sup> )	Burst (m s <sup>-1</sup> )	Maximum Jump Height (m)
<b>Juveniles (&lt;50 mm)</b>	0.1	0.3	0.4	0.3
<b>Juveniles (50-125 mm)</b>	0.4	0.7	1.1	0.6
<b>Non- Anadromous Adult Rainbow Trout</b>	0.9	1.8	4.3	1.5
<b>Anadromous Adult Rainbow Trout (i.e., Steelhead)</b>	1.4	4.5	8.1	3.4

For most Salmonids in BC, stream temperatures below 18°C are considered safe. Water temperatures between 18-21°C are classified as stressful under strenuous activity (e.g., migrating upstream), and spawners tend to migrate downstream to deeper and cooler water if temperatures reach or exceed 21°C (Sullivan *et al.*, 2000; Hicks, 2000; Hyatt *et al.*, 2003; Klomes and Richter, 2006; McGrath, 2010). If the fish are unable to locate cold-water refuge, then disease is likely to spread among the population. Should temperatures reach the upper incipient lethal temperature (UILT), approximately 24°C, for a sustained period of several days, upwards of 50% of the population can be expected to die from metabolic failure. For Bull Char and Cutthroat Trout, which occupy colder habitat than other native salmon, the stress thresholds and UILT are lower at about 16 °C and 20-21°C, respectively (Selong *et al.*, 2001; Bear *et al.*, 2007; Gutosky *et al.*, 2017).

Timber harvesting activities in small BC watersheds can have impacts on riparian vegetation and thereby influence streamflow and water temperature (Slaney and Zaldokas, 1997; Lewis *et al.* 2004; Pike *et al.*, 2010). Thus, logging is generally regulated in a manner that will lead to beneficial outcomes such as: 1) creating stable discharges during large precipitation events; 2) retaining a dense tree canopy along stream banks to provide overhead shade from direct insolation, which can reduce daytime high temperatures by as much as 8°C; and 3) retaining or replenishing instream large woody debris (LWD), which leads to the creation of pools and cover.

### 2.1.2 Winter Incubation and Egg Survival

The geomorphic character of the channel bed at spawning sites is of critical importance for reproduction efforts to be successful (Pike *et al.*, 2010). Redds are created by spawning pairs scouring out a large pit in the substrate, into which the female will deposit her eggs and

subsequently bury them with gravel from immediately upstream of the red, after fertilization by the male. The eggs must survive incubation until early spring in the case of most Pacific Salmonids, or late spring in the case of Rainbow and Cutthroat Trout, with only the structure of the redd for shelter.

For the eggs to survive incubation, there are a few key hydrological and geomorphic conditions required. The first is that the redd must be constructed at a site that will remain below water for the entire incubation period. In small interior streams, this can be a challenge as precipitation is almost entirely stored in the snowpack during the winter months. If groundwater inputs become depleted due to extended periods of drought, baseflow discharges may be unable to support the survival of the eggs.

Second, the size, sorting, and packing geometry of the channel substrate must be suitable. By necessity, the particles must be small and loose enough that adult fish can mobilize them, initially to excavate a redd during spawning and later to mobilize upstream gravels to bury the eggs within the redd. But, the particles also need to be large enough such that they are not mobilized during the spikes in discharges during the incubation period (Pike *et al.*, 2010). Areas where the substrate is dominated by sands or finer sediments are avoided because the substrate is both too easily mobilized and lacks suitable porosity. Porosity is critical to egg survival, as water must flow through the pore spaces to provide the developing eggs with a continuous supply of oxygen and to remove metabolic wastes during incubation (Quin, 2004; Pike *et al.*, 2010).

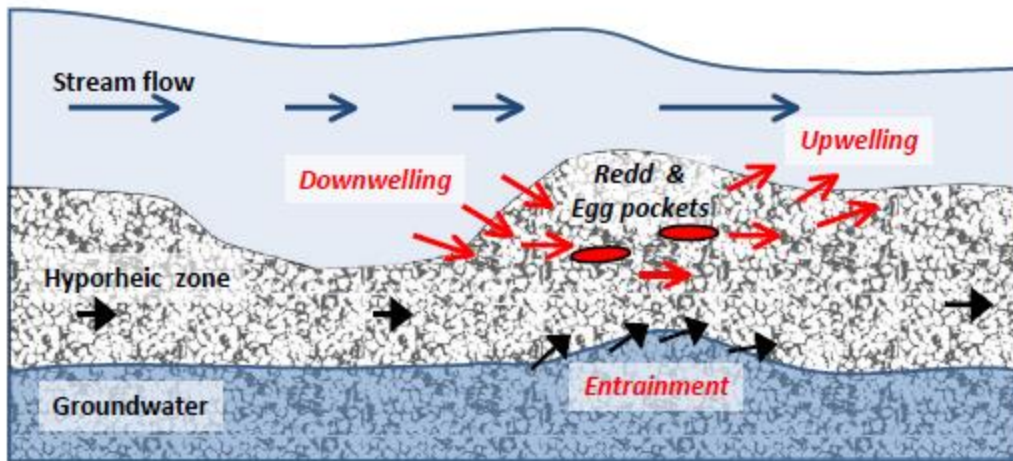


Figure 2.1 Schematic of intergravel water flow through a salmonid redd. (from Pike *et al.*, 2010).

As a generalization, Salmonids favour digging their redds where well-sorted and loosely-packed gravels are present. The most common criteria for assessing and restoring salmonid habitat is the median grain size of the substrate, which Kondolf and Wolman (1993) noted is dependent on fish size, with larger species and individuals able to mobilize larger materials and occupy areas of stronger flow.

### 2.1.3 Spring Hatching

The rate and timing of egg development to the fry stage are largely dependent on water temperature, usually described as the accumulation of “thermal units” over the incubation period (Quin, 2004; Pike *et al.*, 2010). Upon hatching, the fry will continue to remain within the pore spaces between the gravel for days until the yolk sack is fully absorbed (Quin, 2004; Pike *et al.*, 2010). Afterwards, the fry will begin to emerge from gravels and migrate to suitable rearing habitats. The timing of emergence from the gravel coincides with warming water temperatures but often precedes peak discharges, (Pike *et al.*, 2010).

Rainbow and Cutthroat Trout migrations tend to coincide with the peak flow following a brief incubation period because the eggs are typically laid in April-May when other Salmonid fry begin their emergence. In the case of most Salmonids, the fry will migrate upstream and along the shallow margins of the banks of tributaries where the prevalence of cover and reduced predation is advantageous to survival (Pike *et al.*, 2010). Sockeye and their non-anadromous variant, Kokanee Salmon, are an exception to this because they migrate downstream to nearby

lakes to capitalize on the pelagic plankton as a critical food source.

From the perspective of managing habitat, the key parameter during this relatively short period following incubation and hatch is for discharges to be within a certain range. Discharge should be above the minimum level for channel connectivity to be continuous as well as to provide enough cover available to protect from predation, but small enough that flow velocities do not exceed the sustained swimming abilities of the fry (Slaney and Zaldokas, 1997; Pike et al., 2010).

#### **2.1.4 Summer Rearing and Feeding**

For Salmonids that reside and rear in small streams for at least one year, a few hydrogeomorphic parameters have to be satisfied. However, these conditions are rarely as strict as those required during the spawning and incubation stages.

The first condition is for there to be sufficient available cover in the form of woody debris, overhanging banks, and pools to shelter small individuals from large discharge events that might otherwise displace them downstream into more inhospitable environments (Slaney and Zaldokas 1997). Second, the combination of substrate size and shear stress along the channel bed should be conducive to the production and drift of macroinvertebrates (Slaney and Zaldokas, 1997; Newbury, 2004; Rosenfield and Ptolemy, 2012). Loosely consolidated gravels and cobble with moderate flow velocities (e.g., 0.2 -1.0 m s<sup>-1</sup>) are usually found in riffle habitats upstream of pools, and they provide optimal conditions for macroinvertebrate breeding and survival. However, the flow velocity has to be great enough that small or weak individuals will be entrained in the flow, much like smaller sediment particles, drifting downstream and becoming a readily available food source for resident Salmonids (Rosenfield and Ptolemy, 2012).

If the substrate becomes clogged with fine particles (e.g., silts and clays), the macroinvertebrates within the pore spaces will be smothered. Moreover, there would be no shelter in the boundary layer for the population to persist and no oxygenation of the pore spaces. If flow velocities and shear stress are too large, the bed sediments may be mobilized thereby pulverizing much of the macroinvertebrate population. In both cases, the key food source for young Salmonids is severely reduced, limiting the overall productivity of the fishery.

During the rearing stage, the presence of cool and well-oxygenated water is critical for fish

survival (Sullivan et al., 2000; Selong et al., 2001; Klomes and Richter, 2006; Bear, McMahon and Zale, 2007). As discharges decrease following the freshet and into the summer, the thermal capacity of the stream to accommodate temperature changes decreases at a time when insolation is at its greatest. Thermal loading is important because a combination of warmer and less oxygenated waters can place major stress on the health of Salmonids, often leading to limited growth rates, secondary infections, and shorter lifespans. For most Salmonids, this occurs when temperatures increase above 15-18°C, depending on the population. Major die-offs can start to occur when water temperatures in a stream reach above 24°C (Sullivan et al., 2000; Selong et al., 2001; Klomes and Richter, 2006; Bear, McMahon and Zale, 2007). In warmer regions of the Southern Interior of British Columbia, this is an increasingly important concern given climate warming, and there are now efforts underway to start incorporating models of water temperature into environmental flow needs assessments (e.g., Parkison *et al.*, 2016; MacDuff *et al.*, 2019).

## **2.2 Incremental Flow Instream Methodology**

### **2.2.1 Introduction**

'Instream flow needs' or 'environmental flow needs' are relatively recent terms that refer to the amount of water needed to sustain stream habitat and aquatic health on a year-round basis (Cooperrider *et al.*, 1986). In the Pacific North-West (PNW) of North America, the predominant methodology for conducting detailed assessments of instream habitat conditions is the Instream Flow Incremental Methodology (IFIM), which now has many regional variants such as the BC Instream Flow Incremental Methodology (BCIFM) (Navarro *et al.*, 1994; Lewis *et al.*, 2004; Ahmadi-Nedushan *et al.*, 2006; McParland, 2014; Booth *et al.*, 2016). Formally developed in the late 1970s by the US Fish and Wildlife Service (USFWS) (Bovee and Milhous, 1978), the IFIM uses instream empirical measures of hydraulic conditions and simulations of hydraulic responses to changes in discharge to estimate the quality and availability of instream habitat available for an aquatic species of interest (Bovee and Milhous, 1978; Navarro *et al.*, 1994; Lewis *et al.*, 2004; Reiser and Hilgert, 2018). The foundational data requirements for this methodology are:

- A topographic survey, sampling the topography/bathymetry of the channel at a series of transects over a study reach, perpendicular to the direction of flow.
- A series of hydrological surveys, measuring the flow depth and velocity at each of the

previous sampling points, at a minimum of three different dates when discharges are between 5%-40% of the mean annual discharge (MAD).

- Measurements of the substrate particle size distribution at each transect, most often sampled with a Wolman Pebble Count (Wolman, 1954; Kondolf, 2000).
- Estimates of the overhead cover provided at each transect, often associated with overhead riparian vegetation or large woody debris in the channel (Bovee and Milhous, 1978; Lewis et al. 2004; Ahmadi-Nedushan, *et al.* 2006).
- Other water quality criteria, such as oxygen content and water temperature, can also be incorporated into IFIM assessments depending on objectives and available resources (Bovee and Milhous 1978; Lewis *et al.*, 2004).

From the measurements of channel geometry, slope, flow hydraulics, discharge, and substrate distribution, the friction coefficients (e.g., Manning's  $n$ ) can be estimated alongside other modelling parameters such as expansion and contraction coefficients. Simulations of channel hydraulics across a range of discharges not previously surveyed can then be realized using hydraulic models (Bovee and Milhous, 1978; Navarro *et al.*, 1994; Lewis *et al.*, 2004; MacParland *et al.*, 2016). Such simulations can provide estimates of the flow depth, velocity, and other associated values (e.g., Froude number, shear stress, Reynolds number, stream power) for each transect, at each increment of discharge simulated.

The next step in the IFIM process is to apply a habitat suitability index (HSI) to each measure of the selected criteria (e.g., each simulated value of flow depth or flow velocity). An HSI assigns a relative score of habitat quality, from least suitable (0) to most suitable (1), for different ranges of the criteria (e.g., flow depth) based on the statistical analyses of data previously collected or collated regarding the relative abundance of fishes observed across those ranges at similar measurement locations (Bovee and Milhous, 1978; Navarro *et al.*, 1994; Lewis *et al.*, 2004). Figure 2.2 provides an example of an HSI curve for adult Rainbow Trout based on flow velocity. The principal assumption in this approach is that the hydraulic conditions are the primary factor in determining how many individuals occupy any given location with the stream, and thus habitat suitability (Bovee and Milhous, 1978; Navarro *et al.*, 1994; Resier and Hilgert, 2018).

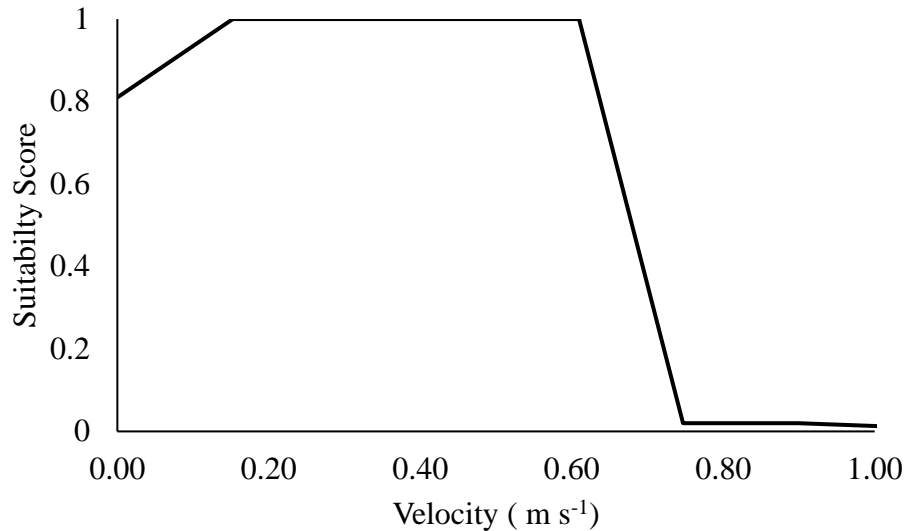


*Figure 2.2 Habitat suitability for adult Rainbow Trout according to flow velocity (m s<sup>-1</sup>) (from Raleigh et al., 1984). The curve shows that flow velocities above about 0.75 m s<sup>-1</sup> are not suitable for Rainbow Trout.*

At each transect, the habitat suitability scores are cross-multiplied to produce a combined suitability index (CSI), which is the relative habitat suitability score for that transect. The transect-specific CSI is then multiplied by the wetted width of the transect to generate the transect-specific wetted-usable-width (WUW), which is a relative measure of how much of the wetted width at that transect would be considered desirable habitat by the species of interest (Bovee and Milhous 1978; Navarro *et al.*, 1994; Resier and Hilgert, 2018).

Some of the software packages that have been commonly used to perform these habitat modelling exercises include Physical Habitat Simulation (PHABSIM 2021), the Hydrologic Engineering Centre – River Analysis System (HEC-RAS 2019), River 2D (River2D 2021), and the System for Environmental Flow Analysis (SEFA 2021). The collective term for combinations of models that assess hydraulic conditions and habitat suitability is ‘habitat simulation models’ (HSMs) or ‘habitat association models’ (HAMs) (Lancaster and Downes, 2011; Stalnaker *et al.*, 2017).

The key advantage of the IFIM that led to its widespread adoption in the PNW is that it provided a standardized approach for biologists, hydrologists, geomorphologists, and engineers to make predictions of the likely impacts to freshwater habitat in response to alterations in channel morphology or the availability of water (Stalnaker *et al.* 2017, Nester *et al.* 2019). The manual

for conducting IFIM in British Columbia states that the methodology “provide[s] a standardized approach to the collection of instream flow information in relation to fish and fish habitat” (Lewis *et al.*, 2004, 63) in order to identify the range of discharges required for ecological functions to be maintained throughout the year (McParland *et al.*, 2016).

Another critical factor that contributed to the popularity of the IFIM was its flexibility to apply to a broad range of species, instream environments, and specific assessment objectives (Stalnaker *et al.*, 2017; Nester *et al.*, 2019). IFIM assessments may have several different objectives, ranging from an evaluation of the impacts of discharge alterations due to the construction of large hydroelectric projects to the restoration of spawning habitat in formerly channelized reaches to assessments of how physical habitat may limit macro-invertebrate production in small creeks (Ahmadi-Nedushan *et al.*, 2006).

### **2.2.2 Challenges with habitat suitability modelling**

As with any well-studied methodology, the IFIM and PHABSIM modelling approach is not without specific nuances and limitations that have been the source of criticism (Lancaster and Downes, 2011; Kondolf, 2011; Booth *et al.*, 2016; Railsback 2016; Stalnaker *et al.*, 2017; Nester *et al.*, 2019). The most common criticism relates to the technical and logistic challenges of data collection, which include: 1) considerable expense associated with fieldwork; 2) limited spatial coverage for assessments; and 3) difficulties in accounting for habitat complexity and watershed-scale processes (Rumps *et al.*, 2017; Kondolf, 2011; Booth *et al.*, 2016; Wheaton *et al.*, 2017).

As previously stated, the IFIM relies on the collection of reliable topographical and hydrological data to generate realistic simulations of hydraulic habitat. Traditionally, the topographical data would consist of a series of transects sampled following standard surveying conventions. Most commonly the equipment utilized includes an engineer’s level, tripod and stadia rod, although Total Stations and Real-Time Kinematic Global Positioning Systems (RTK-GPS) are increasingly being used to perform more detailed surveys. Likewise, hydrological measurements are sampled using wading rods mounted with flow meters, have become increasingly sophisticated and expensive, with flow meters evolving from rotating-cup devices such as the Price-style velocimeters to high-frequency instruments incorporating acoustic technologies based on the Doppler principle.

The logistical challenges with these data collection methods are that surveys are limited to sections of the stream that are: 1) accessible by foot; 2) safe for crews to wade into whilst carrying equipment, and 3) have clear lines of sight upstream and downstream (Lewis *et al.*, 2004; Tamminga 2016). Where these criteria are met, the preparation and survey of each transect require a fair amount of time, often in the range of 1-2 hours per transect for an experienced crew; thereby significantly limiting the number of transects that can be surveyed on any given day.

These constraints often limit the study reach to less than 1 km so that 'detailed' assessments can be conducted with a sampling density of 5-15 transects per km for purposes of evaluating potential alterations to channel morphology (e.g., restoration of a formerly channelized reach) (Payne *et al.*, 2004; Williams, 2010; MacParland *et al.*, 2014; Tamminga 2016; Gronsdaahl, 2019; Backes *et al.* 2020, Gronsdaahl *et al.* 2021). Alternatively, a reach length of several kilometres with a sampling interval of fewer than 2 transects per km might be required, perhaps for managing water licences (Williams, 1996; Payne *et al.*, 2004; Williams, 2010). Clearly, there will be trade-offs between transect density and reach length. In a meta-analysis of 600 IFIM assessments, Payne *et al.* (2004) found that the median transect density for surveys was 3.74 transects per km. Assessments for water licensing had a density of 2.09 transects per km, whereas detailed project evaluations had a median sampling density of 6.71 transects per km (Payne *et al.*, 2004).

The impact of transect density on the uncertainty of HSM outputs is perhaps the most studied aspect of the IFIM (Williams, 1997; Payne, 2004; Gard, 2005; Williams, 2010; Alleyon *et al.*, 2012; Inuo 2019). Bovee and Milhous (1978) recommended that the length of a study reach be at least 10-14 times the average channel width. This was proposed to ensure that two riffle-pool sequences would be included in the study, based on the generalization that riffle-pool sequences in alluvial reaches typically repeat over a distance of five-seven times channel width (Leopold *et al.*, 1964). Within the study reach, the guideline for minimum transect density has been to sample at least one of each habitat unit type (e.g., pool, riffle, run) and each major hydraulic control point (e.g., a weir). The inclusion of additional transects is recommended mainly to address specific project objectives (Bovee and Milhous, 1978; Navarro *et al.*, 1994; Lewis *et al.*, 2004).

Payne *et al.* (2004) relied on visual comparisons of how WUA curves changed with alterations to the number of transects incorporated in previous studies to characterize how the confidence intervals surrounding HSC outputs changes in response to the reduced number of transects. The recommendation from the meta-analysis was that for reaches with relatively ‘simple’ (i.e., consistent) morphology, no more than 6-10 transects per reach were necessary (e.g, a meandering reach with deep flows and no LWD). For reaches with complex morphology, such as those that dominate mountainous environments, 18-20 transects per study reach were recommended. After this number, minimal change in the WUA curves was observed, even if the number of transects increased to 70 transects per reach. Williams (1996) found that regardless of reach complexity, a minimum of 15 transects per study was needed to produce reliable PHABSIM results for adult populations of Chinook Salmon in California, USA.

Williams (1996, 2010), Gard (2005) and Alleyon *et al.* (2012) relied on a series of bootstrap analyses to quantify the impacts of transect density on uncertainty in habitat estimates. Each of these studies generated a detailed set of habitat models with WUA curves based on WUW estimates from 15 to 107 transects, with a base habitat model created using the complete set of transects available. Several variations of the model were generated, each using a different combination of transects and a reduced transect density (e.g., only 40 of 107 transects may have been used), with transect density decreasing at set intervals. For each specified interval of transect density, the combination of transects and final WUA estimates was resampled randomly with the replacement of transects, for up to two thousand simulations (Williams, 2010). The range of WUA outputs for each scenario, compared to those in the complete model, demonstrated how the spread in confidence intervals exponentially increases, with often uniform separation from the ‘best-practices’ HSC, in response to either an increase in modelled discharge or a decrease in transect sampling density.

Work on the Feather River, California, Williams (1996) was among the first to demonstrate that significant uncertainty can be introduced into the IFIM assessments for Salmonids as transect numbers are less than fifteen. In Gard (2005) a similar bootstrap exercise was performed with each analysis resampling between six to forty transects from a pool of 107 transects overall. Resampling was done without replacement for adult and juvenile Rainbow Trout in the Cache la Poudre River, Colorado, USA. This study observed that WUA estimates could deviate from the

‘true values’ by 28% whilst remaining within the 95% confidence intervals when including 40 of the 107 transects. As the number of transects decreased below 40, the deviation from the true WUA increased up to a maximum of 70% when six transects were used. In response to Gard (2005), William (2010) used the same transect data and habitat indexes for the Cache la Poudre River; however, this time the bootstrapping exercise increased the sample size to 100 transects, rather than 40, and resampling was done with replacement. While this analysis observed similar magnitudes of uncertainty as Payne *et al.* (2004) and Gard (2005) at smaller transect numbers (e.g.,  $n < 20$ ), William (2010) highlighted that uncertainty in WUA estimates could remain substantial even when transect numbers far exceeded what is often practical to survey (i.e.,  $n > 40$ ). William (2010) recommended that all PHABSIM assessments include some measure of uncertainty when reporting the results, even if transect sampling density is relatively dense ( $n > 15$  transects per km).

In consideration of Brown Trout (*Salmo trutta*) in the mountains of Northern Spain, Ayllon *et al.* (2012), noted that WUA estimates could vary by little as 3% from the ‘true value’ within the 95% confidence interval if the bootstrapping sample was complete (40 transects, 1 m sampling interval). However, as the number of transects decreased from 40 to 9, with distances between transects increasing by 5 m in each scenario, the width of WUA estimates within the confidence interval increased from 3% for year old fry to 226% for adult Brown Trout at peak discharges. Similar, to Gard (2005), Ayllon *et al.* (2012) concluded that the two largest sources of uncertainty could be traced to small sample sizes and the density of transects.

Inuoé (2019) evaluated the impact that transect density had on the accuracy and precision of model estimates for flow depth, velocity, and the wetted width of the channel for seven study reaches in Japan. The first conclusion was that predictions for wetted width, mean depth and mean velocity could achieve sufficient precision and accuracy when transects were sampled at a spacing equal to 0.5 x channel width. Precision was defined by the coefficient of variation (100% x standard deviation/mean), which at half-channel width was less than 10%. The correlation coefficient for the regression between predicted and measured values was  $R^2 \approx 1.0$ . Likewise, reasonable precision and accuracy could be achieved so long as the transect spacing was equal to or less than 1.5 x channel width, with precision  $< 15\%$  and  $r > 0.95$ . However, if study objectives were to achieve ‘reasonable’ levels of accuracy and precision for other measures of variance

(e.g., standard deviation) for wetted width, flow depth, and velocity, rather than just the means, then the spacing had to be reduced to 1.0 x channel width at a minimum and down to 0.5 x channel width in an ideal situation.

In addition to increasing transect density, these studies also recommended that transect surveys be repeated at multiple dates and discharges (Williams, 1996; Lewis *et al.*, 2004; Payne *et al.*, 2004; Gard, 2005; Williams, 2010; Ayllon *et al.*, 2012; Stalnaker *et al.*, 2017; Reiser and Hilbert, 2018). Repeating the transect surveys was suggested as a way to reduce uncertainty in WUA in two ways: 1) by identifying and correcting, previous sampling errors, such as a slight misplacement of the stadia rod or miscommunication between crew members; and 2) providing the necessary information to calibrate the hydraulic models for more than one discharge event, greatly improving the reliability of habitat predictions at both small and large discharge conditions.

Further highlighting the logistical challenges of conducting repeatable and detailed instream habitat surveys in the PNW, Rumps *et al.* (2007) surveyed forty-seven managers involved in stream restoration projects. Fully 34% of the forty-seven projects were unable to “conduct sufficient monitoring to evaluate effectiveness” of the work done (Rumps *et al.* 2007, 509). Among the 70% of respondents that did report the project to be a ‘success’, 43% either had no success criteria or were unaware of any criteria for their project (Rumps *et al.* 2007). More critically, only 12% of the respondents reported their answers were based on in-field measurements. The majority of respondents (66%) stated that there was a need for ongoing project maintenance or monitoring but only 43% had the funds to do so.

### **2.2.3 Recent Advancements – Hydraulic modelling**

Many of the strengths and weaknesses of IFIM have been tied to the associated modelling programs, such as PHABSIM and HEC-RAS. Until recently, these software packages were only capable of performing one-dimensional (1D) hydraulic modelling in the streamwise direction. This meant that hydraulic parameters for a transect are cross-sectionally averaged and do not address spanwise complexity such as depth changes from bank to bank or velocity profiles in the vertical or horizontal direction, which are all relevant to fish habitat (Gibson, 2013; Stalnaker *et al.*, 2017; Reiser and Hilbert, 2018; Benjankar *et al.*, 2018). While the consensus has been that

PHABSIM is still a valuable tool for assessing general habitat conditions at a transect (Payne *et al.*, 2004; Gard, 2005; Williams, 2010; Ayllon *et al.*, 2012; Gibson and Pasternack, 2016; Stalnaker *et al.*, 2017; Reiser and Hilbert, 2018; Benjankar *et al.*, 2018), this 1D limitation has been a lightning rod for criticisms against the IFIM. Critics claim that the uncertainty tied to the hydraulic modelling outputs and the limited scale of calculations imply that the results have minimal real-world significance (Lancaster and Downes, 2011; Railsback, 2016). Hence, a great effort has been expended to improve the accuracy, precision, and resolution of IFIM habitat estimates, with significant advancements made during the past two decades in the field of hydraulic and habitat modelling (Rosenfield and Ptolemy, 2012; Gibson and Pasternack 2016; Wheaton *et al.*, 2017; Benjankar *et al.*, 2018).

The key products of these efforts have been the development and application of laterally distributed one-dimensional models, sometimes known as 1.5D or Quasi 2-D models (Jowett and Richardson, 2008; Gibson and Pasternack, 2016), and recently, two-dimensional hydraulic modelling programs (e.g., River 2D) as well as three-dimensional modelling packages (e.g., Delft3D). Laterally distributed one-dimensional hydraulic models differ from a purely 1D model in that the space between each sampling point functions as a unique prism (Gibson, 2013). This allows the models to predict hydraulic conditions for each prism (see Figure 2.3) along a transect, compared to previous versions that were only capable of estimating the general conditions at a transect. The critical advantage that this provides is improved accuracy of hydraulic estimates at both smaller and larger discharges than what was used during calibration (Gibson, 2013).

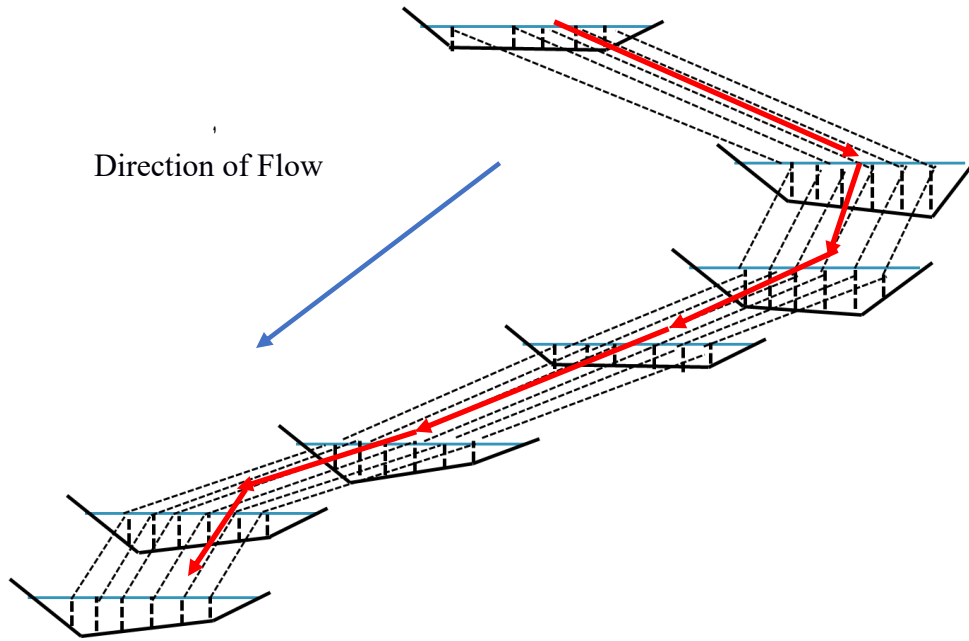


*Figure 2.3 A 3D representation of seven theoretical transects with six sampling points each. Dashed lines show the interpolation between transects, forming the lateral prisms of the 1.5 D hydraulic model. Whereas the red arrows show the pathway for interpolation in 1D hydraulic models for the same transects.*

HSCs can now be applied to each prism and the WUW of each prism can be tallied to generate an estimate of WUW for the area between neighbouring transects rather than calculating WUW as a linear measure across a single transect. For transects where there is significant variance in the hydraulic conditions, such as a pool on a meander bend where flow depth and velocity of the thalweg on the outside are much greater than on the shallow inside bank, a 1.5D hydraulic model would be able to distinguish the number and size of prisms suitable as habitat, rather than assigning a habitat value for the entire transect based on the channel-averaged conditions.

Another key criticism of the PHABSIM approach has been that HSIs, which are based on sampling hydraulic conditions at points where individuals of the species of interest are observed, can not be directly applied to 1D model estimates of habitat conditions because transect means are rarely equivalent to specific point measurements (Lancaster and Downes, 2011; Railsback 2016; Booth, 2016). However, in the progression to laterally distributed 1.5D models, where estimates of flow hydraulics and habitat are now computed as an average between sampling points rather than across the entire transect, the differences in scale between the HSIs and the model outputs have been significantly decreased, with hydraulic outputs of each prism becoming a close equivalent to the empirical point measurements done for the HSIs (Gibson, 2013).

The development of fully two-dimensional hydraulic modelling programs has improved the situation even more (Gibson, 2013; Winterhault, 2013; Gibson and Pasternack, 2016; Benjankar *et al.*, 2018). The first factor that distinguishes two-dimensional models is the incorporation of survey points and hydraulic measurements that are reported in three-dimensional space (e.g., longitude, latitude, and elevation or x, y, z). Each survey point functions as an individual node, with hydraulic responses modelled on the relationship between each node and the nodes that directly surround it. Flow parameters can therefore be assigned as a vector with speed and direction rather than assuming that the flow is orthogonal to the transect orientation as in 1D models. The space between each node then functions as a prism with predictions of hydraulic habitat generated for each one. The advantages of these modelling packages are several, including: 1) finer-scale estimates of hydraulic conditions, directly comparable to the empirical measurements used to build the HSIs; 2) the ability to model multiple flow pathways, with the elevations of the waterlines not always being equal (e.g., a perched side channel in a braided reach); 3) ability to assign frictional resistance values to individual cells rather than the entire transect; and 4) typically greater accuracy at predicting hydraulic conditions at extremely small or large discharges when flow patterns become more complex due to increased interaction with either the channel bed at small flows or contact with debris and vegetation along the banks and floodplains.

However, 2D models are also not without disadvantages, most of which relate to the resources required to generate and successfully calibrate the models. First, the models require a fully continuous digital elevation model (DEM) of the study reach, with each survey point in the DEM becoming a node in the hydraulic model. This requires field surveys to sample the latitude, longitude, and elevation at each point along a grid, with a minimum point density of 1 m x 1 m, preferably tighter, that comprises the entire channel and immediate flood zones (Gibson and Pasternack, 2016). Traditionally, instream measurements of these data would be done with an RTK-GPS, and occasionally with the addition of a Total Station when resources allow precision and accuracy to be prioritized. However, this procedure is very labour intensive and costly, often limiting the study reach to 300 m or less in length (Winterhault, 2013). Additionally, if field crews are unable to survey a location due to issues with access or safety or because there is no GPS signal, a 2D hydraulic model will simply treat those sections as blank spots in the DEM. Interpolation is therefore required, as is the case with 1D and 1.5D models.

Gard (2009) compared the accuracy and precision of 1D hydraulic models, generated with PHABSIM, against 2D models created with River2D for a study reach on the Merced River, California. What Gard (2009) found was that in four out of five cases, both the 1D and 2D models achieved sufficient accuracy and precision in replicating field measurements of channel hydraulics. However, in an earlier study, Gard (2005) concluded that where channel morphology and flow patterns are complex, the use of 2D hydraulic models should be favoured, despite the increased cost.

Gibson and Pasternack (2016) similarly conducted a comparison between a laterally distributed 1D model and 2D models for the Lower Yuba River, California. This study found that while 2D modelling was more accurate and precise, the advantages were not significant enough to warrant the full transition to 2D modelling at the present. The decision about which approach to follow should be informed by the available budget and project objectives (Gibson, 2013; Gibson and Pasternack, 2016). Hence, the majority of IFIM assessments continue to be conducted with either 1D or preferably 1.5D hydraulic models (Gibson and Pasternack, 2016).

#### **2.2.4 UAV-Supplementation of Channel Surveys**

As has been noted, logistical challenges with data collection remain the greatest source of uncertainty in IFIM-type habitat assessments. However, recent developments in the application of remote sensing techniques to supplement traditional methodologies for data collection are showing potential for improvement in the efficiency of stream channel surveys.

The use of unmanned aerial vehicles (UAV) to acquire structure-from-motion multi-view stereo (SfM-MVS) photogrammetry has been emerging during the past two decades as a cost-effective supplement to traditional ground-based topographical surveys (Marcus and Fonstad, 2008; Fonstad *et al.*, 2013; Tamminga, 2016; Shintani and Fonstad, 2017; Wheaton *et al.*, 2017; Benjankar *et al.*, 2018; Lane *et al.*, 2020; Conesa-García *et al.*, 2020). Using an orthographic photo composite generated from a series of aerial images, which are georeferenced from both the point of image capture (i.e., location of the aircraft) and with a series of control points on the ground, SfM software packages assign each pixel a full 3D coordinate set (latitude, longitude, and elevation) (Carrivick *et al.*, 2016; James *et al.*, 2019). The coordinates from each pixel are then used to generate a DEM and can be combined with the orthographic photo to create a three-

dimensional model of a study site.

Modellers have the option to either extract transects from any location in the DEM for a 1D hydraulic model or potentially use the entire DEM for 2D modelling exercises. While DEMs of the same nature have been sampled in the past using Total Stations on the ground, the significant change with the UAV-based SfM approach is reduced field effort and increased coverage (Tamminga 2016).

For a UAV-based survey, data collection in the field typically encompasses: 1) a series of flights with the UAV to collect the aerial images; 2) a survey with an RTK-GPS of selected ground control points, and 3) two or more transect surveys with a wading rod and flow meter to measure discharge during the flight period for hydraulic model calibration. For study reaches shorter than a kilometre, this can often be accomplished by a crew of three members in as little time as one day. The primary factors that will limit the length of the study reach are a clear line of sight from the drone to the spotter, clear GPS signal, instrument failure, the number of batteries available to power instruments in remote locations, and inclement weather. In comparison, a very large field crew (greater than five) would be needed to sample a study reach at the recommended transect density (e.g., greater than 15 transects per km) within one day or to establish a robust DEM with a total station and RTK-GPS (MacParland *et al.*, 2014; Winterhault, 2015; Richardson, 2019; Hettrich 2020, Gronsdahl *et al.*, 2021).

By reducing the field time to one day for a complete survey, including DEM and hydraulic parameters, the UAV-SfM approach has great potential to increase the density of transects, thereby reducing uncertainty in habitat estimates, as well as allowing for surveys to be repeated on multiple dates, again reducing uncertainty and providing some temporal monitoring of habitat shifts.

Airborne Light Detection and Ranging (LiDAR) systems have also been deployed in the same capacity to remotely sample elevations, often with gains in accuracy or precision over the photogrammetric approach. However, at the present, the costs of the LiDAR equipment and the drone platforms to support it are significantly more than what is required for a photogrammetric survey. LiDAR, therefore, remains outside the budgetary constraints that most studies can afford (Carbonneau and Piégay 2012, Biron *et al.* 2013, Tamminga 2016).

The UAV-SfM approach is not faultless, as the accuracy and precision of SfM DEMs have been a focus of significant study during the past decade (Carbonneau and, Piégay 2012; Biron *et al.*, 2013; Woodget *et al.*, 2014; Tamminga, 2016; Dietrich, 2016; Lane *et al.*, 2020). The root cause of this relates to the derivation of elevation because it is based on the behaviour of light observed in the camera sensor, which is due to the natural variability of light. Early usage in fluvial settings focused on the application of photogrammetry to generate 3D models of channel features such as banks, gravel bars and pools from static images photographed at ground level (Pyle *et al.*, 1997; Carbonneau *et al.*, 2001). The purpose of generating these models was to develop a cost-effective tool for assessing the change in channel morphology, such as volume lost to bank erosion or the gains and losses of gravel bar area over a season (Pyle *et al.*, 1997; Carbonneau *et al.*, 2001; Carbonneau and Piégay, 2012; Shintani and Fonstad, 2017).

While these studies found photogrammetric analysis to be an effective tool for measuring morphometric features, with model accuracies for point distances within 12 mm of true values (Pyle *et al.*, 1997; Carbonneau *et al.*, 2001), the use of UAVs for image collection, combined with the application of photogrammetric techniques to survey channel bathymetry was not heavily explored upon until the mid-2010s (Carbonneau and Piégay, 2012). Woodget *et al.* (2014) applied the UAV-SfM approach to derive three-dimensional models of two separate study reaches in the UK. Each reach was no more than 100 m in length and flow depths did not exceed 0.7 m, but the error associated with the photogrammetric derivations of bathymetry did not exceed 0.089 m, which was reduced to 0.053 m after applying a refraction index correction proposed by Jerlov (1976).

Tamminga (2016) investigated the potential of the UAV-SfM for assessing the hydraulic habitat potential for Salmonids (specifically *Salmo trutta*) on a 1 km reach of the Elbow River in Southern Alberta, Canada. Comparing the photogrammetric derived elevations against 297 ground control points, the mean-square error after applying the Jerlov (1976) refraction index correction and a spectral correction was 0.088 m for points above water and 0.119 m for submerged points (Tamminga 2016). After the DEM was processed in River2D, model depths had a mean error of -0.004 m and an absolute maximum error of 0.5 m at a real depth of 0.98 m. The root-square-mean-error (RSME) and standard deviation (SDE) were 0.125 m (Tamminga, 2016). The hydraulic outputs from this model were then processed with an HSI in combination

with substrate and large woody debris mapping to predict Trout habitat. Tamminga (2016) concluded that employing photogrammetrically sourced DEMs to operate hydraulic models was an efficient, economical, and reliable way to assess stream habitat.

Working on a ~250 m reach of the White River Idaho, Dietrich (2016) tested the effectiveness of different refraction indexes (both site-specific calibrations and Jerlov's), with class riffle-pool sequences and depths between 0 -1.5 m. The objective of this was to test an "iterative approach that calculates a series of refraction correction equations for every point/camera combination in an SfM point cloud". With data from two flights, over nine months apart, SfM photogrammetric errors after correction were found to have a mean of -0.011-0.014 m, SDE between 0.077-0.059 m, an RMSE between 0.003-0.006 m, maximum errors of 0.291-0.381 m. Unique to this study, Dietrich (2016) took the height of the UAV into account and relative to the positions of the camera sensor, accuracy (mean error) was with 0.02% of height above ground and the precision in DEM was 0.1% of the flying height.

More recently, Lane *et al.* (2020) applied the UAV-SfM approach to characterize the hydraulics and morphology of the Turtmännna River in the Swiss Alps, for modelling sediment transport in response to the management flows from an upstream hydro dam. The study reach was a 300 m long braided reach typical of a high alpine gravel-bed stream. This study was unique in that it combined the photogrammetric surveys with the traditional data collection method including long-term turbidity monitoring and select Wolman Pebble Counts to create a model of in-channel hydraulics and sediment transport that was robust being rich in both spatial and temporal data. Lane *et al.* (2020) concluded that it was only when using both datasets in conjunction that the confidence in the results was maximized, with each methodology helping overcome the shortcomings of the other.

Despite the excellent results from the previous studies, there were significant doubts about the UAV-SfM approach in terms of which environments its application is feasible. All the studies previously cited, conducted the UAV flights over study reaches that were shallow (most less than 1 m deep), had clear water with little tannins, limited rough water (i.e., riffles and rapids) and were completely clear of overhead obstructions (e.g., riparian vegetation or log jams). While ideal, this was a concern because deeper flows and a healthy riparian zone with some overhead

cover combined with LWD are all features associated with the most productive habitat zones for Salmonids.

One of the few studies to evaluate the effectiveness of SfM photogrammetry for surveying channel morphology in such conditions was by Shintani and Fonstad (2017). The study site was a 140 m riffle-pool sequence on the Lower Salmon River, Oregon with such optical challenges as large riffle zones and some shading from bank vegetation. The purpose of the study was to compare the effectiveness of the SfM approach against the spectral depth approach for deriving estimates of channel bathymetry. For a quick context, the spectral depth approach utilizes regressions that match in-field measurements of the flow depth to specific spectral bands (i.e., colour), to extrapolate and map flow depths for each pixel that intersects the stream channel in an orthographic photo.

The conclusions were that the SfM approach was the most accurate of the two methods, and similar to Dietrich (2016), using a site-specific index to correct for refraction provided the best results instead of Jerlov's index of 1.34. While the mean error of the photogrammetric approach was small and comparable to previous results at 0.009 m, the optical challenges were apparent in reducing the precision, with the standard deviation increasing to 0.17 m and the  $R^2 = 0.67$ , compared to values of 0.82-0.9 m previously (Tamminga, 2016; Dietrich, 2016).

The results of Shintani and Fonstad (2017) suggest that while the application of UAV and SfM techniques to survey channel bathymetry has a promising future, there are still significant gaps in our understanding of how these techniques will perform in challenging environments typical of many watersheds in the Pacific Northwest. This is especially significant because often these same environmental conditions have constrained traditional surveys in vital Salmonid habitats, and any gains in the number and scale of assessments being conducted would have a significant net impact. Thus, the objective of this study is to evaluate how well UAV-sourced imagery and SfM photogrammetry can be used to supplement traditional IFIM surveys of Salmonid habitat in the mountainous terrain of the Southern BC Interior, which remains a worthwhile undertaking.

## Chapter 3 . Methods

### 3.1 Study Site

The study site was located on Upper Mission Creek in the Southern Interior of British Columbia (Figure 3.1). Mission Creek headwaters off the Graystokes Plateau 33 km due east of Kelowna and is the primary tributary to Okanagan Lake.

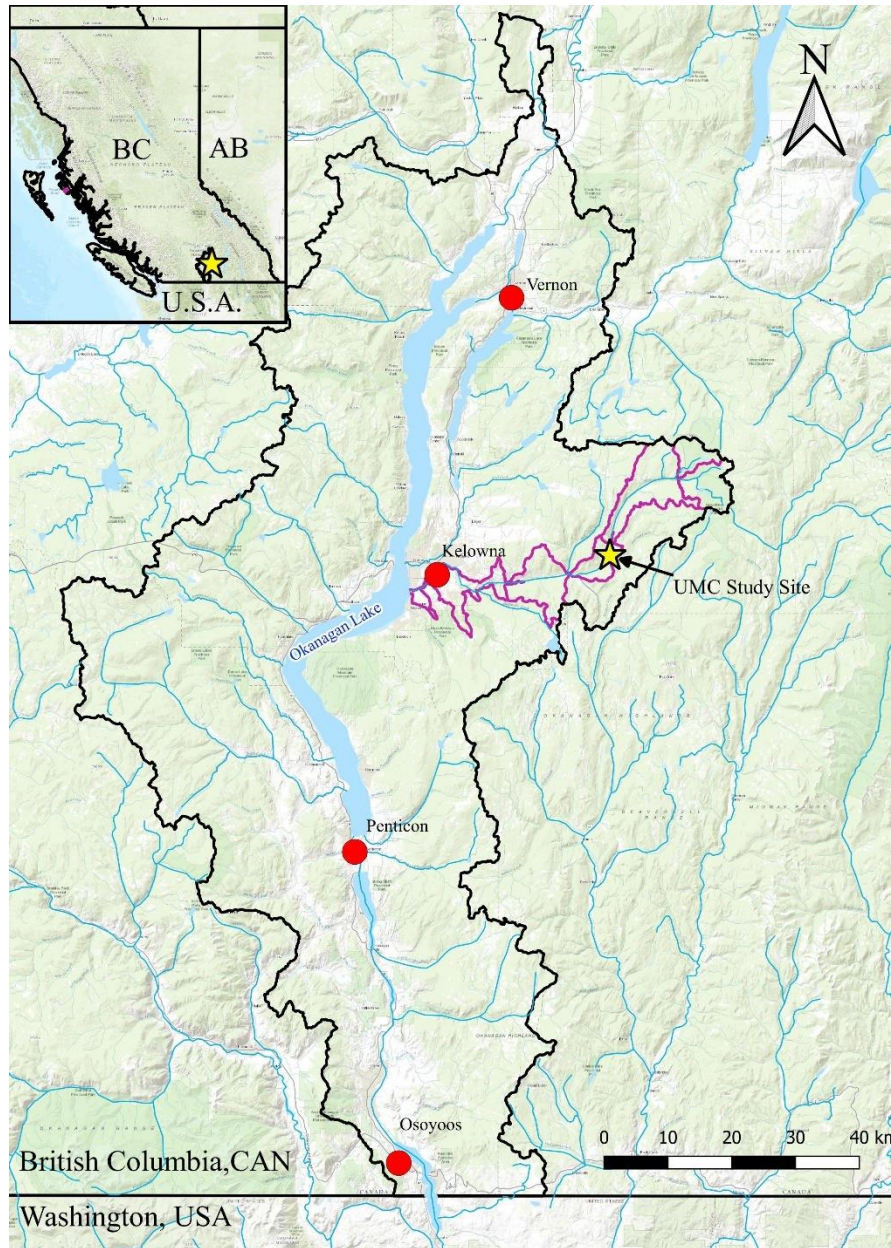


*Figure 3.1 Location of study reach, within the Mission Creek (pink outline) and Okanagan Watersheds (black outline) of the Southern Interior of British Columbia.*

The experimental reach was a 780 m stretch of Mission Creek between  $49^{\circ} 53' 19''$  W  $119^{\circ} 03' 51''$  N and  $49^{\circ} 53' 37''$  W  $119^{\circ} 03' 37''$  N, at an average elevation of 930 m above sea level. The reach is located immediately upstream of the Graystokes Forest Service Road (FSR) bridge crossing and  $\sim 100$  m upstream of the confluence with Pearson Creek (Figure 3.2).



*Figure 3.2 Orthophoto of the study reach on Upper Mission Creek, taken Sept 30th, 2019.*

This site was chosen for four key reasons: 1) human development in the study area is minimal, aside from cattle ranching and limited timber harvesting, with the riparian vegetation largely undisturbed; 2) the reach morphology varies between anabranching and braided with channel stability being variable, providing morphological complexity (Figure 3.2); 3) the average slope of the channel is 0.016 or 1.6% which is an order of magnitude greater than streams in the valley bottom, but still well within the slope preferences of many salmonids, and 4) the aerial visibility of the channel is excellent in comparison to many other watersheds in the region but still comparable to many streams of a similar size in the BC Interior.

The resident population of Rainbow Trout (*Oncorhynchus mykiss*) was chosen as the species of

interest for this study because it is the only salmonid present in the watershed upstream of Gallagher's Falls. Within that population, juvenile Rainbow Trout during the summer rearing stage were selected as the specific life-stage of interest for assessments of hydraulic habitat available, as observations of trout during early reconnaissance surveys were almost entirely of this age group (Figure 3.3).



*Figure 3.3 A juvenile Rainbow Trout (Oncorhynchus mykiss) observed within the study reach, July 13th, 2019.*

## **3.2 Field Data Collection**

### **3.2.1 Topographical Surveys**

The topography of the channel was surveyed at 30 transects along the 780 m study reach. Of these 30 transects, 27 were in the main channel at locations where either a key habitat feature was present (e.g., a pool) or the geometry of the channel significantly changed (e.g., the slope became noticeably steeper, or the curvature of the channel changed). The objective was to characterize key features of the channel and keep distances between transects to less than 30 m whenever possible, following guidelines for best practices in hydraulic modelling (HEC-RAS

2019) and implementation of IFIM (Lewis *et al.*, 2004). The average interval between transects was 28.9 m, yielding a relative sampling density of ~34 transects per km. In a few instances, the distance between transects exceeded the 30 m recommendation to bypass areas where channel morphology was dominated by long sets of shallow braids (mean depth < 0.1 m) and perched channels. These zones were not surveyed and excluded from the hydraulic model for three reasons: 1) HEC-RAS recommends exclusion of areas where challenges in reliably modelling channel hydraulics can be assumed; 2) the flow depth was often insufficient for accurate measurements of in-channel flow velocity with a flow meter and wading rod, and 3) the habitat function of these units for juvenile Rainbow Trout was most often limited to the short-term passage and for the production of invertebrate prey.

The three remaining transects were established across the entry into back channels (Figure 3.4). While expected to be of limited habitat value, these small back channels were surveyed to assist with estimating changes in discharge in the main channel between transects to ensure the accuracy of the hydraulic models.



*Figure 3.4 Transect A, looking at downstream side-channel A at its uppermost extent, near the main channel junction at transect 18 (Aug. 1st, 2019).*

Once a location for a transect was decided upon, the outer bounds of the cross-section were monumented on the left and right banks with rebar pins. A tape measure was strung tautly between the pins perpendicular to the direction of the thalweg, and the topography of the channel was sampled following standard surveying conventions, utilizing an engineer's level, tripod, and stadia rod (Figure 3.5). A minimum of 20 points per transect were taken in the wetted area with additional points characterizing the banks. For the bank areas above the current water level, the emphasis was on sampling points of geomorphic significance, such as a break in slope or the high-water mark (if discernable). Within the wetted area of the main channel, survey points were taken at fixed intervals (0.5 m) because verbal communication between team members could be challenging because of white-water noise at steeper transects and at larger discharges. Team members would regularly check in at regular intervals utilizing both verbal communication and hand signals to confirm the status of the survey.



*Figure 3.5 A topographical survey following the standard surveying convention, transect 20, July 20th, 2019.*

### **3.2.2 Georeferencing**

All rebar pins delineating the transects were georeferenced using a Topcon GR5 Real-Time Kinematic Digital Global Positioning System (RTK-DGPS). Both the top of the pin as well as the ground at the base of the pin were surveyed. In addition, a semi-permanent benchmark pin was

positioned on a wide-open gravel bar located near transects 13-16, and it was used as a common reference for positioning of the base station during all field visits (Figure 3.6). This location was chosen as it had the optimal line of communication between the base station and rover at all transects.

Data from the RTK-DGPS was post-processed using the Natural Resources Canada, CSRS-PPP direct online application (NRCAN, 2019) and plotted on Google Earth for confirmation of horizontal coordinates. NAD83 (CSRS)(2019) and CGVD2013 (CGG2013a) were chosen as the horizontal and vertical datums, respectively. Quality control on rebar elevation estimates from the RTK-DGPS survey was performed using data from the engineer's level to verify the relative elevation differences between various pairs of neighbouring pins (see Section 3.3.1).



*Figure 3.6 Location of the RTK - DGPS base station and drone lunch pad (Green Cross), within the UMC study reach.*



Figure 3.7 Ground level photo of the RTK -DGPS base station and drone lunch pad, at the gravel bar mid-reach, between transects 14-16 (August 13th, 2019).

### 3.2.3 Instream Flow Measurements

Following the topographical surveys, the transects were reoccupied over a two-day interval to sample the in-channel hydraulics and characterize the substrate. The flow rate exceeded 40% mean annual discharge (MAD) as recommended by Lewis *et al.* (2004) during this sampling period.

For each transect, the depth and mean velocity of the flow was measured at each survey point. Mean flow velocity was measured using a portable electromagnetic flowmeter (Marsh McBirney Flow Mate) mounted on a wading rod at 0.6 of depth below the surface, over a 30-second interval, as is the standard convention for single-point measurements of average flow conditions (Lewis *et al.* 2004).

Estimates of water surface elevations at each transect were generated twice utilizing different techniques. The primary method combined the topographic profiles at each transect with the water depths taken at every point along the transect during the flow velocity measurements to

generate a series of water elevations that defined the water surface during the sampling period. The average water surface elevation for each transect was then calculated. The water surface slope at each transect was estimated using water surface elevations from upstream and downstream transects.

The second method for estimating water surface elevation was from direct measurement of the waterlines on the left and right banks using an engineer's level and standard surveying techniques. These measurements were performed earlier in the experimental period when flow discharge was above 40% MAD. The discharge was measured twice during this water surface elevation survey, once at the downstream end of the study reach (transect 4) in the morning and then later in the day at the upper end (transect 25). In both cases, the discharge was sampled at glides.

The channel substrate was also characterized at each sample point while taking the flow velocity measurements. A visual assessment was made of the relative percentages of each sediment size class (i.e., cobble-boulder, gravel, sand, silt-clay) following the Wentworth nomenclature as described by Lewis *et al.* (2004), within a  $\sim 0.25$  m radius of the sample point.

### **3.2.4 Drone Flights**

Three drone flights were conducted between late July and late September 2019. The drone was flown by a certified pilot, following Transport Canada Guidelines (Transport Canada 2021) for basic operations, noting that the study site is outside classified airspaces. The drone employed was a DJI PHANTOM™ 4 RTK, with a horizontal position accuracy of  $\pm 1$  cm, a vertical position accuracy of  $\pm 1.5$  cm, and absolute horizontal accuracy in associated photogrammetric models of  $\pm 5$  cm when flying at or below 100 m in sunny conditions (DJI, 2018).

The first two flights served as preliminary tests of flight paths, camera settings, visibility of ground control markers, and line-of-sight communication between the drone and base-station setup at the benchmark.

In setting up the flight paths, the first test flight attempted (July 25<sup>th</sup>, 2019) to fly a total of four flight paths, with the drone utilizing the onboard RTK-DGPS to automatically adjust its flying elevation at a constant  $\sim 30$  m above the ground. However, this combination had two key issues.

The first was that with the elevation of the drone being auto-adjusted by interval systems, the sensitivity of the onboard safety mechanisms seemed to increase as a precaution. This in turn resulted in the collision avoidance systems engaging multiple times and the drone automatically returning to the base station, despite the spotters visible observing ten or more metres of spacing between the drone and forest canopy below. Combined, with the greater number of flight paths, this resulted in the excessive use of battery power, with all spare batteries needing to be utilized. Steps were then taken in the second test flight (August 14<sup>th</sup>, 2019) to reduce the flight paths to three and set the flying to a fixed elevation, to avoid engaging the collision avoidance systems and maintain battery life. These goals were successfully achieved, and a quick check of the processed DEM later confirmed that despite the relative distance of the ground and drone, changing significantly throughout the reach, no noticeable trends were introduced in the error, with overexposure and rover communication at specific ground control markers remaining the only observed source of error at this point.

The high albedo of the exposed gravel bars, combined with the prevalence of white water, washed out the images when working in sunny conditions near noon. Adjustments were made before the final flight with the application of a polarized lens filter to the camera and the installation of higher contrast ground control markers (Figure 3.8).



*Figure 3.8 Examples of ground control markers deployed in the field, including the initial test markers (left) used for the July 25h and Aug. 14th test flight, as well as the high contrast markers (right) employed on the final Sept. 30th flight.*

The third and final flight was flown on September 30<sup>th</sup>, 2019, with the drone flying a total of

three flight paths at a fixed elevation (958 m) corresponding to an average height above ground of approximately 29 m for three flight paths. A total of 15 high contrast ground control markers were utilized and surveyed by RTK-DGPS during the Sept. 30<sup>th</sup> flight.

Images and positional data from Sept. 30<sup>th</sup> were then processed following the Structure-from-Motion (SfM) approach using the software package Pix4D (PIX 4D 2021) to generate both the high-resolution orthographic photo and photogrammetric digital elevation model (DEM) of the study reach. The final resolution for both the orthographic photo and DEM is 1.6 cm<sup>2</sup> per pixel.

### **3.3 Data quality control**

#### **3.3.1 Survey Data**

The first quality control step for the topographic survey data was to compare the engineer's level survey results to the GPS survey results. Four metrics were used to identify errors and to assess the overall quality and reliability: 1) horizontal distance across the transect from pin to pin; 2) absolute elevation of rebar markers; 3) the relative difference in elevation between left bank and right bank markers, and 4) elevation of the mean waterline for the same date at each transect.

These four criteria were chosen because of how well they characterize the variance between the engineer's level and GPS surveys at the same transects. Specifically, the GPS provides absolute coordinates in XYZ space relative to a national reference frame (e.g., NAD83, CGVD 2013), whereas the engineer's level provides relative height and distance from an arbitrary set-up point for each transect. Ties between transects and, ultimately, the tie to the benchmark pin located on the gravel bar allow for referencing to NAD83 if the true location of the benchmark pin is known (or measured via GPS). Nevertheless, both methods are prone to uncertainty and error. The engineer's survey is susceptible to human errors associated with accurate levelling of the instrument after each re-positioning of the level along the study reach. Small errors in levelling the instrument to a 'perfect bubble' yield progressively larger errors in height measurements at increasing distances from the instrument. These can be recognized as a consistent bias rather than random errors. Additional errors occur when numbers are miscommunicated, misread, or transcribed incorrectly. In contrast, errors in the GPS measurement arise when there is a poor signal from satellites due to vegetation canopies and unsteadiness in the rod position. Most rebar pins were in areas where the satellite signals allowed for 'locked-in' positions as indicated by

sequential measurements within predefined uncertainty bounds, but a few of the pins were beneath vegetation canopies where strong signals were not possible.

### **3.3.2 Photogrammetric Data**

Photogrammetric transects were extracted from the DEM of the study reach using the Global Mapper GIS Software package (Blue Marble Geographics, 2022). Cut lines were created using the path tool by tracing across every surveyed transect between the GPS coordinates for each pair of bank marker (rebar) pins. Along each of these cut lines, elevation was extracted for 1025 points (the default setting). Rather than extract elevation along a path that was one pixel in width (the default setting), a spatial sampling approach was adopted that extracted the minimum bed elevation over a 0.1 m wide band centred on the transect line. This approach accommodates the uncertainty in horizontal distance associated with the placement of a stadia rod or rover rod during the survey as well as the likely differences in horizontal positions between the engineer's level and GPS surveys, which were conducted on different days. Since the average size of the substrate material was also of the order of 0.1 m, it is entirely reasonable to expect that the rod holder may have placed the rod in a position that was not precisely where the photogrammetric transect was located.

The decision to sample the minimum elevation (rather than the maximum or average elevation) at each point along the band was made after preliminary tests using the mean elevation produced topographic profiles with large errors at steeper transects associated with riffles and rapids where large cobbles and boulders exist (e.g., transect 6). The prevalence of white water and the associated refraction at these locations also influenced the quality of penetration into the water column. Qualitative comparisons of channel bathymetry profiles sampled using the minimum elevation along with the 0.1 m band produced channel geometries similar to those sampled by the engineer's level, so this approach was adopted without further refinement.

The industry standard refraction index (Jerlov 1976), which multiplies depth estimates by 1.34, was applied during the initial stages of analysis, however, this index was developed for clear, tannin-free streams (Shintani and Fonstad 2017), which is not the case for Upper Mission Creek. Application of the index yielded unacceptably greater flow depths than in field measurements (e.g., increased depths by 15-30 cm), and it was not adopted in the final analyses.

To validate the accuracy of the photogrammetric DEM cut lines, the elevations of ~ 900 sampling points common to both photogrammetric and engineer's surveys were compared. The results from this analysis were then summarized following the standardized procedures in Carrvick *et al.* (2016) and James *et al.* (2019). This included reporting on the: mean error (ME), median error (MDE), coefficient of determination ( $R^2$ ), mean absolute error (MAE), the standard deviation of error (SDE), and root-mean-square error (RSME) in the residuals between the measured and modelled elevations.

The final step in the preparation of the photogrammetric transects was to reduce the number of sampling points by one-half (i.e., every second point). This was necessary because the maximum number of points that HEC-RAS 5.0.7 can accommodate in a single transect is 515.

### **3.3.3 Channel Hydraulics**

The general accuracy and precision of instream hydraulic measurement were evaluated using two different criteria.

The first was an evaluation of in-field measurements of flow depth, which was done by comparing the depth profiles produced by the engineer's level surveys against those from the wading rod surveys at each transect. This was accomplished by first converting elevation points from the engineer's level into estimates of 'assumed depth', for the same date as the wading rod survey to ensure a direct comparison.

Assumed depth, was simply calculated by subtracting the elevation of the channel bed from the transect mean water-surface elevation on the survey date (e.g., Aug 14<sup>th</sup>) for each sampling point. In principle, the values for measured flow depth and assumed flow depth at each point should be identical; however, some error in sampling the same points was expected due to factors such as replicating the same tension in the tape measure for both survey and slight differences in the base profile of the stadia and wading being slightly off. Discrepancies between the two sets of flow depth estimates were evaluated at each transect based on the mean, median, standard deviation and maximum absolute error.

With the measurements of flow depth evaluated with confidence, the general quality of flow velocity measurements was assessed. Without a secondary set of velocity measurements, this

was done through an indirect evaluation of discharge measurements. To do so in-field measurements of discharge for each survey date were validated against discharges recorded downstream at the East Kelowna station, checking that the discrepancies between locations closely matched the historical differences between the East Kelowna station and the historical hydrometric station (station 08NM233 previously located that study site), now inactive. With discharge calculations being a product of flow depth and velocity estimates, if the flow depths and discharge measures were validated, it, therefore, can be assumed that the velocity measurements were also reasonably accurate.

### **3.3.4 HEC-RAS Modeling**

The Hydraulic Engineering Center River Analysis System (HEC-RAS), produced by the US Army Corps of Engineers, was used in this study to estimate transect-specific flow parameters. HEC-RAS was chosen because: 1) it is freely available; 2) has been tested extensively and is used broadly by professionals; 3) is supported by extensive documentation, including user manuals and user-group forums; 4) is functional on a laptop computer or PC; 5) has a GIS-like mapping module; and 6) has a broad range of modules for hydraulic modelling including one-dimensional steady flow analysis, one- and two-dimensional unsteady flow analysis, sediment transport-mobile bed modelling, and water quality analysis (HEC-RAS, 2021). To estimate habitat conditions in this study, only the one-dimensional steady flow analysis was used. Conducting a 2D hydraulic unsteady analysis was ruled out as it requires a fully continuous DEM of the channel bathymetry to generate reliable results, which was assessed as not being viable due to the prevalence of overhead riparian cover and channel spanning large woody debris (LWD).

## **3.4 Experimental Design**

The purpose of the research was to determine whether information obtained from photogrammetric methods could be used reliably to improve the assessment of habitat conditions in salmonid-bearing streams. A strategy was devised to incrementally remove measured transect information from the HEC-RAS model of the study reach and replace it with information obtained from the DEM. Each step required a different hydraulic model, so a large number of hydraulic models had to be created using different combinations of measured field data and extracted photogrammetric data. The results were then used to assess habitat conditions for each simulation to address the level of uncertainty associated with different combinations of measured

and extracted transects.

### 3.4.1 Hydraulic Modelling

In total, twenty 1-D hydraulic models were created with different combinations of surveyed and photogrammetric transects (Table 3.1). Estimates of the transect-specific averages for flow velocity, hydraulic radius, Froude number, and wetted width at each transect were extracted for 40 discharge events between 0.5 - 20 m<sup>3</sup> s<sup>-1</sup> (at 0.5 m<sup>3</sup> s<sup>-1</sup> intervals).

*Table 3.1 Summary of the number and combinations of surveyed and photogrammetric transects included in each scenario for the hydraulic models.*

Scenario	Sampling Interval for Surveyed Transects	Number of Surveyed Transects	Number of Photogrammetric Transects	Distribution of Transects Incorporated
<b>'Best-Practices' Scenario</b>				
0	Every transect	27	0	1,2,3,4,5,6,7...27
<b>Reduced Scenarios</b>				
1 – A	Every 2 <sup>nd</sup> transect	13-14	0	i.1,3,5,7,9...27
				ii.2,4,6,8, 10...26
2 – A	Every 3 <sup>rd</sup> transect	9	0	i.1,4,7, 10...
				ii. 2,5,8, 10...
				iii.3,6,9, 12...
3 – A	Every 4 <sup>th</sup> transect	5-6	0	i. 1,5,10,15,20, 25
				ii. 2,6,11,16,21,26
				iii.3,7,12,17,22,2
				iv. 4,11,13,18,23
<b>Supplemented Scenarios</b>				
1 – B	Every 2 <sup>nd</sup> transect	13-14	13-14	1,2,3,4,5,6, 7...27
2 – B	Every 3 <sup>rd</sup> transect	9	18	
3 – B	Every 4 <sup>th</sup> transect	5-6	21-22	
<b>Photogrammetric Scenario</b>				
4	No surveyed transects	0	27	1,2,3,4,5,6,7...27
<b>Number of Traditional Models</b>				<b>10</b>
<b>Number of Supplemented Models</b>				<b>10</b>
<b>Total Number of Models</b>				<b>20</b>

The first of these HEC-RAS models was developed around a 'Best-Practices' scenario that includes all 27 surveyed transects in the hydraulic model with no supplementation of photogrammetric transects (Table 3.1, Figure 3.10). The calibration process for this model involved adjusting the Manning's n friction factor, and occasionally the contraction/expansion

factors at each transect in a repetitive trial and error approach, until the elevation of the modelled water surface matched, as closely as possible, the measured elevation in the field for a given discharge. The measurements of water surface elevation and discharge used to calibrate the HEC-RAS models were derived from the two wading rod surveys (Aug. 14<sup>th</sup> and 24<sup>th</sup>) and not from the additional engineer's level survey on Aug. 15<sup>th</sup>, 2019.

The field measurements were conducted over several different days with different discharges. Thus, groups of transects with similar discharges were considered separately during model calibration. The total number of steady flow simulations doubled because of the need to calibrate the model to two different sets of boundary conditions. The first set utilized a boundary condition for known elevation of the water surface at the upper and lowermost transects in the reach (transect 27 and 1) for the measured discharge; whereas, the second set utilized the normal depth boundary condition based on the local thalweg slope at transects 1 and 27. This two-step process of calibrating the model was done to ensure that the model was robust and capable of handling both smaller discharges, similar to the conditions during calibration, and larger discharge events that proved unsafe to survey. All simulations for the steady flow analyses assumed mixed flow conditions, with both super-critical and sub-critical flows potentially present, due to the morphological variability and the steep gradient of the reach. This scenario with all 27 measured transects incorporated into the model is referred to as the 'Best-Practices' scenario or Scenario 0.



Figure 3.9 Map showing the distribution of transects across the study reach for the 'Best-Practices' scenario' (Scenario 0).

To evaluate how predictions of overall channel hydraulics and habitat might be influenced by the number of measured transects included in the model, nine additional models were created, each with smaller and smaller numbers of transects based on decreasing the measured transect spacing so that every second, third, and fourth transects were incorporated in the model in sequential models. Because there are potentially different ‘starting’ transects, several scenarios for each spacing are possible. For example, if every third transect is included, the starting transect could be 1, 2, or 3, leading to a different combination of transects included in each of the three models (Table 3.1). This strategy was adopted to mimic situations where time and resources for conducting detailed surveys are limited. With each increase in the scenario designation (i.e. Scenario 0 →1) the sampling interval (spacing) between transects increases by one, to a maximum of four by Scenario 3. Accordingly, the number of measured transects incorporated into the model drops from 27 for Scenario 0 to 5 for Scenario 3 (Table 3.1).

Scenario 1 is comprised of two HEC-RAS models, each representing a different combination of transects with a fixed sampling interval of two for a total of 13-14 surveyed transects depending on the starting transect. For transect 1 as the starting transect (Model 1Ai), the sequence of transects included is 1, 3, 5, 7, ... whereas for transect 2 as the starting transect (Model 1Aii) the sequence is 2, 4, 6, 8, and so on. Scenario 2 comprises three models at a sample interval of three with nine transects in each model, whereas Scenario 3 is a collection of 4 models with an interval of four leading to either 5 or 6 transects incorporated in the model.

In each model, discharges and calibration parameters were unchanged from the ‘Best-Practices’ scenario to facilitate direct comparisons (i.e., no re-calibration of the model was performed). It was thought that the ‘Best-Practices’ scenario, with the greatest number of transects, was the best representation of the actual flow conditions in the study reach with optimized values for bed roughness parameterization due to the model calibration process.

For scenarios 1 to 3, the models with only a few measured transects were duplicated and additional transects derived from the photogrammetric DEM were added to create a secondary model. The photogrammetric transects were extracted and inserted in precisely the same positions as the surveyed transects that had been previously removed in the progression from scenario 0, thereby restoring the total number of transects in each model to 27 (see example in

Figure 3.11). Scenario 3, therefore, had the largest proportion of photogrammetric transects (i.e., 22 extracted versus 5 measured). This allowed for an assessment of whether the supplementation of photogrammetric transects improves or degrades the accuracy of hydraulic models in terms of reproducing the results of the ‘Best-Practices’ scenario. The secondary models supplemented with photogrammetric transects were designated with a B in labelling, and models with only surveyed transects were designated with an A (Table 3.1 and Figure 3.12). A final model using only transects extracted from the DEM, with no measured transects, was also created (Scenario 4).

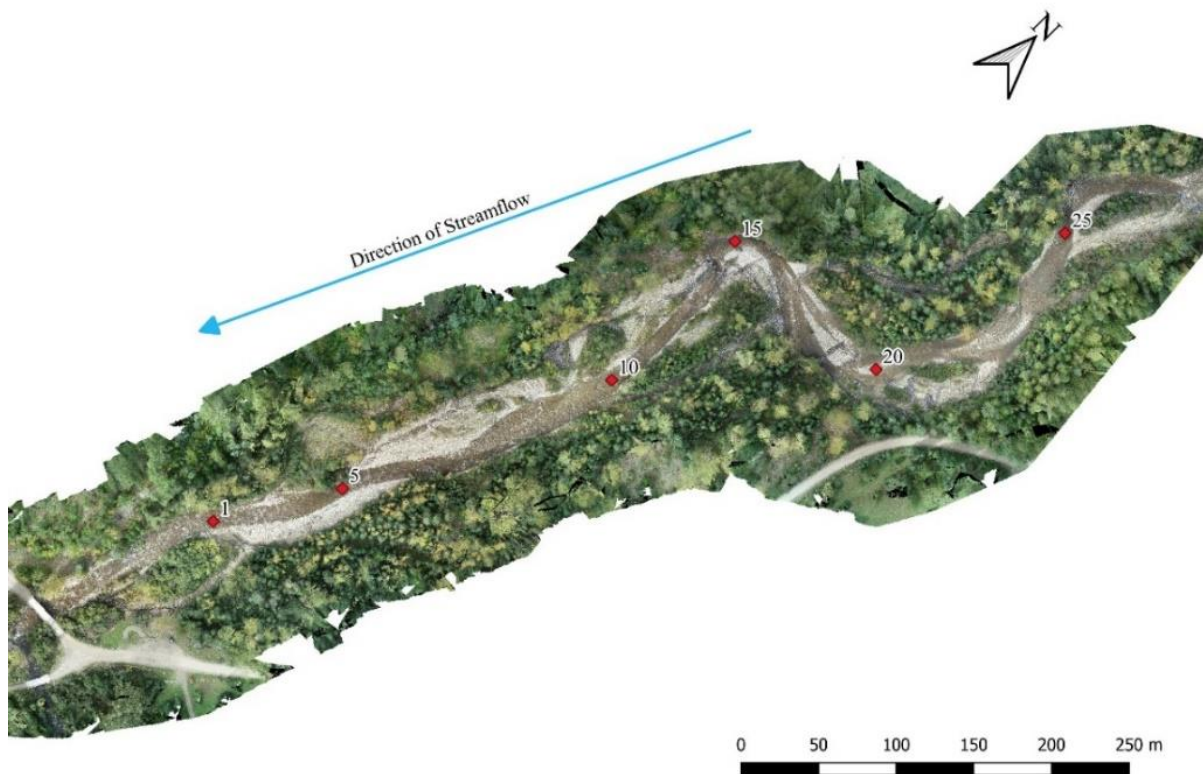


*Figure 3.10 A map showing the distribution of transects for the reduced model, Model 3Ai with only 5 surveyed transects incorporated into the model.*

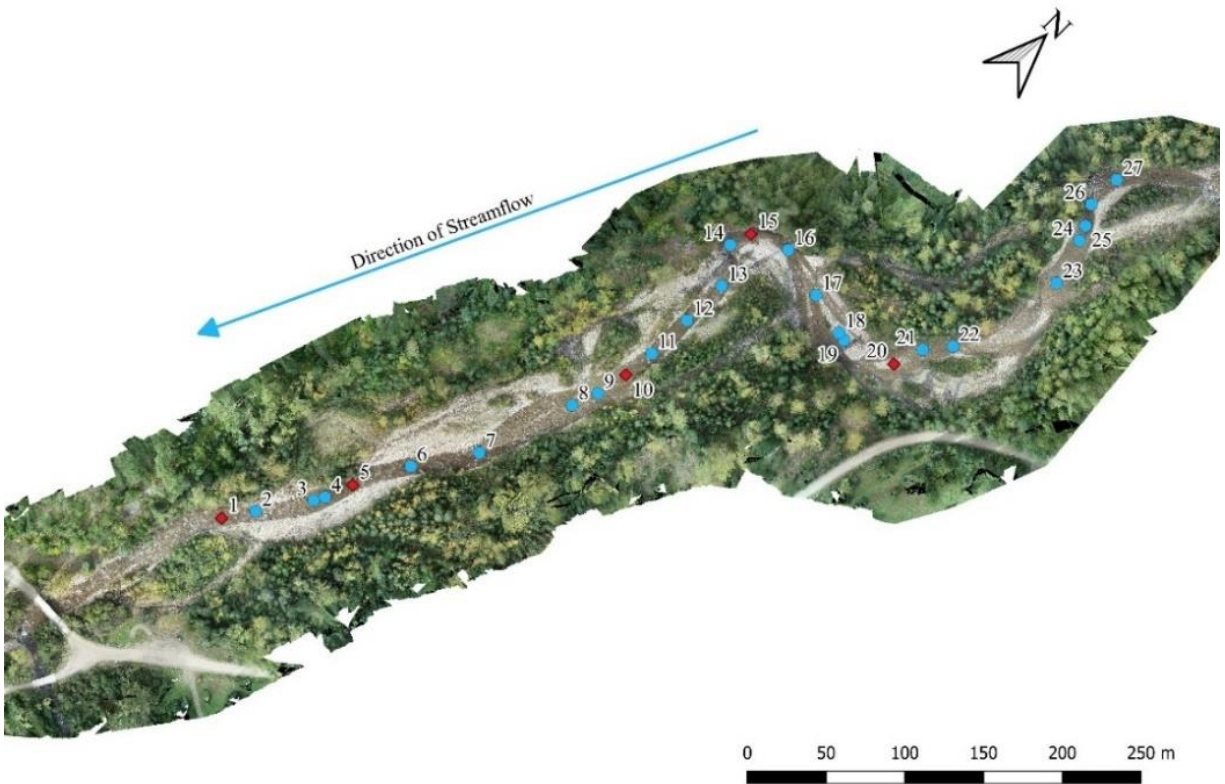


*Figure 3.11 A map showing the distribution of transects for the supplemented model, Model 3Bi, with 5 traditional transects (red diamonds) and 22 photogrammetric transects (blue circles).*

Following the creation of the twenty different hydraulic models, every model was used to perform a mixed-steady flow analysis for 40 discharge events utilizing intervals of  $0.5 \text{ m}^3\text{s}^{-1}$  between  $0.5\text{-}20 \text{ m}^3\text{s}^{-1}$  for a total of 800 simulations. This range of discharges was chosen to simulate conditions present at the smaller discharges that dominated the study period (less than  $8 \text{ m}^3\text{s}^{-1}$ ) and larger discharges that immediately preceded the study period (early June), towards the end of the spring freshet, which peaked at  $31 \text{ m}^3\text{s}^{-1}$  on May 31<sup>st</sup>, 2019.

Such a wide range of discharges is important to the lifecycle of Rainbow Trout, but more importantly, is expected to highlight discrepancies in model performance as a product of notable differences compared to calibration conditions. The transect-specific outputs for hydraulic radius (an approximation for mean flow depth), mean channel velocity, mean Froude number and wetted perimeter were then extracted for each discharge event to assess habitat suitability across the range of expected discharges in Mission Creek.

### 3.4.2 Habitat Modelling

Estimates of flow velocity and depth at each transect were converted to habitat suitability index (HSI) scores for juvenile Rainbow Trout, using the habitat suitability curves (HSC) derived for the US Fish & Wildlife Services (USFWS) by Raleigh *et al.* (1984) (see Figures 3.13 and 3.14). The purpose of these curves is to assign a relative value for the quality of habitat from 0 (not suitable) to 1 (most suitable) for comparison of habitat availability as a function of discharge at different locations rather than providing direct estimates of carrying capacity.

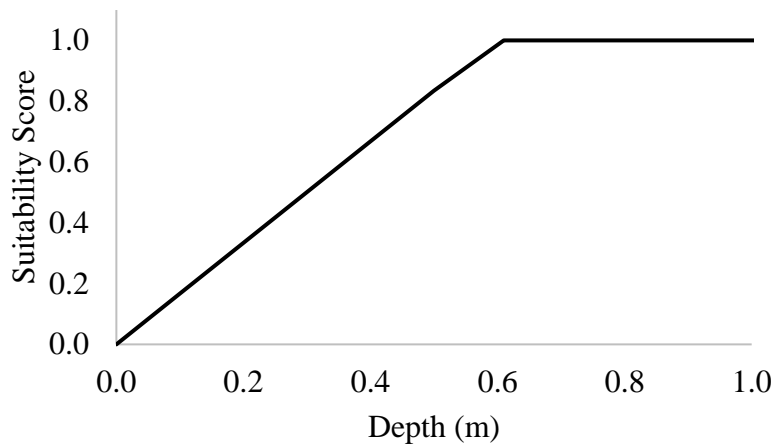


Figure 3.12 Habitat suitability for juvenile Rainbow Trout according to flow depth (m) (Raleigh *et al.* 1984).

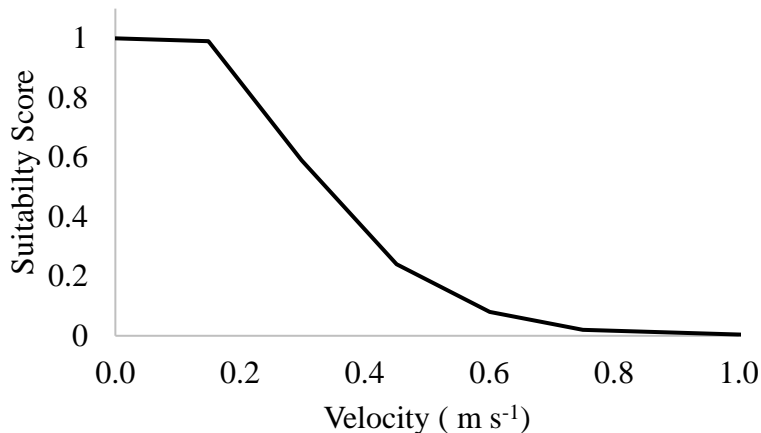


Figure 3.13 Habitat suitability for juvenile Rainbow Trout according to flow velocity (m s<sup>-1</sup>) (Raleigh *et al.* 1984).

The suitability indices for depth and velocity are cross-multiplied to calculate the combined suitability index (CSI) for each transect at the modelled discharges (Equation 1).

$$\text{Combined Suitability Index} = \text{Depth Suitability Score} \times \text{Velocity Suitability Score} \quad (\text{Equation 1})$$

Combined suitability scores are then multiplied by the modelled wetted perimeter to generate estimates of the “Wetted-Usable-Width” (WUW) for juvenile Rainbow Trout at each transect for a given discharge (Equation 2).

$$\text{WUW (m)} = \text{Wetted Perimeter (m)} \times \text{Combined Habitat Suitability Index} \quad (\text{Equation 2})$$

The “Wetted Usable Area” (WUA) was estimated by cross-multiplying each transect WUW estimate by the half-distance upstream and downstream to neighbouring transects (Equation 3).

$$\begin{aligned} \text{WUA (m}^2\text{)} = & (\text{WUW}_1(\text{m}) \times (\frac{\text{Distance Upstream}_1 + \text{Distance Downstream}_1}{2})) + \\ & (\text{WUW}_2(\text{m}) \times (\frac{\text{Distance Upstream}_2 + \text{Distance Downstream}_2}{2})) + \\ & \dots (\text{WUW}_n(\text{m}) \times (\frac{\text{Distance Upstream}_n + \text{Distance Downstream}_n}{2})) \end{aligned} \quad (\text{Equation 3})$$

The total WUA for the entire study reach was simply the sum of the transect-specific WUAs multiplied by their representative area. These results from a combination of 800 different simulations serve as the basis for addressing the study hypotheses.

## Chapter 4 . Results

### 4.1 Site Conditions

#### 4.1.1 Hydrological conditions

The hydrology of Mission Creek is typical of streams in the Southern Interior of BC, with a prominent, snowmelt-dominated spring freshet and a lengthy low-flow period in the summer and early fall. This is exemplified by the Water Survey of Canada (WSC) discharge records for station 08NM116, located in East Kelowna, BC, downstream of the study site and close to the valley bottom at ~400 m ASL (Figure 4.1). As a generalization, the spring freshet starts in the lower reaches of the watershed during the last week of March, with discharges ramping up to peaks of around  $30 \text{ m}^3\text{s}^{-1}$  during the last two weeks of May through the first week of June. The discharge then rapidly decreases through the months of June-July and typically reaches the level of baseflow in August at about  $0.5\text{-}2.5 \text{ m}^3\text{s}^{-1}$  until the onset of the next freshet in March.

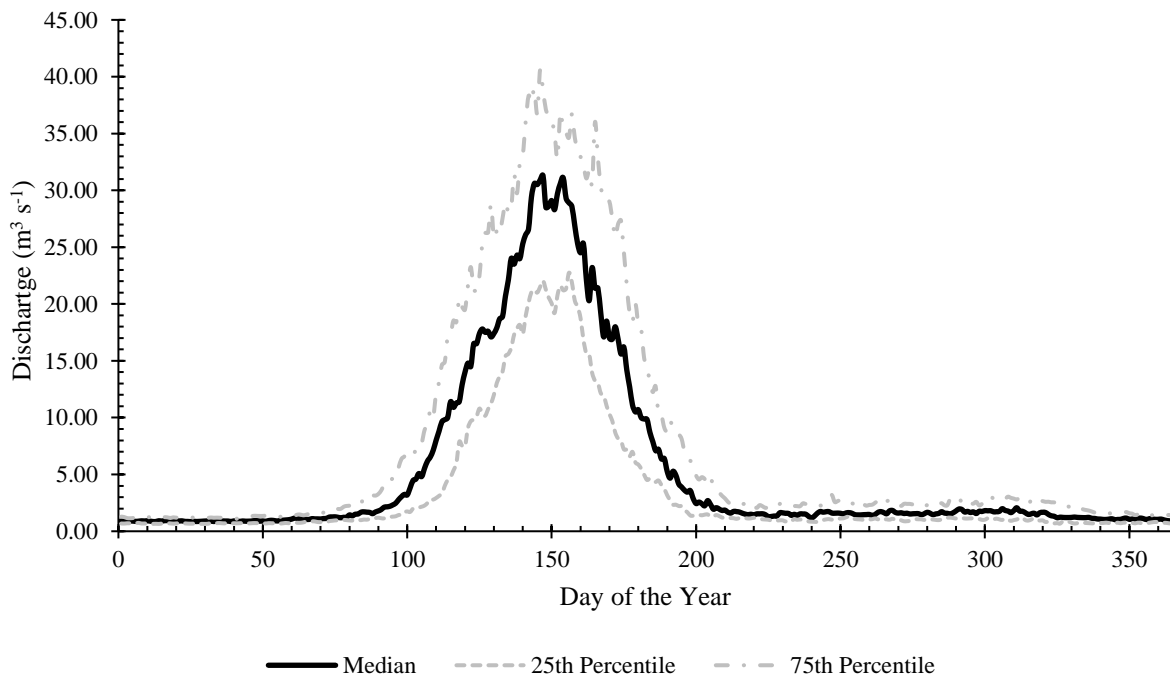


*Figure 4.1 Hydrograph for Mission Creek recorded near East Kelowna, BC (Station 08NM116) by the Water Survey of Canada from 1967 to 2017.*

The WSC maintained a hydrometric station close to the study site (Station 08NM233) between the years 1977-1982. The data from this station are incomplete, but they demonstrate that the freshet in the upper portion of the watershed is often delayed until the end of April with peaks in

late June due to colder temperatures at higher elevations (~930 m ASL). In addition, a comparison of discharges between stations 083NM233 and 08NM116 shows that discharges within the study reach are only 33-52% (average of 42%) of the total discharge recorded farther downstream. This is consistent with the discharge measurements taken at the study site during the 2019 field campaign relative to the East Kelowna discharge records on the same days.

During the summer of 2019, discharge levels at the East Kelowna station were below normal at the start of the study period (June 23<sup>rd</sup>); however, rainfall increased towards the end of June, with discharge levels remaining at or above the historical median for the remainder of the study period (June 23<sup>rd</sup> – Nov 11<sup>th</sup>) (Figure 4.2).

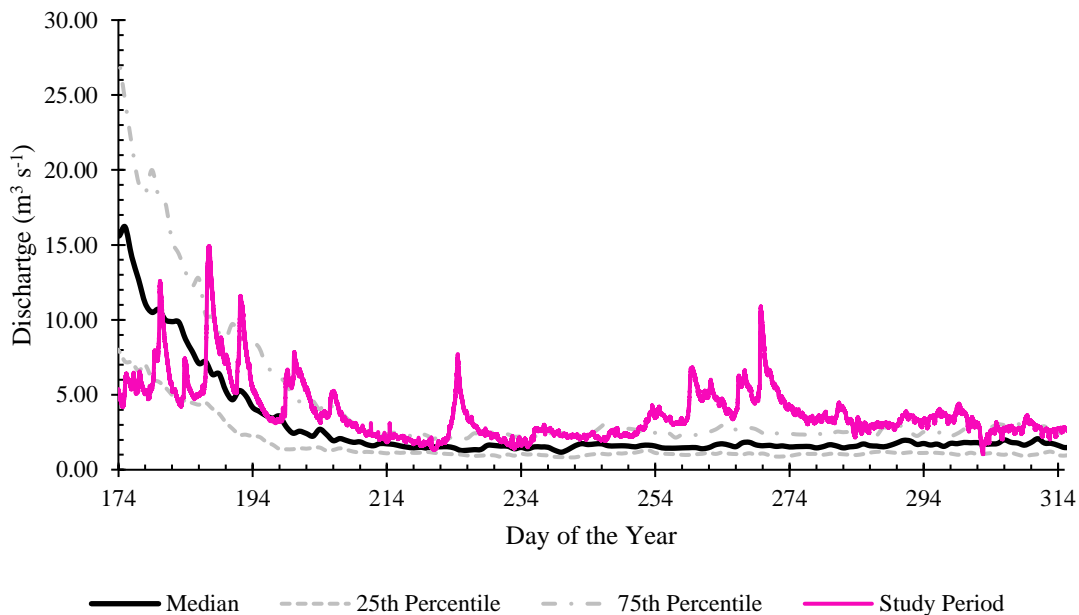


*Figure 4.2 Hydrograph for Mission Creek (Station 08NM116), between the June 23 to Nov. 11, 2019, Study Period. Day 200 corresponds to July 19 whereas Day 300 corresponds to October 27<sup>th</sup>, alternatively July 1 is Day 182 and Sept 1 is Day 244.*

During the field surveys, several large convective thunderstorms travelled through the area, each generating short-lived discharge peaks equivalent to ~25-50% of peak freshet (~8-15 m<sup>3</sup> s<sup>-1</sup>) (Figure 4.2). While discharges returned to background levels (2-4 m<sup>3</sup> s<sup>-1</sup>) within 24 hours after each peak, these events were significant for two reasons. The first was that surveys during these large discharge events were not possible, for safety concerns, and several transect surveys had to be rescheduled. Attempts to survey during or shortly after peak events demonstrated that a

discharge reading above  $6 \text{ m}^3\text{s}^{-1}$  was the safety threshold. At discharges greater than this, even experienced crew members could not safely cross the channel with equipment, due to a combination of strong flows, slick algae cover on the substrate, as well as the prevalence of small rapids and chutes upstream of LWD hazards.

While discharges were still below the peak of a typical spring freshet, these flow events introduced some uncertainty as to whether the channel bed was mobilized and reorganized in locations where the substrate was dominated by loose gravel, such as the braided reach between transects 17-22. Observations from the Aug. 1st survey date noted some minor shifts in the position of side channels on the braids between transects 17-20. Additions of LWD to the log jam at the end of transect 18 (Figure 4.3) also suggested that the previous surges had been sufficient to recruit and transport large debris downstream. These observed changes in channel geometry were limited to the stretch between transects 17-22, and are believed to be relatively inconsequential, on the order of a few centimetres, and within the broader uncertainty levels of the methods.



*Figure 4.3 a log jam immediately downstream of transect 18, at the junction of side-channel A, with fresh additions of woody debris noted by the bright colouration at the base of the jam, Aug. 1st, 2019.*

### 4.1.2 Geomorphological character

Using the classification scheme of Mollard and Janes (1984), the study reach was classified as a wandering channel pattern. The stream is only loosely confined by valley walls and not deeply entrenched. The bank materials are dominated by alluvial cobble and gravels that are easily mobilized. The channel pattern is semi-regular with different sub-reaches varying in morphology from riffle-pool sequences to short series of rapids to broad sets of braids and numerous side channels (both active and inactive) throughout the reach (Figures 4.7 and 4.8). On average, the slope of the channel was 0.016 or 1.6%, although several sections dominated by rapids and chutes had slopes greater than 2% (Table 4.1 and Figure 4.4)

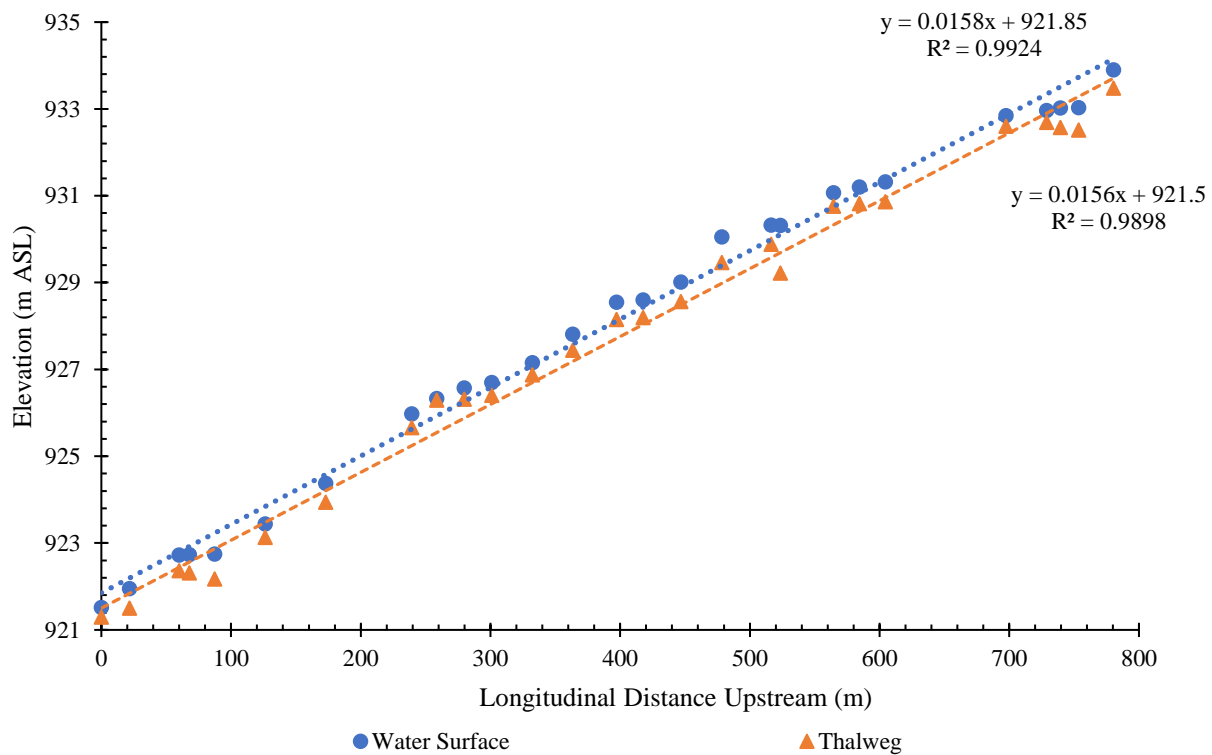


Figure 4.4 Longitudinal slope profile of the Upper Mission Creek Study reach.

Table 4.1 Summary of morphological characteristics by transect.

Transect	Morphological Unit	Distance Upstream (m)	Transect Width (m)	W.S. Slope (m/m)	Thalweg Elevation (m)
1	Rapid	0	19.86	0.020	921.29
2	Rapid	21.7	19.67	0.020	921.50
3	Rapid	60.0	18.21	0.011	922.36
4	Glide	67.9	16.48	0.001	922.31
5	Deep Run	87.4	12.51	0.009	922.17
6	Rapid	126.3	15.28	0.019	923.13
7	Rapid	172.9	15.92	0.022	923.94
8	Broad Riffle	239.3	22.94	0.021	925.66
9	Riffle	258.6	21.79	0.015	926.29
10	Run	279.9	14.32	0.009	926.31
11	Run	301.0	13.03	0.010	926.40
12	Chute	332.3	11.04	0.018	926.87
13	Chute	363.3	11.93	0.021	927.44
14	Riffle	397.1	15.48	0.012	928.15
15	Shallow Run	417.7	9.64	0.008	928.19
16	Run	446.7	10.35	0.023	928.56
17	Chute -Rapid	478.5	32.37	0.020	929.46
18	Deep Glide	516.4	32.82	0.003	929.88
19	LWD Pool	523.6	30.32	0.009	929.22
20	Braided Riffle	564.4	26.27	0.012	930.76
21	Shallow Run	584.4	17.05	0.006	930.82
22	Run	604.5	16.19	0.011	930.86
23	Broad Riffle	697.5	24.28	0.010	932.60
24	Glide	728.8	20.95	0.005	932.69
25	Run	739.3	15.6	0.003	932.57
26	Run with LWD	753.4	12.49	0.016	932.51
27	Riffle	780.3	16.5	0.032	933.48

At an average elevation of ~928 m ASL, the study site is located midway between the outlet at Okanagan Lake in the valley bottom and the headwater lakes on the Graystoke Plateau. The dominant bedrock material beneath the alluvial deposits in the upper portion of the watershed is volcanic basalt (Neilson and Allen 2007). As a product of the short distance travelled and the strength of the parent material, the alluvial deposits within the reach are dominated by cobble size particles (diameter between 0.0064-0.256 m), with boulders common and finer sand and

gravels largely limited to the imbrication zones behind boulders.



*Figure 4.5 Upstream view from transect 2 showing cobble-boulder substrate materials (July 8th, 2019).*



*Figure 4.6 Downstream view from transect 6 (July 8th, 2019) showing the transition from rapids to pool-riffle sequences.*



*Figure 4.7 View from transect 7, looking upstream towards transects 8, 9 and 10 (July 13, 2019).*



*Figure 4.8 Transect B, looking downstream on active side channel B (Aug. 1st, 2019).*



*Figure 4.9 One of two inactive side channels behind the right (north) bank of transects 7-12.*

The exceptions to this trend were the sub-reaches between transects 18-22 (Figures 4.9 and 4.10) where the slopes were consistently less than 2% (Table 4.1) and finer materials (sands and gravel) were observed within the substrate of the inside banks and eddy zones.



*Figure 4.10 Transects 18 and 19, with the flow moving from left to right and photographed from the outside bank of the mid-channel gravel bar (July 13th, 2019).*



*Figure 4.11 Transect 20, looking upstream (Aug 1st, 2019).*

LWD was observed in the channel at seven locations within the active channel. These included transects 5, 8, 18, 19 and 26, as well as another location not surveyed. This location was a pool between transects 13-14, and it was excluded from the survey due to safety concerns related to the nature of the log jam, constricted fast-moving flow (less than 2 m wide) and depth (~1.5 m).

#### **4.1.3 Observations of Rainbow Trout**

During the July 13<sup>th</sup> stream walk, visual observations and angling techniques were employed to assess the presence of Rainbow Trout (RBT) throughout the study area. This was done to ensure that the distribution of transects would capture the full range of habitat conditions utilized by resident trout populations. Juvenile RBT were observed to be plentiful wherever lateral refuge from strong flow velocity was present. Even sections of the channel that were dominated by rapids or the turbulent zones in the downstream wake of boulders or LWD were well utilized with each 'pocket' of calm water containing a minimum of five RBT, and upwards of twenty individuals in certain locations (Figure 4.12). Areas of deep and complex flows, such as transects 3,5,7, 18,19, 20 and 26 were especially well occupied with some locations holding more than 30 individuals. Larger RBT approaching maturity (~30 cm in length) were only found

in the deep pools around transects 18-20 and upstream of the study reach.

While July 13<sup>th</sup> was the only date when angling techniques were employed, RBT were observed during other transect survey dates (July 23<sup>rd</sup> and Aug 1<sup>st</sup> ) after peak discharge events. On these two occasions, upwards of twenty RBT had temporarily occupied the side channel habitat, some of which were only active during the large discharges. However, by late September, the side channel habitats were no longer utilized. In locations where in-channel cover provided by LWD or boulders was not available, RBT were largely absent even if flow velocities and depths were perfectly suitable and there was the presence of macroinvertebrate prey.



*Figure 4.12 Example of turbulent 'pocket' water, July 13th, 2019.*

## **4.2 Data Quality Control**

### **4.2.1 Evaluation of Field Data**

Before performing any modelling exercises, it was necessary to validate the quality of field data collected. Fourteen field trips were conducted throughout the study period, nine of which

produced quantitative data sets that needed to be assessed (Table 4.2). The two-stream walks were principally qualitative surveys, assessing the general morphology of the stream, documenting the presence of Rainbow Trout, and mapping transect locations. Likewise, the first drone flight on July 13<sup>th</sup> served as a test of flight paths, line of sight and ground control markers. As previously discussed in the Methods chapter, issues with the images being over-exposed due to white water refraction and glare from the exposed channel bed, disqualified the photogrammetric outputs from the July 25<sup>th</sup> and Aug. 13<sup>th</sup> flights.

*Table 4.2 Summary of field trip dates, sorted by type and including estimates of discharges at the time, both at the Water Survey of Canada station in East Kelowna and measured in the field.*

Survey Type	Dates Conducted	WSC Discharges (m <sup>3</sup> s <sup>-1</sup> )	Measured Discharges (m <sup>3</sup> s <sup>-1</sup> )
<b>Stream Walk</b>	Jun. 23 <sup>rd</sup> , Jul. 13 <sup>th</sup>	4.69, 4.96	N/A
<b>Transect – Engineer’s Level (Eng. Lvl.)</b>	Jul. 8 <sup>th</sup> , Jul 20 <sup>th</sup> , Jul 23 <sup>rd</sup> , Aug. 1 <sup>st</sup>	7.85, 5.94, 3.66, 2.08	N/A
<b>Transect – Wading Rod (WR)</b>	Aug. 14 <sup>th</sup> , Aug 24 <sup>th</sup>	3.24, 2.69	1.61, 0.63
<b>Drone Flight</b>	July 25 <sup>th</sup> , Aug. 13 <sup>th</sup> and Sept. 30 <sup>th</sup>	3.96, 4.16	1.64, 1.88
<b>Secondary Waterlines for Calibration (Cal.)</b>	Aug. 15 <sup>th</sup>	2.74	1.15
<b>RTK-DGPS</b>	Sept. 30 <sup>th</sup> and Nov. 11 <sup>th</sup>	4.16, 2.61	1.15, N/A

Initially, only one RTK-DGPS survey was planned for September 30<sup>th</sup>, but a second survey was done on November 11<sup>th</sup> due to concerns of poor rover-base station communication on the first trip. Except for four transects (6,14, 15 and 17), the easting and northing coordinates for twenty-three transects on these two trips differed by less than 0.02 m E and -0.05 m N on average, with a standard deviation of 0.07 m E and 0.09 m N (Appendix B). This was within the range of expectations for measuring error with the GPS surveys. However, at transects 6,14 and 15, the pin coordinates were off by several metres, and elevations between the two dates differed by -0.52 m on average (Appendix B), with the Sept. 30<sup>th</sup> survey producing the highest elevations. Both sets of pin coordinates were overlaid onto existing maps, including visually mapped pins on Google Earth, to test the validity of both surveys. The November 11<sup>th</sup> survey was found to fit pre-existing maps extremely well, and without the large errors observed at transects 6,14 and 15 in the Sept 30<sup>th</sup> survey. Therefore, the November 11<sup>th</sup> RTK-DGPS survey was treated as the principal GPS survey for this study. All further references to the GPS survey will be referring to

only those measurements from the November 11<sup>th</sup> survey; a detailed comparison of pin coordinates between the two survey dates can be found in Appendix B.

The first assessment of different field techniques compared the elevation differences between left bank and right bank pins at each transect for 1) the initial transect survey with an engineer’s level (Eng. Lvl); 2) the Nov. 11<sup>th</sup> RTK-DGPS (GPS) survey; and 3) the Aug. 15<sup>th</sup> waterline surveys (Cal.), also conducted with an engineer’s level. The results of these comparisons are summarized in Table 4.5.

*Table 4.3 A comparison of three topographical surveys (Eng. Lvl., Cal. and GPS) measurements for the elevation difference between left and right bank markers at each transect.*

<b>Error</b>	<b>Eng. Lvl. vs Cal.</b>	<b>Eng. Lvl. vs GPS</b>	<b>Cal. vs GPS</b>
<b>Mean (m)</b>	0.00	0.01	0.00
<b>Mean Absolute Error (m)</b>	0.06	0.06	0.07
<b>Median (m)</b>	0.00	0.00	0.00
<b>Standard Deviation (m)</b>	0.11	0.11	0.10
<b>Maximum Absolute Error (m)</b>	0.44	0.50	0.36
<b>Number of XS with an absolute difference &gt; 0.05 m</b>	7	7	10
<b>Number of XS with an absolute difference &gt; 0.1 m</b>	6	3	4

Of the three comparisons between surveying methodologies, all produced a similar range of uncertainty, with the mean and median among the residuals of the comparisons varying by less than 0.01 m (Table 4.5). However, there were instances in which the maximum absolute error (MAE) was quite large, requiring a close assessment of which method was associated with greater uncertainty. For example, the largest value of MAE was associated with the same survey point, the right bank pin at transect 2, regardless of the survey technique. This was the only anomalous point for that transect and has been identified as an error in both the engineer’s level and GPS surveys. Achieving a clear line of sight with the engineer’s level to this location proved challenging, and the communication link between the RTK rover and base station was weak because of the dense foliage interfering with antennae communication. This single point with maximum error also contributed to the rather large standard deviation of about 0.1 m. Ignoring this pin in the overall assessment, led to the conclusion that the survey data from the water level

calibrations (**Cal**) were the least reliable because of the impact of imprecise levelling of the instrument on long-distance shots to the stadia rod, of which there were many. Table 4.3 shows that the comparison of the engineer’s level and GPS surveys yielded only three transects where pin elevations disagreed by more than 0.1 m (including transect 2). For twenty of the twenty-seven transects, the methods were within 0.05 m of each other, which was deemed acceptable but not ideal.

To further validate the survey data, the horizontal span from the right bank to left bank pins was compared using the tape measured distances and the RTK-DGPS measurements. A summary of the results appears in Table 4.4.

*Table 4.4 Summary of discrepancies between the measurements from engineer’s level and GPS surveys for the horizontal distance of each transect, with error, reported as the difference from tape measurements, both in metres and as a percentage of transect length.*

	<b>Metric Error (m)</b>	<b>Percentage of Transect Length (%)</b>
<b>Mean (m)</b>	0.06	0.25
<b>Mean Absolute Error (m)</b>	0.11	0.67
<b>Median (m)</b>	0.04	0.26
<b>Standard Deviation (m)</b>	0.15	1.01
<b>Maximum Absolute Error (m)</b>	0.50	2.59

Similar to the results for pin elevations, the discrepancies in horizontal distance between the tape measure and GPS were minimal for the majority of transects with a mean error of 0.06 m or 0.25% of transect length. This variance was expected due to a combination of reasons, including stretch and sag in the tape measure, tilting of some pins over a three-month survey period, and interference with GPS readings at some locations due to dense vegetation cover. Again, Transect 2 was found to have an inordinately large error (0.5 m), supporting earlier observations that interference between the GPS rover and base station due to vegetation cover on the right bank may have influenced GPS measurements for the right pin. The tape measure distance seems more reliable, and following this logic, greater faith is placed in the engineer’s level data for this pin elevation and location.

Excluding transect 2, attempts were made to assign a spatial context to observed errors to rule out any systematic bias. No such systematic spatial patterns were found and there was no

significant correlation between error in the pin elevations or transect lengths. Therefore, it can be assumed that the error in survey data was random and inherent to the methods used and human fallibility. Nevertheless, the average errors are smaller in magnitude than the average diameter of the substrate ( $\sim 0.1$  m), which provides reassurance that the measurements were generally quite accurate and reliable.

#### **4.2.2 Evaluation of Photogrammetric Data**

Twenty-seven photogrammetric transect profiles were extracted from the Sept. 30<sup>th</sup> flight with Global Mapper, using the GPS pin coordinates (as quality controlled by the engineer's level survey) to ensure that the photogrammetric transects exactly matched the locations of the surveyed transects. The accuracy of the transects extracted from the photogrammetric DEM was then assessed according to two criteria.

The first criterion was the accuracy and precision of the photogrammetric survey at replicating the absolute elevation of each sampling point in the previous engineer's level surveys. Three linear regressions were performed on the entire data set of pairwise point elevations: one for the whole dataset, a streamlined dataset with vegetation points removed, and a final dataset that included only survey points below the waterline.

Accuracy and precision of channel bathymetry was the second criterion evaluated. This assessment differed from and was complementary to the first, as it compared measurements of flow depth of each sampling point, rather than absolute elevation. By doing so, direct instream measurements of depth sampled with a wading rod could be added to the comparison; thereby conformity between the photogrammetric and engineer's level survey results could be compared against the agreement between engineer's level and wading rod surveys, which are both traditionally used survey techniques.

For each of the pairwise comparisons of absolute elevation estimates, a measurement of elevation was extracted for every sampling point that was common to both the surveyed and photogrammetric transects. The first of three regression analyses compared elevation estimates from the raw DEM in its entirety with no corrections for refraction or known interference from overhead vegetation. This dataset had a total of 908 common sampling points, each with two estimates of elevation (surveyed and photogrammetric) and the results of the regression are

summarized below in Figure 4.12 and Table 4.6.

The second regression followed a similar procedure, but any outliers that could be identified as a direct product of overhead vegetation were excluded, yielding a dataset with a total of 861 sampling points. The results of this 'corrected' regression analysis with the outliers are summarized in Table 4.5 below.

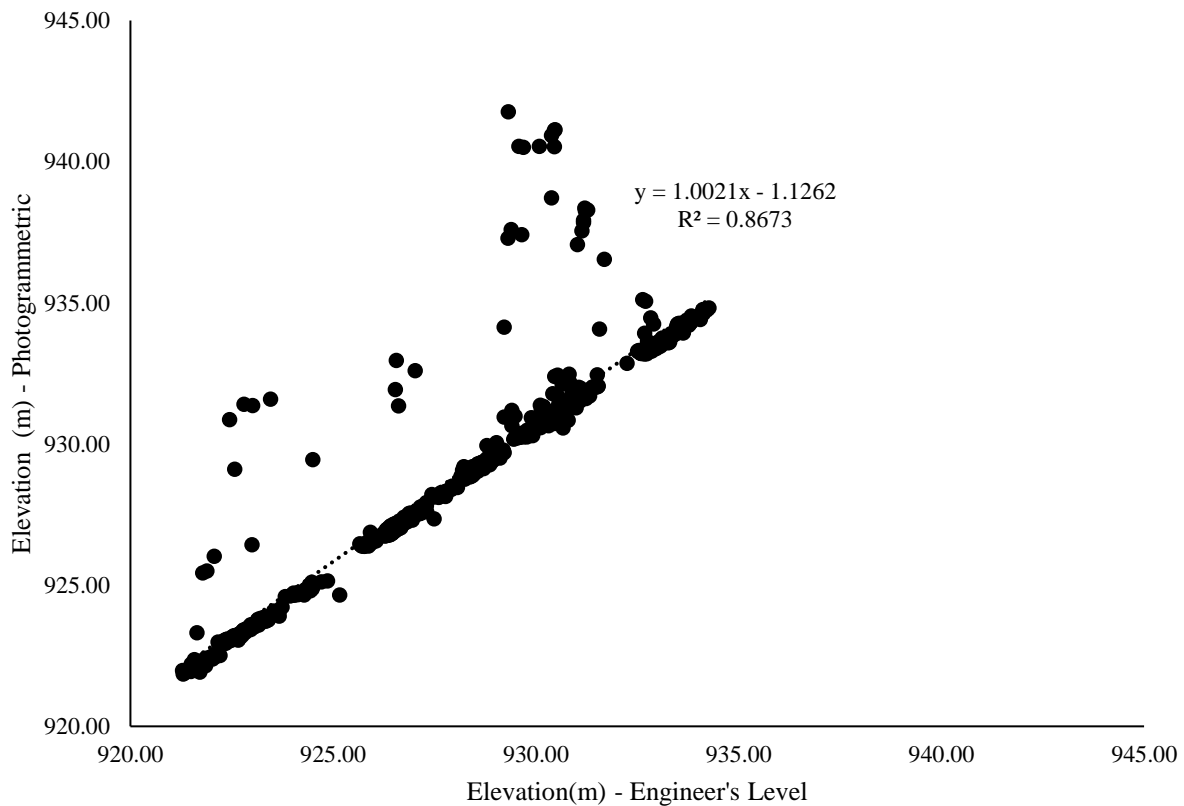


*Figure 4.13 Regression plot comparing uncorrected photogrammetric transect points versus elevations from standard surveying techniques using an engineer's level.*

For the third comparison of absolute elevations, 666 sampling points that were both clear of overhead vegetation and below the waterline during the Sept. 30<sup>th</sup> flight were compared. This was done to evaluate the accuracy of the photogrammetric survey at deriving channel bathymetry only. The results are summarized below in Figure 4.13 and Table 4.5.

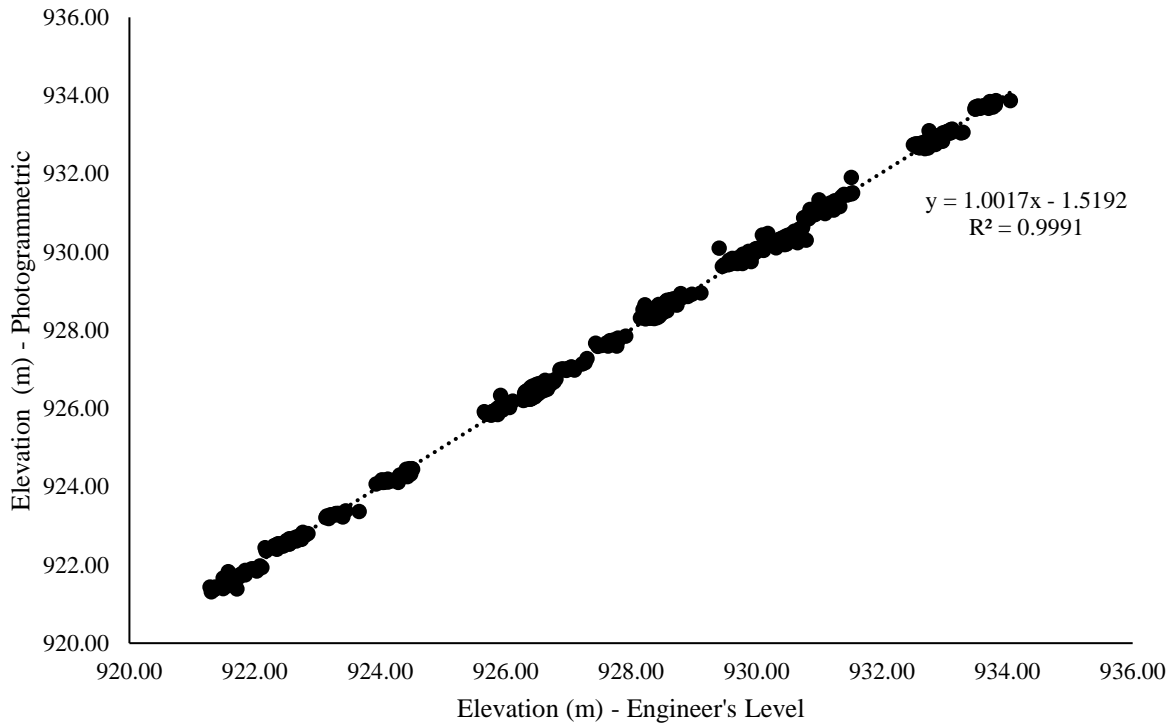


Figure 4.14 A regression plot comparing corrected photogrammetric transect points versus elevations from standard surveying convention. Outliers have been deleted and only sampling points below the water surface were included in this analysis.

Table 4.5 Summary of error for photogrammetric measurements of elevation at survey points compared to measurements sampled following the standard surveying convention.

	Uncorrected	Corrected	Corrected – Bathymetry Only
<b>Mean Error (m)</b>	0.31	0.02	0.02
<b>Mean Absolute Error (m)</b>	0.37	0.09	0.06
<b>Median Error (m)</b>	0.04	0.02	0.03
<b>Standard Deviation (m)</b>	1.41	0.15	0.11
<b>Root Mean Square Error (m)</b>	1.43	0.15	0.11
<b>Correlation Coefficient (R<sup>2</sup>)</b>	0.867	0.998	0.999
<b>Number of Sample Points</b>	908	861	666

Upon examining the results of the first regression analysis, it was immediately clear that for the majority of points the error was small, as indicated by a median error of 0.04 and an R<sup>2</sup> of 0.867.

However, the presence of overhead vegetation at several locations resulted in a mean error of 0.31 m and a standard deviation of 1.41 m (Table 4.5). After the points of overhead cover were removed the mean error, standard deviation and RSME decreased to 0.02 m, 0.15 m and 0.15 m, matching the respective error range as the engineer's level and GPS surveys and that is comparable in magnitude to the diameter of the cobble substrate. Additionally, the correlation coefficient increased to 0.998, and as seen in Figure 4.13 no outliers were evident. Somewhat unexpectedly, the results for the bathymetry only data set (no points above the waterline) showed additional improvement in nearly all metrics. The median error increased slightly to 0.03 m, however, the mean absolute error, standard deviation, and RMSE decreased to 0.06 m, 0.11 m and 0.11 m, respectively.

To compare how the photogrammetric survey performed against the wading rod survey at replicating channel bathymetry, two pairwise linear regressions were conducted. In each regression, the reference flow depth for each sampling point was the assumed depth calculated from the difference between the bed elevation derived from the engineer's level survey and the elevation of the water surface on the day of the wading rod survey. Estimates of flow depth from the photogrammetric survey were derived for the same locations. The residuals between the photogrammetric and engineers level survey were then compared against the residuals between the wading rod and engineer's level surveys.

The first regression analysis compared the discrepancies between each pair of surveys for all sampling points simultaneously with equal weighting. Whereas the second, averaged the error by transect to assign an equal weighting to each transect, rather than individual points. This was done to highlight issues that may have been transect specific, such as the presence of LWD. The results of this comparison are summarized in Tables 4.6 and 4.7 below

*Table 4.6 Comparison of discrepancies between the final photogrammetric bathymetry and wading rod depth measurement, with residuals taken against measurements from the engineer’s level survey and summarized for the whole study reach with no statistical weighting.*

	<b>Corrected – Bathymetry Only</b>	<b>Wading Rod Depth Measurements</b>
<b>Mean Error (m)</b>	0.02	0.01
<b>Mean Absolute Error (m)</b>	0.06	0.03
<b>Median Error (m)</b>	0.03	0.00
<b>Standard Deviation (m)</b>	0.11	0.07
<b>Root Mean Square Error (m)</b>	0.11	0.07
<b>Number of Sample Points</b>	666	572

*Table 4.7 Comparison of discrepancies between the corrected photogrammetric bathymetry and wading rod depth measurement, with residuals taken against measurements from the engineer’s level survey, with transects assigned equal weight.*

	<b>Corrected – Bathymetry Only</b>	<b>Wading Rod Depth Measurements</b>
<b>Mean Error (m)</b>	0.03	0.01
<b>Mean Absolute Error (m)</b>	0.09	0.04
<b>Median Error (m)</b>	0.04	0.01
<b>Standard Deviation (m)</b>	0.09	0.07
<b>Root Mean Square Error (m)</b>	0.10	0.07

Comparing the results for the whole set, as presented in Table 4.7, measurements of channel bathymetry taken with a wading rod had a slightly smaller error when compared to the engineer’s level survey than the photogrammetric estimates with a median error of 0.01 m and standard deviation of 0.07 m, compared to 0.03 m and 0.11 m. Averaging the results by transects did little to change the results for the wading rod survey, while it slightly increased the mean and median error in the photogrammetric estimates to 0.03 m and 0.04 m but decreased standard deviation and RMSE to 0.09 and 0.10 m respectively. However, even comparing mean absolute error, the largest difference between the depth estimates from the two methodologies varied by only 0.05 m. This is smaller than the error observed between the engineer’s level and GPS surveys (Table 4.4) and is approximately half the diameter of the substrate size.

During the analysis, it was noted that the photogrammetric method tended to over-estimate depth consistently (Appendix C). It is not known why the photogrammetric method yields slight

overestimates of depth, but in any case, the discrepancy was relatively small. Applying the industry-standard refraction index of 1.34 (Jerlov, 1976; Dietrich, 2016) only yielded unrealistic overestimates of depth; therefore, no refraction index was utilized in the final data set.

Ultimately, because of the issues with the initial two test flights and relative inexperience on the part of the crew with the methodology, it was hypothesized that of the topographic datasets the photogrammetric DEM would be the less accurate. As all the crew members were experienced in hydrometric sampling and surveying with the standard convention, there was greater confidence in the traditionally derived transect data. Hence the decision was made to utilize the engineer's level and wading rod survey data to generate the calibrated 'Best-Practices' scenario.

## **4.3 Hydraulic Modelling**

### **4.3.1 Calibration Efforts**

Following the procedure laid out in Chapter 3, a base geometric model was constructed with HEC-RAS, using the engineer's level survey data for all twenty-seven transects to create the 'Best-Practices' scenario ( Scenario 0).

As noted previously, the discharge of the main channel varied between transects due to losses and gains into and out of the numerous side channels, along with likely hyporheic exchanges through the cobble substrate. It was necessary, therefore, to calibrate the model taking into account the different sub-reaches. Each sub-reach was defined as a group of transects with similar discharge measurements, in close proximity to each and located either upstream or downstream of major changes in field discharge measurement, such as upstream of the confluence with back-channel A ( Transect 10, Figure 4.15). Within each sub-reach, the mean discharge for all transects in that group was assigned as the sub-reach average. A total of five such sub-reaches were created during the setup of the steady flow data in HEC-RAS with the inputted discharges summarized below in Table 4.8.

Table 4.8 Summary of discharges, sorted by transect, used to calibrate the HEC-RAS model.

Group ID	Transect	Calibration Discharges ( $\text{m}^3 \text{s}^{-1}$ )
<b>Surveyed Aug 14<sup>th</sup></b>		
1	1-9	1.51
2	10	1.09
<b>Surveyed Aug 24<sup>th</sup></b>		
3	11-16	0.49
4	17-18	0.31
5	19-27	0.66

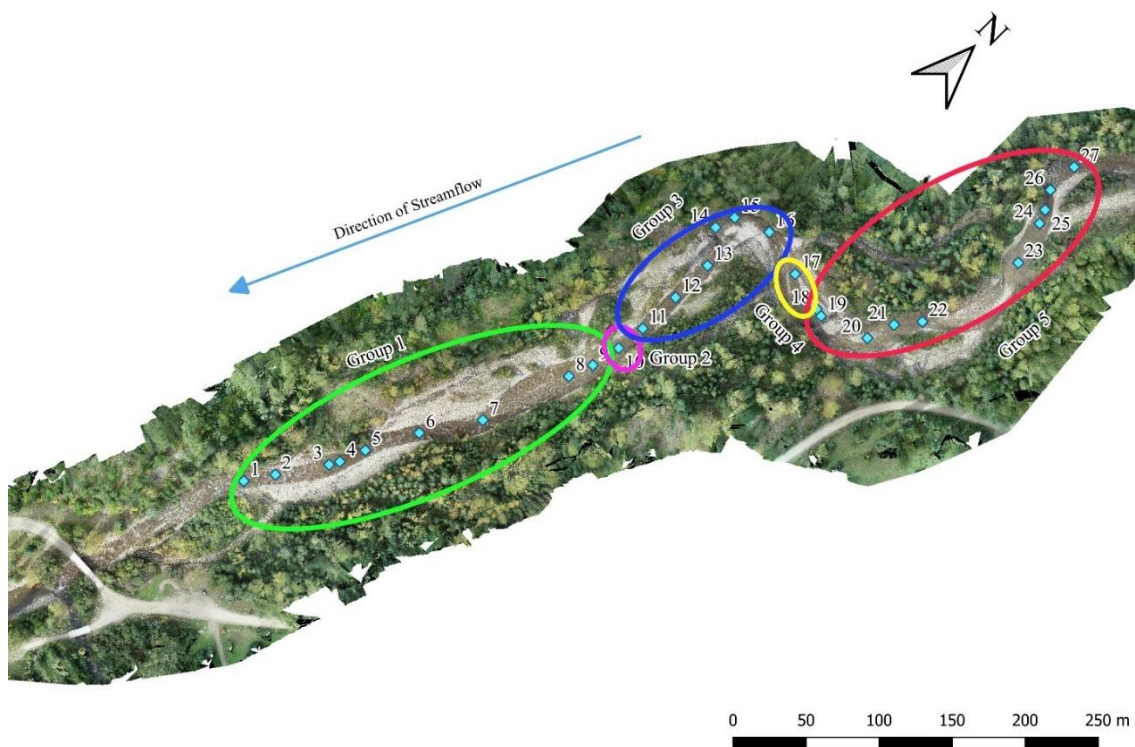


Figure 4.15 Distribution of sub-reaches as defined by transect-specific discharges employed in the calibration exercises (see text for explanation).

With the calibration discharges established, the initial set of upstream and downstream boundary conditions of the model were set to the measured water surface slope at the calibration discharges for transects 27 ( $0.032$ ) and 1 ( $0.01$ ). The simulations were then set up to run mixed-steady flow analyses for forty discharge intervals between  $0.5 - 20 \text{ m}^3 \text{ s}^{-1}$  at the upstream reach boundary (transect 27).

The ‘Best-Practices’ HEC-RAS model was successfully calibrated after eleven calibration iterations using the water surface slope boundary conditions, with the Manning’s n and the contraction and expansion factors adjusted incrementally in each simulation. The adjustments were made for every transect until the modelled elevations of the waterlines matched the measured waterlines for Aug. 14<sup>th</sup> and 24<sup>th</sup> (reach average discharge of 1.63 and 0.63 m<sup>3</sup> s<sup>-1</sup>) or the model outputs ceased to respond to additional adjustments, often at extreme values of Manning’s n (Appendix C). A secondary set of calibration runs was also done for known elevations of the water surface at transects 1 (~921.5 m) and 27 (~933.8 m) on Aug. 14<sup>th</sup> and 24<sup>th</sup>, when calibration discharges were measured within the study reach. A total of three such calibration simulations were run immediately after the first three of the water surface slope calibration runs. However, in each case, the results were found to be identical and the remaining seven calibration runs were done using water surface slope as the boundary condition.

With the model calibrated, modelled mean elevations of the water surface (WS) were then compared to measurements from the engineer’s level surveys. The purpose of this exercise was to evaluate the effectiveness of the calibration efforts within the context of sampling challenges in the field due to natural variability exhibited in mountain streams.

These comparisons were done by evaluating how much the modelled mean for water surface elevation at each transect deviated from measurements at both banks and the mean water surface elevation. To dampen the influence of perched benches, LWD and localized swells, which the HEC-RAS model would not include in its hydraulic outputs, the measured mean water line at each transect was not taken simply as the mean between left and right banks. Instead, the measured mean water surface elevation at each transect was calculated as the average water surface elevation for all wetted sampling points present, with each point weighted according to a portion of horizontal distance it represented at the transect.

Several transects were observed to have tilted waterlines because of perched ridges, braids, woody debris or the high curvature of the channel. Elevation differences as large as 0.11 m between the inside and outside banks were measured in the field, but these cannot be duplicated in a 1D hydraulic model that yields only transect-averaged values. The results are compiled in Figure 4.16 and Table 4.9 below. Both the mean and median error were less than 0.05 m. The

median error was comparable to uncertainty in the measured waterlines. The standard deviation for modelled waterlines was 0.07 m, paralleling the deviation seen in the waterline measurements surveyed with an engineer’s level (Table 4.3) and the previous results for point-specific measurements of depth with a wading rod (Table 4.7).

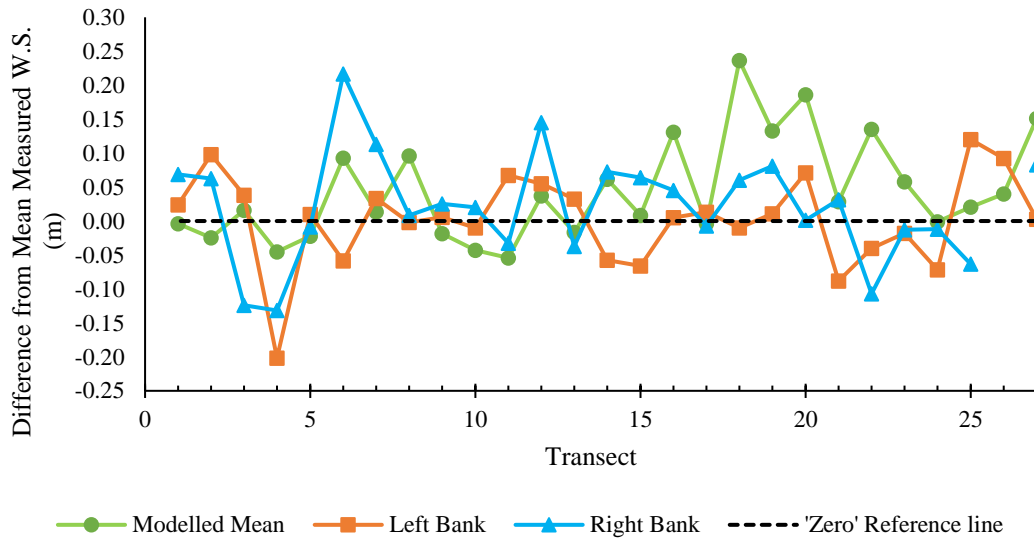


Figure 4.16 Deviation of the water surface elevation from the measured mean at each transect.

The model had a total of six transects that failed to calibrate within 0.1 m of measured waterlines, compared to a total of four transects that had a 0.1 m difference between the measured mean waterline and either the right or left bank water surface. Of the six transects that were difficult to calibrate, one was located at a major break in slope where a steep chute transitioned to a run (transect 16). Two transects were located at pools created by LWD with complex hydraulics, and each had a side-channel diverting some of the flow away from the main channel (transects 18 and 19). Another two were located at riffles with perched braids (transects 20 and 22) and the final one, was a steep riffle zone located at the upstream reach boundary, immediately upstream of a log jam (transect 27). The remaining twenty-one transects had less than 0.1 m of error, with seventeen having less than 0.05 m of error and thirteen below 0.025 m.

*Table 4.9 Summary of calibration efforts, comparing the mean waterlines in HEC-RAS against the mean water line measured in the field on the calibration dates (Aug. 14th and 24th). Discrepancies between the measurements at the left and right banks are also included.*

<b>Error (m)</b>	<b>Modelled Mean Waterline</b>	<b>Measured Waterline – Left Bank</b>	<b>Measured Waterline – Right Bank</b>
<b>Mean</b>	0.04	0.00	0.02
<b>Median</b>	0.02	0.01	0.02
<b>Standard</b>	0.07	0.07	0.08
<b>Absolute Maximum</b>	0.24	0.20	0.22
<b>Number of Transects with deviation greater than:</b>			
<b>0.1 m</b>	6	1	3
<b>0.05 m</b>	10	6	10
<b>0.025 m</b>	13	9	13
<b>Transects with calibration deviation greater than 0.1 m</b>			
16, 18, 19, 20, 22, 27			
<b>Transects with calibration deviation less than 0.05 m</b>			
1, 2, 3, 5, 7, 9, 10, 12, 13, 15, 17, 21, 24, 25, 26			

In summary, six transects with morphology that would be expected to increase modelling uncertainty had errors during calibration that were greater than the sampling variability, however, the vast majority of transects were well within the error bounds of the field surveys. Hence, the model was deemed sufficiently calibrated, and the assessment progressed to evaluating the effectiveness of supplementing photogrammetric transects into hydraulic models with a limited density of surveyed transects.

#### **4.3.2 Modelled Channel Hydraulics**

After the ‘Best-Practices’ model with 27 transects was calibrated, another nineteen HEC-RAS models were generated, each belonging to one of seven scenarios with a reduced number of surveyed transects (refer to Table 3.1 for details). The model outputs for mean depth and flow velocity for every transect were extracted and organized for comparison to field measurements. This was done only for the calibration discharges when field sampling was conducted. The full results of this comparison are provided in Tables 4.10 and 4.11 below.

Table 4.10 A summary comparison of modelled flow depth for each HEC-RAS Scenario against field measurement at the calibration discharges.

Scenario	Model Number	Mean Error (m)	Median Error (m)	Standard Deviation (m s <sup>-1</sup> )	Max. ABS. Error (m)	RMSE (m s <sup>-1</sup> )
<b>Traditional 'Best-Practices' Scenario</b>						
0	i	0.01	0.00	0.06	0.16	0.06
<b>Reduced Scenarios</b>						
1A	i	0.01	-0.01	0.08	0.23	0.08
	ii	-0.01	0.00	0.07	0.18	0.08
	Average	0.00	-0.01	0.08	0.23	0.08
2A	i	0.04	0.01	0.10	0.30	0.11
	ii	-0.01	-0.01	0.04	0.06	0.04
	iii	0.00	0.04	0.10	0.21	0.10
	Average	0.01	0.01	0.09	0.30	0.09
3A	i	0.06	0.04	0.08	0.21	0.10
	ii	-0.01	0.03	0.09	0.17	0.09
	iii	0.00	0.00	0.06	0.09	0.06
	iv	0.01	0.02	0.09	0.14	0.09
	Average	0.01	0.02	0.08	0.21	0.09
<b>Supplemented Scenarios</b>						
1B	i	0.02	-0.01	0.07	0.16	0.07
	ii	0.01	0.00	0.08	0.36	0.08
	Average	0.01	0.00	0.07	0.36	0.07
2B	i	0.01	0.00	0.06	0.14	0.06
	ii	0.02	0.01	0.08	0.35	0.09
	iii	0.02	0.00	0.08	0.37	0.08
	Average	0.02	0.00	0.07	0.37	0.08
3B	i	0.02	0.00	0.08	0.35	0.09
	ii	0.02	0.01	0.08	0.37	0.08
	iii	0.02	0.01	0.06	0.15	0.06
	iv	0.02	0.00	0.07	0.32	0.07
	Average	0.02	0.00	0.07	0.37	0.08
<b>Photogrammetric Scenario</b>						
4	i	0.02	0.01	0.07	0.34	0.08

Regardless of the scenario, both the mean and median error estimates of flow depth, shown in Table 4.10, were found to be minimal (-0.02 - 0.00 m), likely a product of the calibration exercise on all models were based on. The standard deviation of error and the root mean squared

error for flow depth were similar and again matched margins previously seen in the field surveys (0.06-0.09 m), though with a slight variance between scenarios (less than 0.03 m). What did change between the scenarios was the absolute maximum error, which was 0.16 m for scenario 0, increasing to 0.3 m by scenario 3A as the number of surveyed transects included in the model decreased from 27 to 5. The supplemented scenarios that included photogrammetric transects all had a similar error of 0.34-0.37 m, greater than the previously reduced scenarios. This relatively large error of ~0.35 m when photogrammetric transects were inserted into the model was a bit surprising but was thought to be due to photogrammetric error for transect 19, where overhead vegetation over the left bank and thalweg was prevalent. By excluding transect 19, the absolute maximum error for all supplemented and photogrammetric error dropped to 0.13 m, which was smaller than the traditional transect models, including the 'Best-Practices' Scenario 0 (0.16 m).

Unlike estimates of flow depth, model outputs for mean flow velocity were observed to be highly variable between the different scenarios (Table 4.11). The mean error started at 0.23 m s<sup>-1</sup> for scenario 0 and increased to 0.26 m s<sup>-1</sup> when the number of surveyed transects was reduced (scenarios 1A-3A). As the number of surveyed transects was reduced to 9 or fewer, the median error increased from 0.12 to 0.17 m s<sup>-1</sup>. The standard deviation for reduced models also increased significantly from 0.24 to 0.37 m s<sup>-1</sup> when the number of surveyed transects dropped from 27 (scenario 0) to 14 (scenario 1A) and remained high.

Performance statistics improved when photogrammetric transects were used to supplement the models (1B-3B). For example, supplemented scenarios 1B-3B all had similar mean error between 0.19-0.20 m s<sup>-1</sup>, median error 0.13-0.14 m s<sup>-1</sup>, standard deviation around 0.19-0.20 m s<sup>-1</sup>, and root-mean-squared error 0.24-0.26 m s<sup>-1</sup>. The maximum absolute error of 0.72-0.78 m s<sup>-1</sup> was smaller than 0.96 m s<sup>-1</sup> for scenario 1A and 0.78 m s<sup>-1</sup> for scenario 0.

Scenario 4, which was entirely based on photogrammetric transects had the smallest error of all models when compared to real-world measurements with a mean error of 0.17 m s<sup>-1</sup>, a median error of 0.14 m s<sup>-1</sup>, a standard deviation of 0.15 m s<sup>-1</sup>, root mean squared error of 0.2 m s<sup>-1</sup> and an absolute maximum error of 0.63 m. It is interesting to note that this photogrammetric-only model performs better than the 'Best Practices' scenario 0, although it remains difficult to explain why this is the case.

Table 4.11 Summary comparison of modelled velocity for each HEC-RAS scenario against field measurement at the calibration discharges.

Scenario	Model Number	Mean Error (m s <sup>-1</sup> )	Median Error (m s <sup>-1</sup> )	Standard Deviation (m s <sup>-1</sup> )	Max. ABS. Error (m s <sup>-1</sup> )	RMSE (m s <sup>-1</sup> )
<b>Traditional 'Best-Practices' Scenario</b>						
<b>0</b>	i	0.23	0.12	0.24	0.78	0.29
<b>Reduced Scenarios</b>						
<b>1A</b>	i	0.36	0.16	0.36	0.96	0.40
	ii	0.15	0.02	0.33	0.81	0.32
	Average	0.26	0.11	0.37	0.96	0.36
<b>2A</b>	i	0.24	0.24	0.18	0.66	0.21
	ii	0.30	0.15	0.31	0.76	0.36
	iii	0.27	0.26	0.35	0.70	0.36
	Average	0.27	0.18	0.29	0.76	0.29
<b>3A</b>	i	0.10	0.21	0.34	0.71	0.23
	ii	0.04	0.13	0.35	0.76	0.28
	iii	0.02	0.02	0.32	0.70	0.25
	iv	0.01	0.13	0.39	0.81	0.30
	Average	0.03	0.16	0.35	0.81	0.26
<b>Supplemented Scenarios</b>						
<b>1B</b>	i	0.13	0.11	0.13	0.57	0.15
	ii	0.14	0.12	0.15	0.63	0.19
	Average	0.20	0.13	0.20	0.72	0.26
<b>2B</b>	i	0.13	0.12	0.15	0.63	0.17
	ii	0.14	0.14	0.12	0.57	0.17
	iii	0.11	0.09	0.09	0.27	0.13
	Average	0.20	0.14	0.19	0.72	0.25
<b>3B</b>	i	0.13	0.09	0.13	0.57	0.15
	ii	0.14	0.14	0.14	0.65	0.18
	iii	0.11	0.10	0.08	0.32	0.12
	iv	0.12	0.12	0.10	0.31	0.14
	Average	0.19	0.14	0.19	0.78	0.24
<b>Photogrammetric Scenario</b>						
<b>4</b>	i	0.17	0.14	0.15	0.63	0.20

Flow depth measurements were observed to be skewed by the carry-over error in the photogrammetric DEM for transect 19, and similarly, six other transects (8, 12, 14, 16, 20 and 27) were found to skew the model output with an error greater than 0.3 m s<sup>-1</sup>. These transects are

all located at either a riffle zone (transects 8,12 and 14), a transition from the chute to run (transect 16) or a braid (transect 20), with several of them proving difficult to calibrate (e.g., transects 16,20, and 27). When those six transects were excluded from the analysis, the mean error decreased for scenario 0 from 0.20 to 0.11 m s<sup>-1</sup>, scenarios 1B-3B from 0.20 to 0.12 m s<sup>-1</sup> and scenario 4 from 0.17 to 0.12 m s<sup>-1</sup>. However, for reduced models (1A-3A), the mean error increased to 0.27-0.32 m s<sup>-1</sup>.

### 4.3.3 Modelled Habitat Potential

The next objective of the study was to assess the impact of transect density and photogrammetric supplementation on the estimates of habitat potential at a range of discharges. The hydraulic outputs for flow depth, velocity and wetted width at each transect were converted into transect-specific estimates of wetted usable width (WUW) using the HSI curves for juvenile Rainbow Trout (Raleigh *et al.* 1984). Wetted useable width uses the unit m m<sup>-1</sup>, which is the metre width of the channel that is usable habitat per metre length of the channel. The reach average WUW was then calculated based on the mean of all transects, weighted according to the channel length that each transect represented. This was done for each 0.5 m<sup>3</sup>s<sup>-1</sup> discharge interval between 0.5-20 m<sup>3</sup>s<sup>-1</sup>, for a total of 40 WUW-discharge pairings for each of the twenty HEC-RAS models (Table 4.12).

Table 4.12 Summary of transect distribution for all eight modelled scenarios.

Scenario	0	1A	1B	2A	2B	3A	3B	4
Number of Surveyed Transects	27	13-14	13-14	9	9	5-6	5-6	0
Number of Photogrammetric Transects	0	0	13-14	0	18	0	21-22	27
Number of Simulations	40	80	80	120	120	160	160	40
Transect Density (km <sup>-1</sup> )	34.62	16.66 - 17.98	34.62	11.53	34.62	6.41 - 7.69	34.62	34.62
Mean Distance between Transects (m)	28.88	55.71 - 60.00	28.88	86.67	28.88	130.00 - 156.00	28.88	28.88
x Channel Width	1.66	3.19 - 3.44	1.66	4.97	1.66	7.45 - 8.94	1.66	1.66

The WUW results for nine scenarios (1A-3A, 1B-3B, 4) were then compared graphically to the

‘Best-Practices’ scenario (0) by plotting the upper and lower bounds for each reduced and supplemented pairing (e.g., 1A and 1B) in Figures 4.17 to 4.20. For the Scenario 1A and 1B pairing shown in Figure 4.17, both the upper and lower bounds for Scenario 1A are noticeably greater than the outputs for Scenario 0 at 0.5-12 m<sup>3</sup> s<sup>-1</sup>. At all discharges modelled, the range of WUW estimates for Scenario 1B falls within 0.4 m of Scenario 0, unlike the WUW outputs for Scenario 1A which could differ from Scenario 0 by as much as 1.6 m at some discharges. Habitat estimates for Scenario 0 peaked around 0.5 m<sup>3</sup>s<sup>-1</sup> and tapered off to small values less than 0.5 m by discharges 12.5 m<sup>3</sup> s<sup>-1</sup>; whereas in Scenario 1A habitat peaks between 1-4 m<sup>3</sup> s<sup>-1</sup>, and the upper bounds remain well above 1 m of WUW through discharges greater than 12.5 m<sup>3</sup> s<sup>-1</sup>. The results for the Scenario 2A and 2B pairing (Figure 4.18) showed a similar pattern, with the key difference that the minimum bounds for Scenario 2A closely followed the habitat profile for Scenario 0.

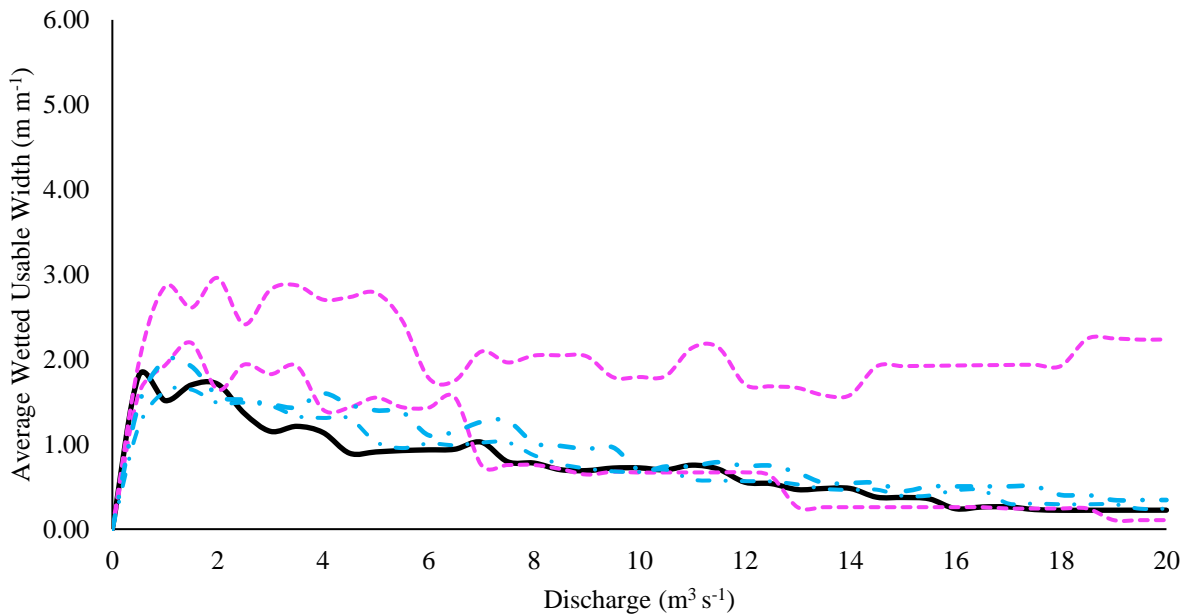


Figure 4.17 Graphical comparison of WUW estimates outputs from the ‘Best-Practices’ Scenario 0 (solid black line) against the upper and lower boundaries for the reduced Scenarios 1A (pink dashed line) and supplemented 1B (blue dashed line).

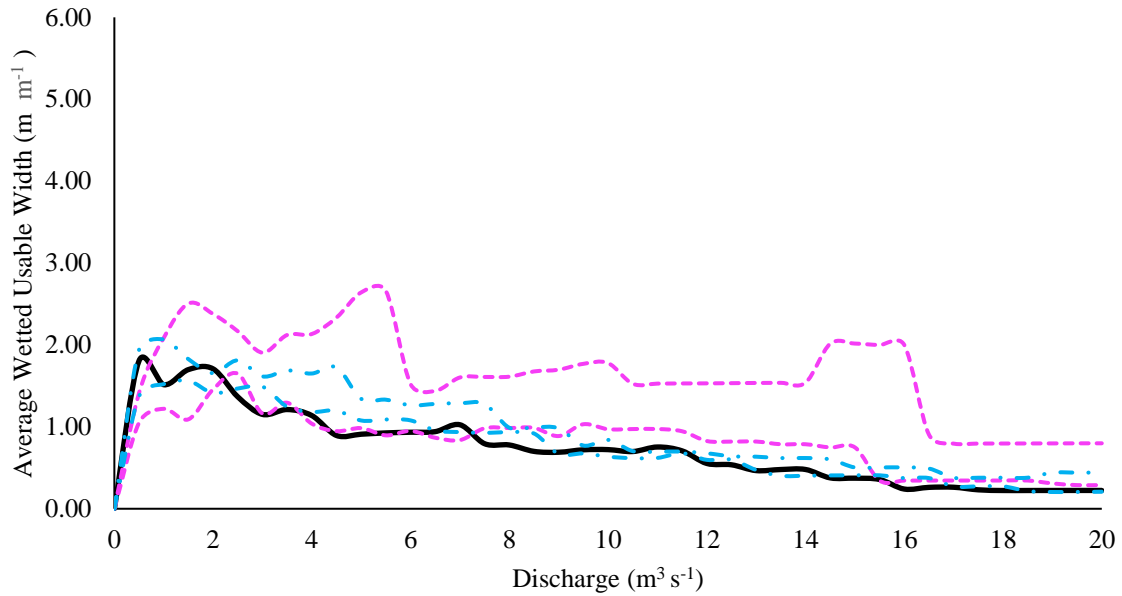


Figure 4.18 Graphical comparison of WUW estimates outputs from the 'Best-Practice' Scenario 0 (solid black line) against the upper and lower boundaries for the reduced Scenarios 2A (pink dashed line) and supplemented 2B (blue dashed line).

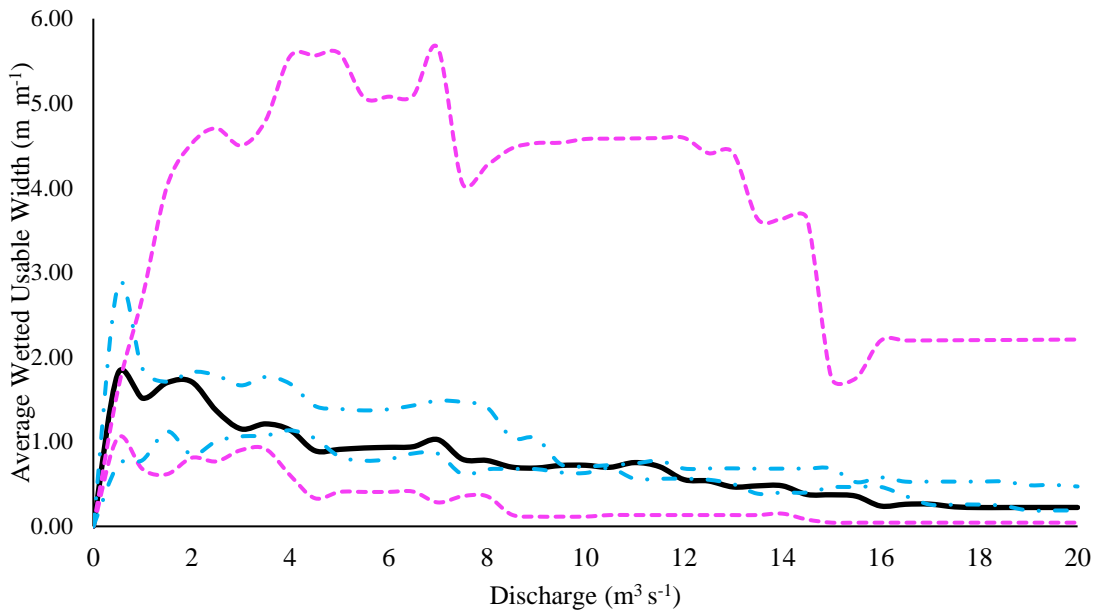


Figure 4.19 Graphical comparison of WUW estimates outputs from the 'Best Practice' Scenario 0 (solid black line) against the upper and lower boundaries for the reduced Scenarios 3A (pink dashed line) and supplemented 3B (blue dashed line).

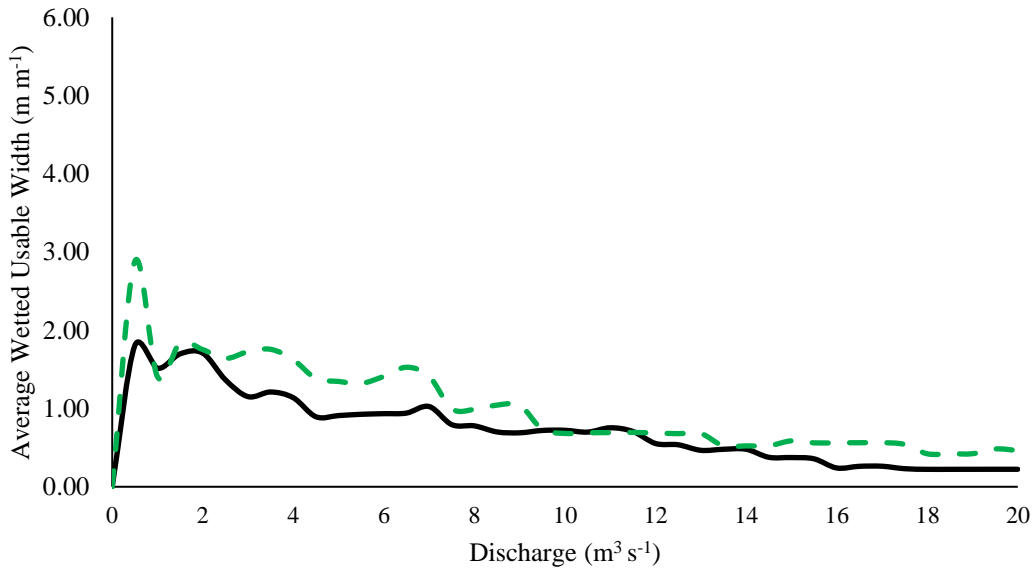


Figure 4.20 Graphical comparison of WUW estimates outputs from the ‘Best-Practice’ Scenario 0 (solid black line) against those from the purely photogrammetric Scenario 4 (thick dashed green line).

For the Scenario 3A and 3B pairing (Figure 4.18), the spread between the minimum and maximum outputs for the reduced model shows a significant increase, varying by ~4.5 m of WUW between discharges of 1.5-12.5 m<sup>3</sup> s<sup>-1</sup>. Additionally, the maximum habitat estimates for Scenario 3A peaked much later (~ 6 m<sup>3</sup> s<sup>-1</sup>) than what was observed in any other scenario and remain high (~2.2 m) through all modelled discharges. The spread between WUW estimates for Scenario 3B also increased compared to the previous supplemented Scenarios, with a maximum difference of ~2.1 m at 0.5 m<sup>3</sup> s<sup>-1</sup> (Figure 4.19). However, this large margin exists only for a short-range and the upper and lower bounds stay within 0.3-0.5 m of each other for the majority of modelled discharges, with the curves closely paralleling the outputs for Scenario 0. Finally, looking at Figure 4.17, the WUW curve for Scenario 4 produced habitat estimates similar to Scenario 0, albeit slightly greater at most discharges. In figure 4.21 below, the overall distribution of WUW estimates for all the supplemented (1B-3B) and photogrammetric scenarios (4) can quickly be assessed as having a much closer to the ‘Best-Practices’ scenario (0); whereas the reduced scenarios (1A-3A) all overestimate WUW quite significantly compared to ‘Best-Practices’ case, with scenarios 1A ( 13-14 transects) and 3A (5-6 transects) showing a far greater spread in WUWs than any of the other scenarios.

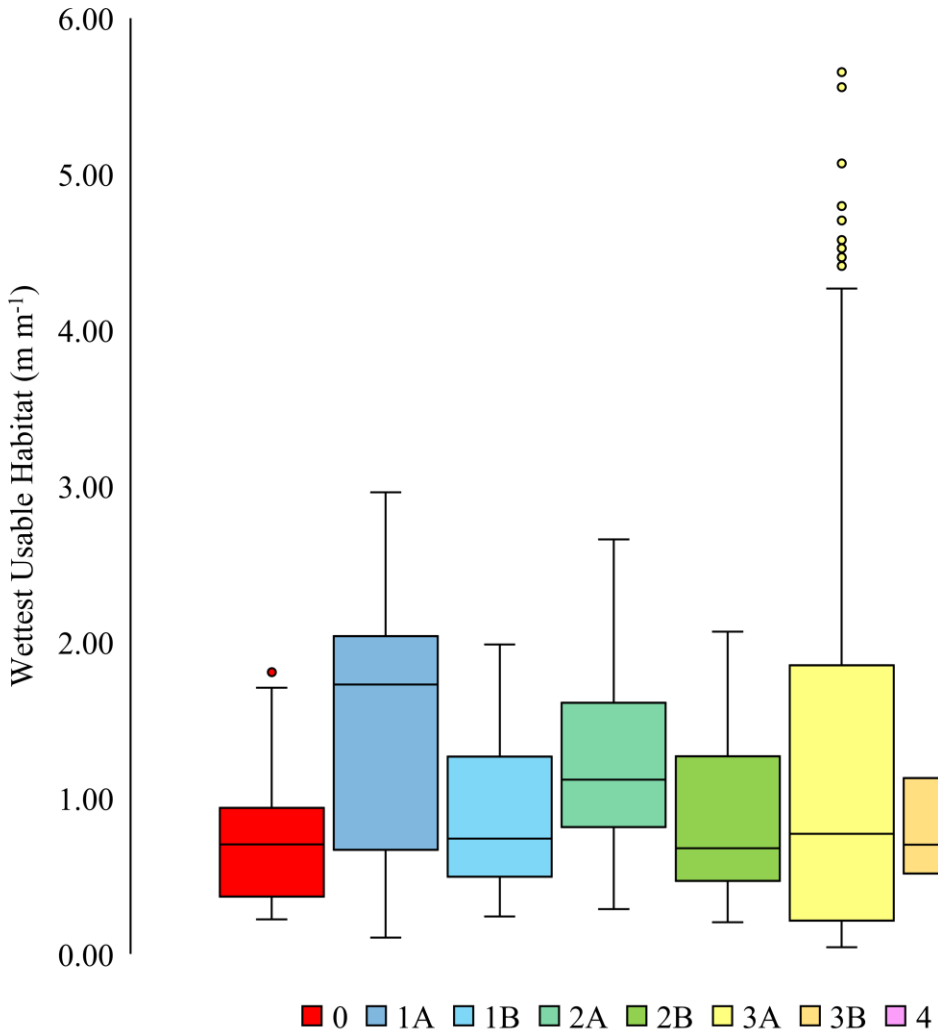


Figure 4.21 Summary box and whisker plot of WUW distributions for the: ‘Best-Practices’ (0) reduced (1A-3A), supplemented (1B-3B) and photogrammetric (4) scenarios.

To assess how the accuracy, precision and uncertainty of reach-scale WUW estimates were impacted by transect density for the UMC study site, a series of linear regressions were conducted. Each regression performed a pairwise comparison, with reach WUW as predicted by either a reduced or supplement model (e.g., Scenario 1A or 1B) matched against WUW from Scenario 0, for all 40 discharge intervals. A total of 25 such linear regressions were conducted, 19 of which were model-specific, with the outputs from only one model being compared against those from Scenario 0. The remaining six regressions followed the same procedure with the exception that the WUW outputs for a whole scenario, rather than individual models, were

simultaneously compared against the Scenario 0 estimates.

Examples of the regressions for each scenario are presented in Figures 4.22-4.28, including both the regression trendlines, as well as the upper and lower 90% confidence intervals. The full regression results, including the regression equation, standard error, correlation coefficient and percentage of outputs within the 90% confidence intervals are summarized in Table 4.13 that follows.

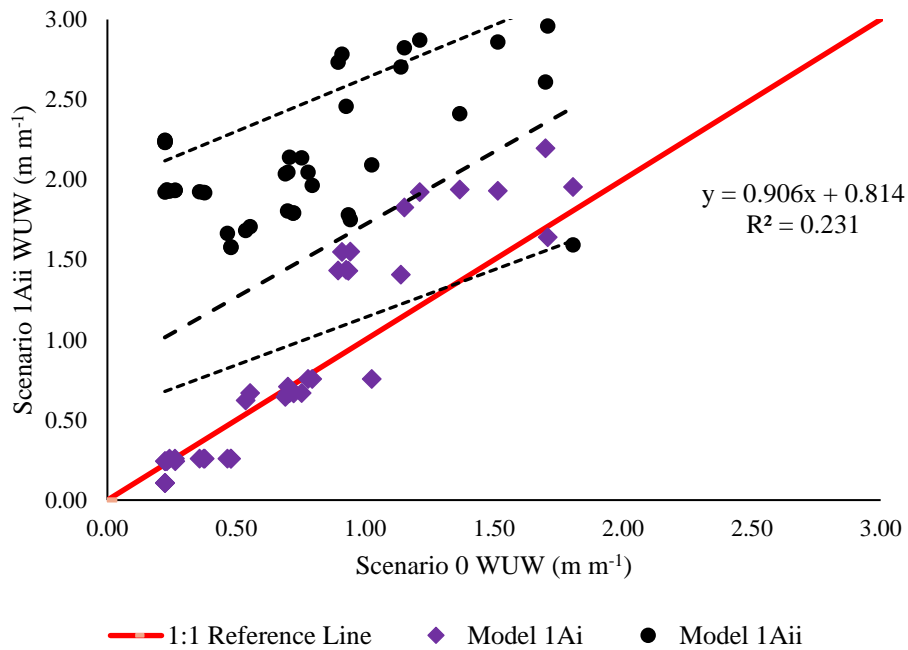


Figure 4.22 A comparison of WUW estimates modelled in Scenario 1A (reduced, transect interval = 2) against WUW outputs from Scenario 0 ( ‘Best-Practice ’ ) with the upper and lower bounds of the 90% confidence interval represented by the two dashed lines above and below.

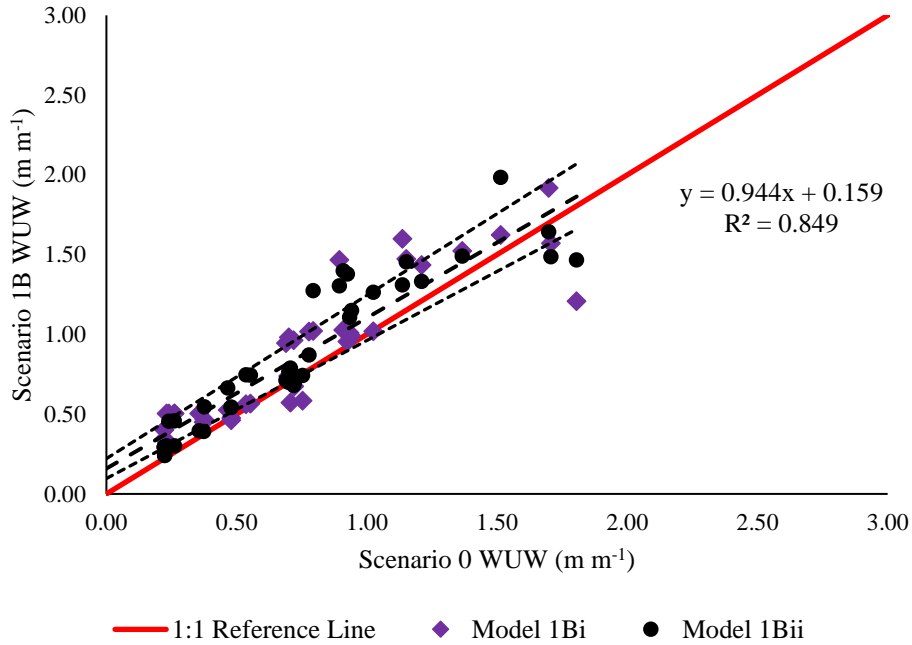


Figure 4.23 A comparison of WUW estimates modelled in Scenario 1B (supplemented, transect interval = 2) against WUW outputs from Scenario 0 ( ‘Best-Practice’ ) with the upper and lower bounds of the 90% confidence interval represented by the two dashed lines above and below.

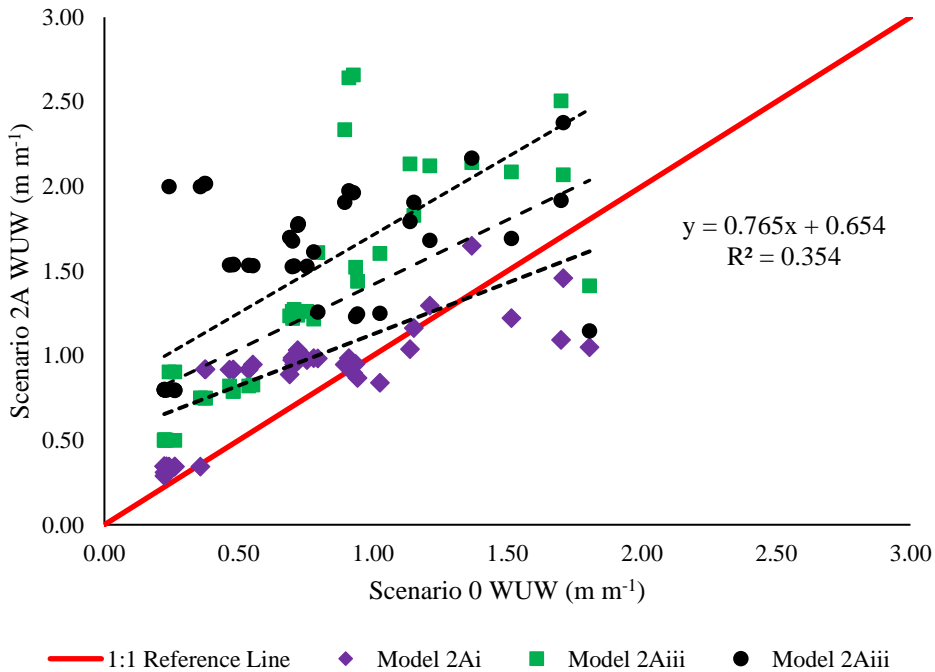


Figure 4.24 A comparison of WUW estimates modelled in Scenario 2A (supplemented, transect interval = 3) against WUW outputs from Scenario 0 ( ‘Best-Practice’ ) with the upper and lower bounds of the 90% confidence interval represented by the two dashed lines above and below.

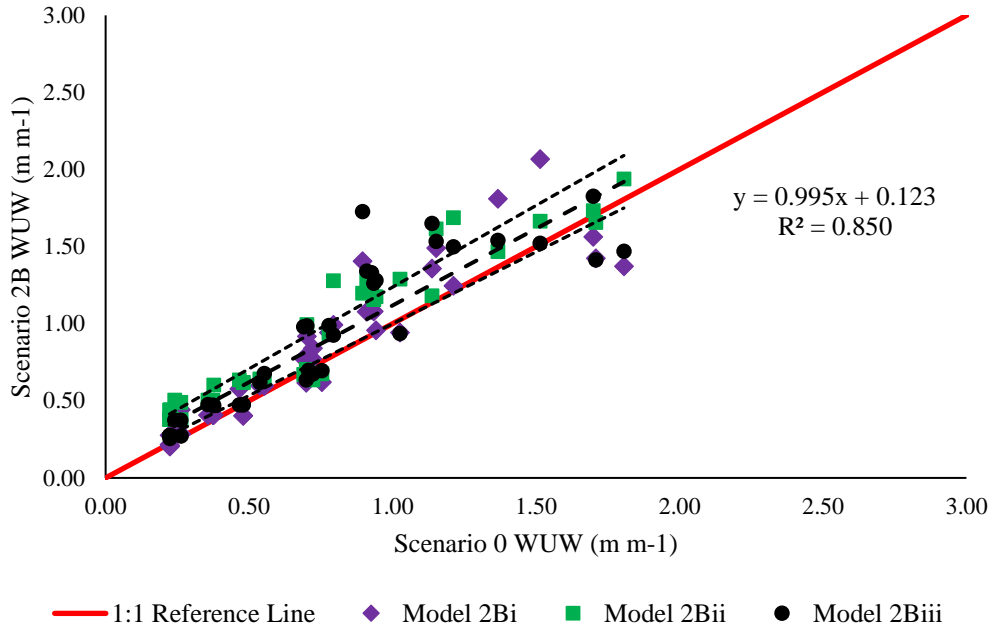


Figure 4.25 A comparison of WUW estimates for each transect modelled in Scenario 2B (supplemented, transect interval = 3) against WUW outputs from Scenario 0 (‘Best-Practice’) with the upper and lower bounds of the 90% confidence interval represented by the two dashed lines above and below.

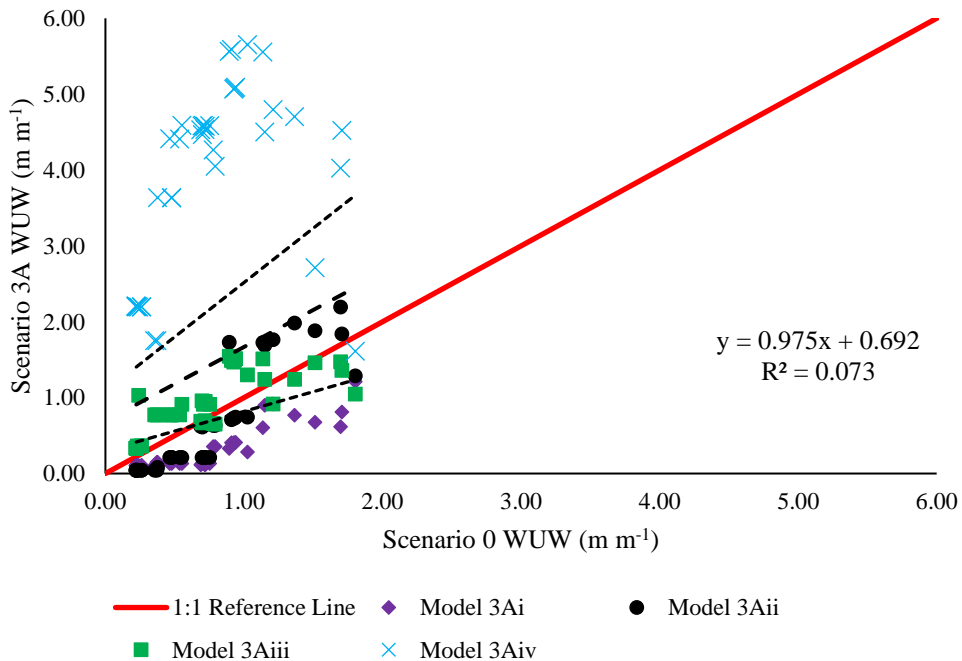


Figure 4.26 A comparison of WUW estimates modelled in Scenario 3A (reduced, transect interval = 4) against WUW outputs from Scenario 0 (‘Best-Practices’) with the upper and lower bounds of the 90% confidence interval are represented by the two dashed lines above and below.

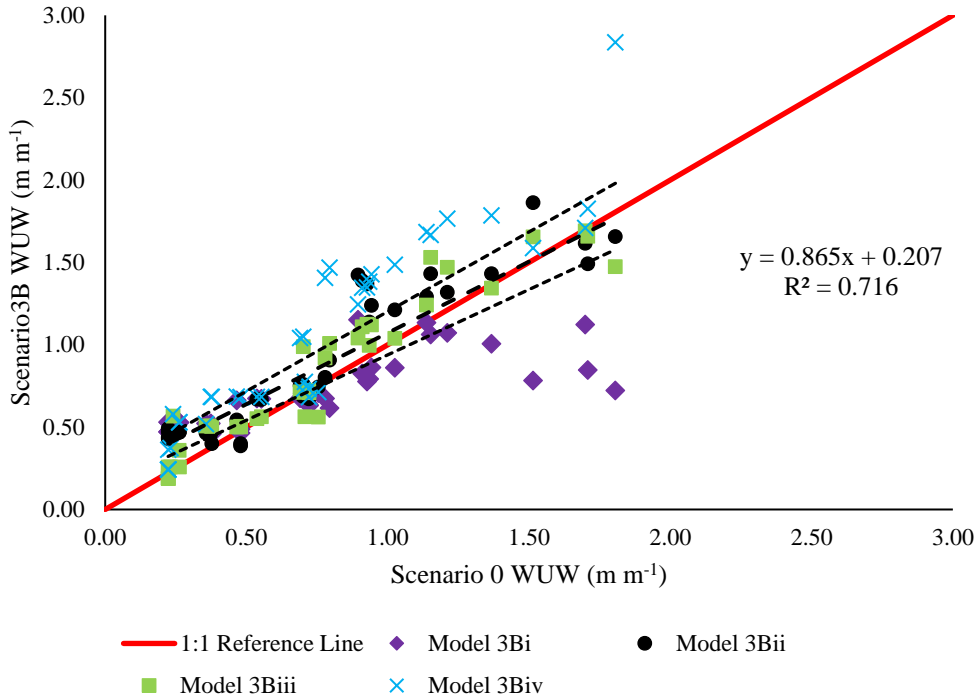


Figure 4.27 A comparison of WUW estimates modelled in Scenario 3B (supplemented, transect interval = 4) against WUW outputs from Scenario 0 ('Best-Practice') with the upper and lower bounds of the 90% confidence interval are represented by the two dashed lines above and below.

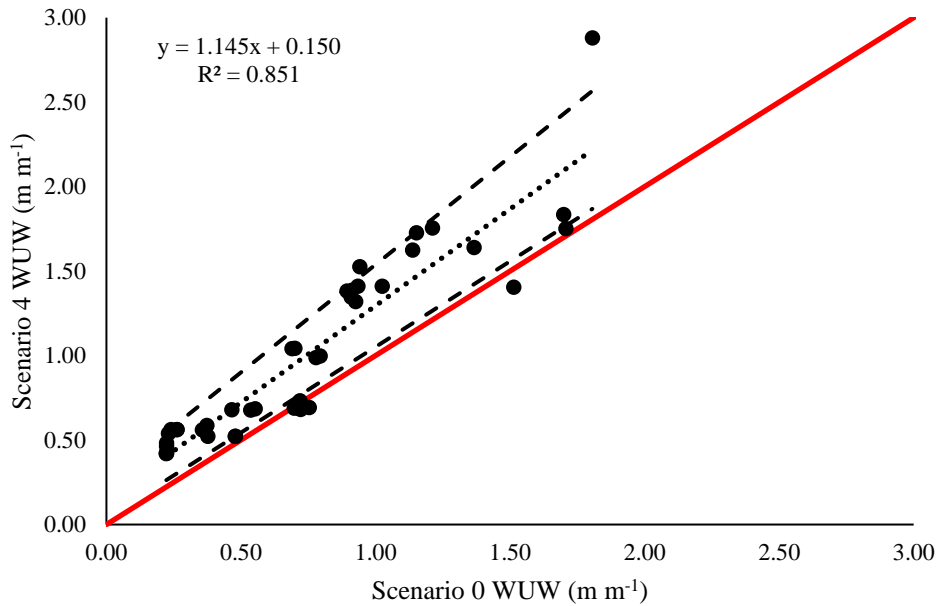


Figure 4.28 A comparison of WUW estimates for each transect modelled in Scenario 4 (photogrammetric only) against WUW outputs from Scenario 0 ('Best-Practice') with the upper and lower bounds of the 90% confidence interval represented by the two dashed lines above and below.

In Table 4.13 the standard error for all three reduced scenarios was observed to be quite large, with Scenario 1A error ( $0.739 \text{ m m}^{-1}$ ) equivalent to  $\sim 103\%$  of the mean WUW for Scenario 0 ( $0.72 \text{ m m}^{-1}$ ); the error in 2A decreasing to  $\sim 63\%$  ( $0.460 \text{ m m}^{-1}$ ) and 3A increasing massively to  $214\%$  ( $1.541 \text{ m m}^{-1}$ ). Similarly, the correlation coefficients for all reduced (1A, 2A and 3A) scenarios were below 0.40, with the outputs for Scenario 3A showing virtually no correlation with the habitat estimates from the ‘Best-Practices’ case with an  $R^2$  of 0.07.

Looking at Figures 4.22-4.22 for each Scenario, on average all the reduced models tended to overestimate habitat available compared to the “Best-Practices” scenario, as indicated by the majority of WUWs plotting well above the 1:1 reference line for Scenario 0. Only models 3Aiii regularly underestimated habitat, which was a surprise as more parity was expected in the model’s chances to either over or underestimate WUW as transects were reduced.

Increases in uncertainty were both visually and numerically assessed by evaluating the spread between the upper and lower 90% confidence intervals (CIs) (Figures 4.22-4.28, Table 4.13), similar to what Williams (1996, 2010), Gard (2005) and Alleyon *et al.* (2012) reported. For Scenario 1A (Figure 4.19), which was comprised of two very distinct models (Table 4.13) the spread between upper and lower CI slope coefficients was quite large. For Scenario 2A, the distance between the upper and lower CIs tightens (Figure 4.23). These improvements disappear when transect numbers are reduced to five or six in Scenario 3A (Figure 4.25) with the spread in confidences increasing to a staggering 0.801, with both large over and underestimates of WUW possible within the 90 % CI.

Table 4.13 Regression result comparing the WUW estimates for each scenario against the ‘Best-Practices’ Scenario 0.

Scenario	Model	n	Standard Error (m m <sup>-1</sup> )	R <sup>2</sup>	Slope Coefficient	Intercept	Upper 90% Slope Coefficient	Lower 90% Slope Coefficient
<b>Reduced Scenarios</b>								
<b>1A</b>	i	40	0.242	0.866	1.362	-0.159	1.537	1.186
	ii	40	0.352	0.251	0.450	1.787	0.706	0.19
	Total	80	0.739	0.231	0.906	0.813	1.217	0.594
<b>2A</b>	i	40	0.207	0.636	0.606	0.400	0.732	0.481
	ii	40	0.388	0.663	1.200	0.405	1.43	0.966
	iii	40	0.399	0.236	0.489	1.157	0.730	0.248
	Total	120	0.460	0.354	0.765	0.654	0.922	0.607
<b>3A</b>	i	40	0.139	0.771	0.562	-0.104	0.645	0.478
	ii	40	0.311	0.800	1.374	-0.391	1.563	1.187
	iii	40	0.268	0.569	0.679	0.406	0.841	0.517
	iv	40	1.156	0.202	1.286	2.858	1.983	0.576
	Total	160	1.541	0.073	0.975	0.692	1.432	0.519
<b>Supplemented Scenarios</b>								
<b>1B</b>	i	40	0.186	0.825	0.894	0.194	1.006	0.781
	ii	40	0.177	0.863	0.979	0.139	1.086	0.873
	Total	80	0.180	0.843	0.937	0.166	1.012	0.861
<b>2B</b>	i	40	0.190	0.848	0.993	0.078	1.108	0.878
	ii	40	0.144	0.906	0.986	0.176	1.07	0.899
	iii	40	0.215	0.818	1.007	0.116	1.137	0.877
	Total	120	0.186	0.850	0.995	0.123	1.059	0.931
<b>3B</b>	i	40	0.131	0.600	0.353	0.441	0.432	0.274
	ii	40	0.162	0.867	0.918	0.192	1.016	0.819
	iii	40	0.137	0.911	0.973	0.083	1.055	0.889
	iv	40	0.216	0.866	1.216	0.111	1.346	1.086
	Total	160	0.242	0.716	0.865	0.207	0.937	0.793
<b>Photogrammetric Scenario</b>								
<b>4</b>	i	40	0.217	0.851	1.145	0.150	1.278	1.014

When the models are supplemented with photogrammetric transects, the standard error is reduced by a minimum of 0.274 m m<sup>-1</sup> (Scenarios 2A-2B) up to 1.30 m m<sup>-1</sup> (Scenarios 3A-3B), which is equivalent to 38-180 % of the true mean WUW from the ‘Best-Practices’ model. Both Scenarios 1B and 2B produced a similar standard error (0.180 and 0.186 m m<sup>-1</sup>) that was equivalent to ~25% of the Scenario 0 mean, whereas Scenario 3B had an error of 0.242 m m<sup>-1</sup> or

33% of the ‘true’ mean, respectively.

Equally dramatic were improvements observed in the correlation coefficients and tightening of the confidence intervals when supplementation occurred. Compared to the reduced scenarios, which all had insignificant correlation values (i.e., less than 0.5), the  $R^2$  for Scenario 1B was 0.86, and Scenario 2B was 0.85, with only Scenario 3B decreasing to 0.72. Likewise, the spread in the 90% confidence intervals was similar for all supplemented models and significantly smaller than seen previously in reduced models (Figures 4.21-4.26). This is visually apparent when comparing the paired regressions (Figure 4.21-4.27), with each of the supplemented scenarios following the ideal 1:1 reference line for ‘Best-Practices’ much more closely than matched reduced scenarios.

Unexpectedly, the photogrammetric only Scenario 4 replicated the results of the ‘Best-Practices’ scenario better than any of the reduced models. This was demonstrated in the regression results for Scenario 4, which included: 1) a standard error of 0.21 m m<sup>-1</sup> or 30%; 2) a correlation coefficient of 0.85, and 3) spread in the 90% confidence interval comparable to the supplemented Scenarios 1B-3B (Figure 4.25). A key difference from the previous scenarios was that habitat was overestimated compared to the ‘Best-Practices’ scenario with a slope coefficient of 1.145, and even the lower bounds for 90% had a slope greater than 1 (Table 4.12, Figure 4.27).

At the chosen significance level of 0.05, the F values for all regressions were found to be significant.

## Chapter 5 . Discussion

The primary objective of this study was to determine whether the application of the SfM-approach to supplement topographic data would lead to significant gains in accuracy and confidence of Salmonid habitat modelling in traditionally challenging mountainous environments. Several key observations made during the study will be discussed in this section, including:

- The need for redundancies in data collection efforts, regardless of methodology, to ensure confidence in the habitat assessment when working in high-gradient streams.
- The effectiveness of the UAV-SfM approach at extracting reliable estimates of channel bathymetry.
- The challenges of utilizing one-dimensional hydraulic models to make habitat inferences in high-gradient streams with complex morphology
- The advantages of the proposed approach using photogrammetric supplementation within hydraulic models for assessing WUW and WUA in mountainous streams.

### 5.1 Field Data Collection Efforts

The study reach for Upper Mission Creek was located at a site that has traditionally been described as challenging for IFIM assessment (Lewis *et al.*, 2004; HEC-RAS, 2021). This is because of logistical and technical challenges including 1) multiple sub-reaches with slopes greater than two percent (Table 4.1); 2) numerous side channels; 3) channel substrate dominated by very coarse material (diameter greater than 0.1 m, Figures 4.6-4.10); and 4) the presence of LWD (Figure 5.1).



*Figure 5.1 Transect 26 as viewed from the right bank of transect 25, Aug. 1st, 2019.*

While these features are common characteristics of mountainous streams, they can introduce uncertainty into IFIM results in two principal ways. The first is that natural channel irregularity produces flow hydraulics with complex three-dimensional patterns. Yet, the majority of freely available modelling programs are only capable of modelling flow in one or two dimensions, and therefore model outputs for locations with complex morphology (e.g., LWD forced pool) may be unreliable (Gibson, 2013; Cienciala and Hassan, 2016). The sampling of channel hydraulics at a broad range of discharges can alleviate some of this uncertainty through better calibration, but this leads to a second source of uncertainty. With more rugged terrain to navigate, and often greater distances from urban centres and passable roads, traditional IFIM surveys of high mountain streams can rarely be completed in one day (Gronsdahl, 2019; Hettrich, 2020; Gronsdahl *et al.* 2021). This study was no exception with fourteen days, each eight to ten hours long, required for a crew of two to three to complete all engineer's level and wading rod surveys for the ~750 m study reach.

This is significant for hydraulic modelling exercises because the model structure presumes that the topographical data for all the transects are acquired during a short period of stable conditions.

If the transect bathymetry changes between surveys, then all transects should be re-surveyed to reflect the new configuration. But this is rarely done due to constraints of time and expense. Rather the assumption is made that there has been no significant change between subsequent survey dates, which may or may not be the case depending on the discharge regime and time between surveys.

Discharge records (Figure 4.2) and field observations of minor alterations to gravel beds, with the addition of LWD (Figure 4.3) at transects 17-22 between the Jul. 23<sup>rd</sup> and Aug. 1<sup>st</sup> surveys indicate that constancy of transect bathymetry cannot be assumed for the surveyed data set. Without repeat surveys, it would be impossible to quantify if any significant morphological alterations (greater than sampling error) did occur during the study period.

Therefore, while this study acknowledges the additional challenges that come with surveying instream habitat in mountainous environments, multiple redundancies were built into data collection efforts, to both reduce and assess the uncertainty (Table 4.2). The principal redundancies included:

- 1) Four measurements of pin elevations, twice with the standard surveying convention and twice with an RTK-DGPS (Table 4.3).
- 2) Two measurements of transect width, once each with a tape measure and RTK-DGPS (Table 4.4).
- 3) Three sets of water surface elevations matched to discharges, for calibrating the hydraulic models. Each data set was sampled with a different technique: engineer's level, wading rod and SfM.
- 4) Three measures of transect bathymetry, the first sampled according to the standard surveying convention, the second with a wading rod and finally using the UAV- SfM approach (Tables 4.6 and 4.7).
- 5) Three drone flights, with two test flights to identify challenges and optimize image quality before the third and final flight.

Upon examining the assessments of data collection efforts (Section 4.2.2) it became apparent that

the redundancies were critical in overcoming the inherent environmental challenges and generating a robust dataset for modelling comparisons. One such outcome of comparing redundant datasets was the identification of discrepancies between the two RTK-DGPS surveys, with the Sept. 30<sup>th</sup> survey, in particular, showing potential errors. The exact reasons for the poor communication between the rover and base station on this survey date cannot be confirmed. Even before this dataset was processed, a decision had already been made to repeat the GPS survey because of communication issues. Several point measurements took upwards of 15 minutes to acquire a signal lock for each control point. Under favourable conditions, the time required for a coordinate lock would be between 30 – 120 seconds. It is possible that satellite coverage during these periods was not as extensive as during the Nov. 11<sup>th</sup> survey. Regardless, the Nov. 11<sup>th</sup> RTK-DGPS survey was found to yield faster point acquisition, and the resulting coordinates fit existing maps for the area very closely.

When the Nov. 11<sup>th</sup> GPS survey was compared to the engineer's level surveys, neither methodology stood out as superior to the other. When transect pin elevations from the surveys were compared (Figure 5.2), the statistical outputs for the mean, mean absolute, median, and standard deviation of error were virtually identical (Table 4.3). That is not to say that the error was insignificant; in fact, the pin-to-pin elevations at four transects (2,9,17 and 22) were off by more than 0.1 m when two surveys were compared. Rather, this implies that the magnitude and frequency of sampling errors are due to human factors (e.g., inexperience, levelling to bubble, placement of rods) and environmental conditions (e.g., inclement weather, tree canopies, etc.) were of the same magnitude for the two contrasting methodologies.

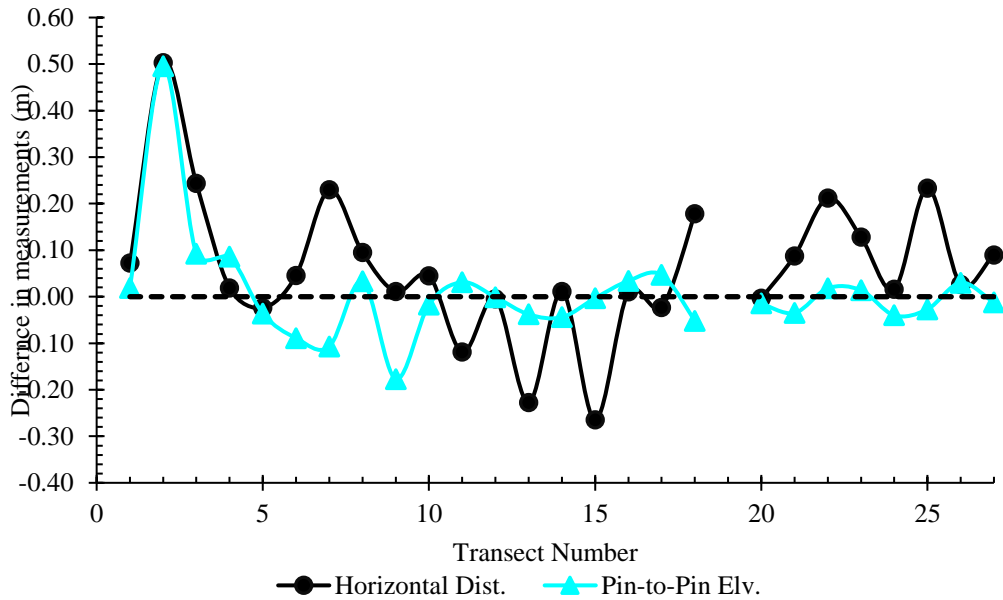


*Figure 5.2 Difference in engineers' level and GPS survey measurements for pin-to-pin differences in elevation and horizontal distances across each transect.*

This hypothesis was further supported by comparisons of pin-to-pin horizontal distances at all transects (Table 4.4, Figure 5.2), with a tape measure and GPS distances aligning within 0.06 m or 0.25 % of each other on average. As previously discussed in Chapter 4, the last three survey points on the left bank of transect 2 were identified as troublesome in both the engineer's level and GPS surveys due to dense foliage obstructing the line of sight for the engineer's level and the line of communication between the base station and rover (Figure 5.2).

Aside from these few points at transect 2, no pattern was observed in the errors (Figure 5.2). Most of the uncertainty appears to have been due to random sampling error, likely associated with human and equipment imprecision. This evaluation of randomness is supported by the median error of ~0.00 m as well as the standard deviation of error being equal to or less than the average diameter of the boulder-cobble substrate that dominated the majority of the channel.

As previously discussed, the conditions for the UMC study site are characteristic for topographic surveys in steep mountain streams of the Pacific Northwest, regardless of the methodology used. Thus, it would not be unusual to eliminate from consideration suspect measurements such as those found on the left bank of transect 2.

In general, there are two strategies available to address transects where environmental challenges

produce results with little confidence. First, if issues are noticed immediately in the field, the location of the transect can be adjusted slightly, either upstream or downstream until a clearer line of sight with the engineer's level or better communication between the GPS rover and base station is achieved. Although this might be considered a best practice, it may contribute to well-known issues of small sample size because of the time required for field crews to re-establish transects. Additionally, unskilled or rushed field crews may not notice points of concern until data compilation and analysis have begun, often long after the opportunity to address the issue in the field has expired.

Second, if the position of the transect cannot be easily adjusted in the field, the only option is to remove the problematic transect from the dataset before any hydraulic modelling is begun. Again, this contributes to the issue of reduced sample size and the possibility that the survey has failed to incorporate sufficient numbers of transects for there to be reasonable confidence in the modelling effort (Payne *et al.*, 2004; Williams, 2010; McParland *et al.*, 2014; Tamminga, 2016; Grons Dahl, 2019; Backes *et al.*, 2020). The obvious solution to this issue is to sample more transects than needed with the expectation that some will need to be removed during quality control exercises. However, the amount of effort required for traditional transect surveys often runs into budgetary and time constraints preventing this from being a practical solution. Hence, there is strong motivation to develop remote sensing techniques, such as the UAV-SfM approach, that may allow for significantly more transects to be captured photogrammetrically in the same amount of time as a traditional IFIM assessment (Carbonneau and Piégay, 2012; Biron *et al.* 2013; Woodget *et al.*, 2014; Tamminga, 2016; Dietrich, 2016; Lane *et al.*, 2020).

## **5.2 Photogrammetric Sampling**

Numerous studies have utilized the UAV-SfM approach for some portion of their data collection efforts (Flener *et al.*, 2013; Woodget *et al.*, 2014; Dietrich, 2016; Tamminga, 2016; Shintani and Fonstand, 2017; Wheaton *et al.*, 2017; Benjankar *et al.*, 2018; Lane *et al.*, 2020), concluding that the methodology was sufficiently reliable and expedient for sampling stream channel topography. Specifically, these studies found that: 1) observed errors were small when using UAV-SfM on small streams; and 2) uncertainty was comparable to that inherent to GPS surveys. The results from this study reaffirm these conclusions.

The measured standard deviation and RSME of 0.11 m for UMC were greater than the 0.077-0.059 m reported in Dietrich (2016) but less than 0.125 m observed in Tamminga (2016) and 0.17 m in Shintani and Fonstad (2017). In the case of Tamminga (2016), which was conducted in the 1 km reach of the Elbow River in Southern Alberta, not too distinct from the mountains of Southern BC, the SDE was comparable to this study even after the application of a refraction index which significantly reduced the mean error. Dietrich (2016) completed a study that observed a smaller SDE on a ~250 m long riffle-pool sequence with minimal white water on the White River, ID. The mean error was likewise somewhat smaller at -0.011-0.014 m (Dietrich 2016), compared to 0.03 m for the Sept. 30<sup>th</sup> survey of UMC. Shintani and Fonstad (2017) studied a reach that was only ~140 m long but had numerous large boulders and issues with white-water refraction and reported a standard deviation greater than for this study.

However, it bears significance that all of the former studies applied a refraction index correction, unlike this study. Prior to the application of a refraction index, Woodget *et al.* (2014) observed that the mean error did not exceed 0.089 m, comparable to this study. Woodget *et al.* (2014) were able to later apply Jerlov's index (Jerlov, 1976) as the study reach was relatively homogenous at only 100 m in length with a maximum depth of 0.7 m, had clear water with little tannin and a gentle gradient. The application of Jerlov's index reduced the maximum error to 0.053 m, considerably less than the UMC study (0.7 m, Appendix C) as well as Dietrich (0.381 m, 2016) and Tamminga (0.5 m, 2016).

Among all of these comparisons of the mean, median, RMSE and SDE for photogrammetric surveys, the discrepancies between pre-existing research and this study were at most 0.05 m and often less than 0.02 m. This is especially significant because it is still comparable to or less than the sampling error in the engineer's level and wading rod surveys for UMC, despite the differences in geography, environmental conditions and equipment used in the other studies.

To provide additional context, Dietrich (2016) reported survey accuracy and precision as mean error and standard deviation measured as a percentage of the flying height (distance from the ground to the UAV sensor), which was 0.02% and 0.1%, respectively. By comparison, this study had a larger relative error with a mean of 0.1 % and a standard deviation of 0.38% flying height. This was expected given the larger and more heterogenous study reach, but the total error was

still less than 1% of the flying height. Critically, as a percentage, this error was significantly smaller than was observed for measurements of horizontal distance with the GPS and tape measure, where the mean error was 0.25 % and the standard deviation was 1.01 %. This suggests as stream width increases so too does the relative accuracy of the photogrammetric surveys as well as those for traditional surveys with an engineer's level, wading rod and tape measure.

Unlike the majority of study sites described in the literature (Carbonneau and Piégay, 2012; Biron *et al.*, 2013; Woodget *et al.*, 2014; Tamminga, 2016; Lane *et al.*, 2020), the water in UMC was rich with tannins and had steep riffles and rapids dominated by white water. At low flows when the sampling was done, the lightly coloured cobbles and boulders that dominated the dry bank had a very high albedo, making the contrast between the much darker, tannin-rich water and bright shoreline intense. The small 1-inch sensor on the DJI Phantom 4, with limited dynamic range, was unable to properly expose the images without additional lens filters. This became apparent when trying to identify the locations of the initial ground control points (see Chapter 3, Figure 3.8). For stretches of white water, the photogrammetry software extracted notably shallower flow depths than reality, due to excessive refraction.

With the application of a CPL filter and high contrast markers (Figure 5.8), these sources of error were not introduced into the final Sept. 30<sup>th</sup> flight in any noticeable way. These photographic adjustments resulted in the ground control marker being easily identifiable during the processing of the orthographic photo and DEM. The results were quickly verified with photogrammetric transect profiles closely matching those measured with traditional techniques (Table 4.4 and Figures 4.12-4.13). In fact, after accounting for the influence of vegetation, the mean and median error for the photogrammetric DEM was minimal and observed to be less than those reported by Woodget *et al.* (2014) and comparable to those in Pyle *et al.* (1997) and Carbonneau *et al.* (2001). The mean and median errors were still slightly greater than was reported in Tamminga (2016), Dietrich (2016), and Shintani and Fonstad (2017), but the discrepancies between studies were well within the drone specifications, with a stated vertical position accuracy of  $\pm 1.5$  cm and absolute horizontal accuracy in associated photogrammetric models of  $\pm 5$  cm (DJI 2018).

### 5.3 Hydraulic Modelling

When evaluating the results of the hydraulic modelling exercises, two key observations need to be discussed: 1) one-dimensional models are inadequate for accurately simulating flow hydraulics at locations with complex morphology; and 2) increasing the number of sampling points at each transect (i.e., increasing the detail in the channel cross-section) had a much greater impact on the accuracy of the hydraulic model than the source of the data (traditional or photogrammetric).

Addressing the first point, after eleven iterations of steady-flow analysis to calibrate the model, there remained notable discrepancies between measured and modelled flow depths and velocities at several transects. This was not surprising as the ability to compute variable hydraulic conditions laterally across transects has long been known as a key weakness of one-dimensional hydraulic models and a source of criticism against the IFIM approach (Gibson, 2013; Stalnaker *et al.*, 2017; Reiser and Hilbert, 2018; Benjankar *et al.*, 2018).

Modelled predictions for flow depth were reasonably precise and accurate with twenty-one of twenty-seven transects having less than 0.1 m of error. While not ideal, six of these transects (with errors between 0.1 - 0.24 m) featured morphological characteristics, such as perched braids or LWD, known to be especially challenging for both 1D and 2D hydraulic models. It is difficult to compare this observed error to other studies as both the literature and the majority of technical manuals for IFIM assessments (Lewis *et al.*, 2004; HEC-RAS, 2019; SEFA, 2020) recommend that these morphological units be excluded from the hydraulic modelling exercises due to reduced confidence in the transect specific outputs. Aside from these six challenging transects, the remaining twenty-one transects had less than 0.1 m of error in the elevation of the water surface, with seventeen having less than 0.05 m of error and thirteen below 0.025 m.

This degree of error was deemed satisfactory and within expectation for 1D hydraulic modelling exercises given the site conditions and observed natural variability. Specifically, the variability in average water surface elevation modelled for each transect was found to be similar in magnitude to both in-field observations and measurements of lateral variability across transects (Figure 4.16, Table 4.9). The mean deviation of the modelled water surface from the measured mean was only 0.04 m (see Section 4.3.1), whereas the measurements of the waterline elevation at the left

and right banks deviated from the measured transect means by 0.00-0.02 m.

When looking at the mean and standard deviation from the measured waterline, the modelled mean was virtually indistinguishable from the natural variability observed in the left and right bank measurements. Given the complex and steep morphology of the UMC study site, a laterally uniform water surface from the left bank to the right bank could only be assumed for three glide transects (transects 4, 18 and 24). At the remaining twenty-four transects, the curvature and gradient of the channel, as well as the large substrate and occasionally LWD, tilting of the water surface, often as great as 0.05-0.1 m. At several of the rapids, the presence of large boulders ( $D \sim 50-100$  cm) caused localized swells and waves where the flow was forced through narrow choke points with depressions in water surface elevation in the immediate wake behind the boulders. For the rapids (e.g., transect 6, Figure 5.6) these swells, and depressions consistently produced differences of 0.10-0.20 m in water surface elevation between the left and right banks on different survey dates.



*Figure 5.3 Transect 6 as viewed from the left bank (July 7th, 2019)*

Overall, though, compared to a reach average depth of 0.21 m (Figure 4.4) the average model error was minimal with a mean of -0.01 m (-5%) and a median of 0.00 m (0%) but with an SDE of 0.06 m (Table 4.11) and a coefficient of variation of ~28%. This suggests that the performance of the 1D model was sufficiently accurate at predicting flow depths for most transects. However, at critical locations with complex morphology and three-dimensional flow patterns (e.g., transects 7, 16, 18-20, 22 and 27), the 1D model produces a larger error, which leads to a relatively large degree of uncertainty for the entire reach taken as a whole.

In much of the referenced literature, the accuracy and precision in hydraulic modelling outputs were evaluated against in-stream measurements of depth only, with no measurements of flow velocity (Tamminga, 2016). Alternatively, the 1D hydraulic modelling outputs were compared against 2D model outputs, with the latter assumed to be the most accurate if correctly calibrated for water surface elevations (Gard, 2009; Gibson and Pasternack, 2016; Benjankar *et al.*, 2018). The UMC study differed in this regard in that model predictions of mean flow velocity were compared directly to instream measurements of mean flow velocity for each transect at the calibration discharge, in addition to the usual assessments of flow depth between model and field measurements.

For the UMC study reaches, the model predictions of flow velocity were notably worse than estimates of flow depth. Compared to the average measured flow velocity of  $0.28 \text{ m s}^{-1}$  for the study reach, simulations from the 'Best-Practices' HEC-RAS model overestimated velocity by  $0.12 \text{ m s}^{-1}$  (+42%) to  $0.23 \text{ m s}^{-1}$  (+82%) according to the median and median error, with an SDE of  $0.24 \text{ m s}^{-1}$  for a coefficient of variation of ~86%. While greater than hoped for, this overestimation of flow velocities was expected because of the tendency for the 1D model to underestimate flow depth and the inability to make reliable inferences in areas with complex 3D flow patterns (e.g., LWD-forced pools) (Gibson, 2013; Stalnaker *et al.*, 2017; Reiser and Hilbert 2018; Benjankar *et al.*, 2018).

Nevertheless, a significant portion of the error in the HEC-RAS model output can be assigned to uncertainty surrounding the instream measurements of flow velocity. Mean flow velocity was measured at each wetted sampling point with a depth greater than 0.05 m, using a Marsh McBirney Flow Mate mounted on a wading rod at 0.6 depth from the surface, following the

standard BC procedures (Lewis *et al.*, 2004). However, several studies have reported that for high gradient, coarse-gravel bed streams, vertical velocity profiles for sampling points can often be irregular and non-logarithmic, especially if there is localized turbulence imparted from the presence of LWD or boulders (Nowell and Church, 1979; Jarrett 1990; Cienciala and Hassan, 2016). “A logarithmic velocity profile does not develop because of the extreme drag from the cobble and boulder bed material and the high-velocity flow near the water surface” (Jarrett 1990, 426). As the standard procedure assumes a relatively steady and uniform flow regime, measurements taken at 0.6 depth in areas of irregular flow may not be representative of the true mean velocity. Jarrett (1990) found that for high gradient, shallow-depth rivers that are common to mountainous areas the standard procedures often produce an underestimate of the true average velocity. Working on two separate ~ 100 m reaches of East Creek along the Southern BC coast, Cienciala and Hassan (2016) reported that the inherent variability around sampling in-channel hydraulics was large, with local values for depth, velocity and shear force having as much uncertainty as 21%. Therefore, it can be stated that the dynamic and turbulent nature of steep mountain streams leads to inherently large degrees of sampling variability even when working at smaller scales and higher densities.

Highlighting the habitat significance of such hydraulic heterogeneity, Naman *et al.* (2020) found that areas of irregular vertical velocity gradients, imparted by extreme bed roughness or flow obstructions (e.g., LWD) are heavily utilized by Pacific Salmonids, such as Rainbow Trout. This is because the low-velocity zones provide ideal holding water, with minimal energy expenditures, yet also provide a regular supply of prey invertebrates, that drift downstream in the nearby high-velocity zones, Naman *et al.* (2020). Field observations from UMC support this, with greater-than-expected numbers of juvenile RBT in the UMC (~ 600 total) observed to be concentrated in areas of ‘pocket water’ in the rapids or immediately downstream of LWD.

In order to more completely evaluate the accuracy of velocity estimates from the HEC-RAS model, the model would have to be calibrated for a broad range of discharges, instead of just two. In addition, more than 100 vertical velocity profiles would need to be sampled for each discharge according to Cienciala and Hassan (2016). This goes far beyond the scope of most IFIM assessments in terms of resources for both data collection and analyses.

On a positive note, increasing the number of sampling points per transect was observed to notably improve the accuracy of flow velocity predictions. Specifically, when comparing error in mean flow velocities, the entirely photogrammetric scenario 4 with ~1000 sampling points had a significantly smaller mean error, maximum absolute error and standard deviation compared to the 'Best-Practices' scenario 0 with ~20-60 sampling points per transect. This was unexpected because the model conditions such as bed roughness, contraction and expansion factors were calibrated for the 'Best-Practices' model to match instream measurements of flow depths. No adjustments were made to accommodate the photogrammetric transects. The implications of this observation are two-fold: 1) the increased resolution (i.e., detail) of the photogrammetric transects was more critical to the hydraulic modelling results for coarse-bed channels with complex morphology than the methodological error in the data sources; and 2) while there may be discrepancies in directly comparing photogrammetric versus traditional sampling points for the same location, the need for interpolation between photogrammetric points becomes unnecessary due to the increased sampling density, and this implies that the photogrammetric transects yield a more accurate representation of real-world conditions.

## **5.4 Supplementing Transects**

Before evaluating the statistical performance of transect supplementation with photogrammetry, it was necessary to address how habitat assessments for UMC from traditional surveys, would be impacted by reductions in the transect sampling density. Visual assessments of the habitat suitability curves (Figures 4.17-4.20) and the regressions of reach average-WUW (Figures 4.22-4.28), all demonstrated that as the number of transects was reduced in each scenario the uncertainty of habitat estimates increases dramatically. Conversely, the probability of model outputs providing a functional representation of real-world conditions decreases significantly with reductions in transect numbers.

Some of this was expected because removing transects alters the slope-energy gradient in the model, which not only requires greater interpolation between transects (Figure 5.4) but generates an energy profile unique to each combination of transects incorporated. Given the numerous sub-reaches with localized slopes varying from 0.003-0.036 m m<sup>-1</sup> in the study reach (Table 4.1) one can expect significant alterations depending on the specific combinations of transects incorporated into the hydraulic model (e.g., Model 1Ai vs Model 1Aii). This was well

demonstrated with the simulated changes in flow velocity, resulting in no regularity or predictable trends, as different combinations of transects were incorporated (Table 4.11). Irregularity in modelled flow velocity would be expected to carry over to habitat estimates, and therefore, habitat availability (i.e., WUW) for individual transects cannot be assumed to remain constant across all model iterations; this matched observations from Section 4.3.3.

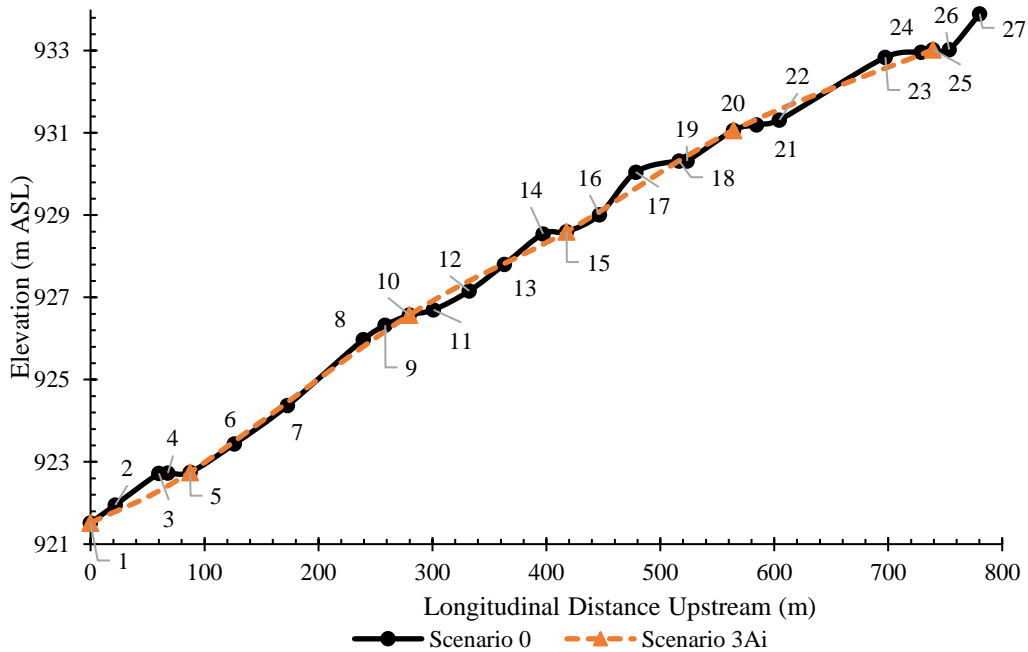


Figure 5.4 Graphical representation of the different slope energy gradients modelled for Upper Mission Creek, in Scenarios 0 (27 transects) and 3A (6 transects). Note, especially the rapid slope changes near transects 3, 14, 17, and 23 that are not reproduced in Scenario 3Ai.

The large degree of heterogeneity in habitat values throughout the UMC reach was another factor hypothesized to have contributed significantly to the observed irregularity in modelled habitat. When modelled in HEC-RAS, assuming ‘Best-Practices’, the majority of transects located in steep rapids or shallow riffles (e.g., transects 2-3, 6-8, 11-14) were found to have insignificant habitat value ( $WUW < 1.0 \text{ m m}^{-1}$ ), regardless of discharge (Figure 5.5). Likewise, the glides, deeper runs or rapids with notable pockets of calm water in the downstream wake of large boulders (transects 1,4-5, 10, 22-26) were predicted to have moderate habitat value ( $2.0 < WUW < 5.00 \text{ m m}^{-1}$ ) at smaller discharge ( $Q < 5 \text{ m}^3\text{s}^{-1}$ ). However, at discharges greater than  $5 \text{ m}^3\text{s}^{-1}$  only transects, 17-20 and 23 were modelled as having significant habitat value for juvenile Rainbow Trout, as most other transects had excessive flow velocities. Transects 19 and 20

consistently dominated the habitat value for the reach (Figure 5.5.) The ramifications of modelled habitat being so unevenly distributed throughout the study reach are significant in that any exemptions or alterations to the WUW (as a product of slope change) of the key transects (4-5,17-20,22-26) has the potential to significantly alter the habitat average for the whole reach.

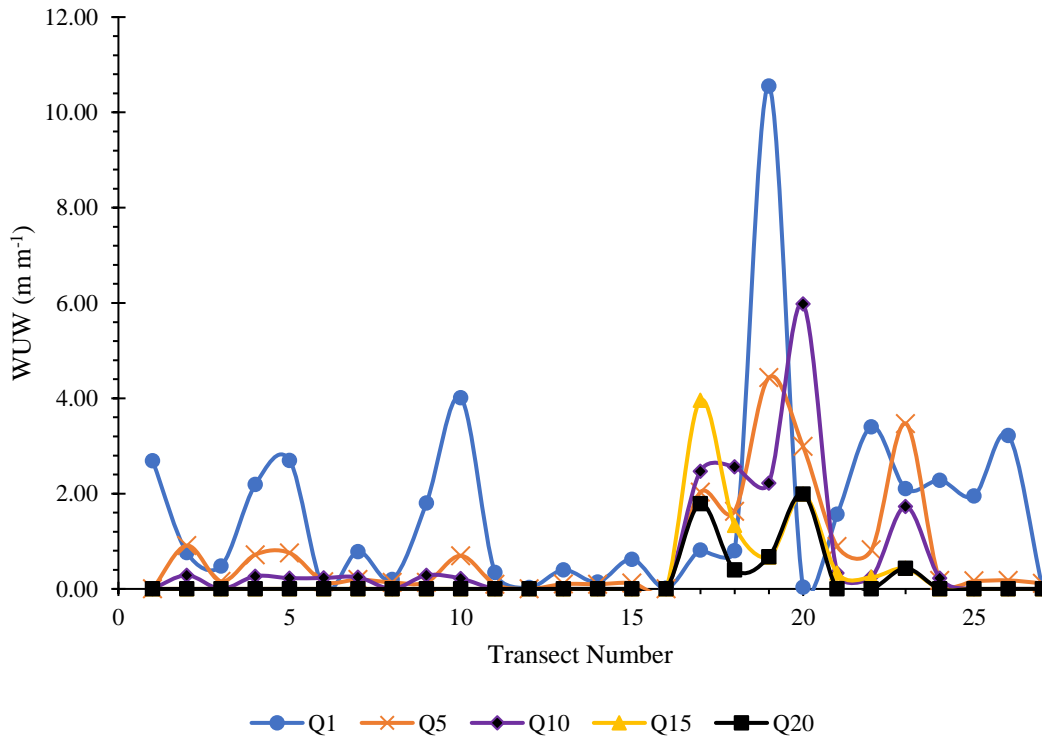


Figure 5.5 Estimates of transect-specific WUW modelled in the 'Best-Practices' Scenario 0. Each coloured line represents the WUW estimates for a specific discharge (e.g., Q1 equates to a discharge of  $1.0 \text{ m}^3 \text{ s}^{-1}$  and Q15,  $15 \text{ m}^3 \text{ s}^{-1}$  respectively)

A quick review of the reduced HSCs (Figures 4.17-4.19) effectively demonstrates this argument that exempting any habitat unit could have large ramifications, with reductions in transects leading to highly uncertain and variable estimates of habitat availability, that rarely parallel the 'Best-Practices' HSC. For example, the maximum WUW bounds for all reduced scenarios were significantly greater than the 'Best-Practices' Scenario 0, with a greater spread as transect density decreased. In all cases though (Scenarios 1A, 2A and 3A), the spread was not centred on Scenario 0 as would be expected based on traditional assumptions that only the uncertainty in the estimates increases but not the mean value (Williams, 1996; Gard, 2005; Williams, 2010; Alleyon *et al.*, 2012). Even when using the minimum and maximum bounds for reach average WUW modelled for each scenario, which theoretically should have a much larger spread than the

90% CI, there were several cases, such as scenarios 1A and 2A (Figures 4.17 and 4.18) for which the minimum WUW estimates were often greater than the HSC for Scenario 0. This indicates that across the five models (1Ai, 1Aii, 2Ai, 2Aii and 2Aiii) that make up Scenarios 1A and 2A, the majority of habitat outputs, including the minima, overestimated available habitat compared to Scenario 0. This is an unexpected result, which indicates how important transect selection can be to habitat assessments. Even though the minimum bounds for Scenario 3A closely paralleled Scenario 0 HSC, albeit, with slightly reduced values, the maximum bounds were several times greater than the HSC. This implies that reducing the number of transects to five for characterizing the study reach could lead to overestimates of available habitat by as much as 6.8 times ( $5.86 \text{ m m}^{-1}$  vs  $0.86 \text{ m m}^{-1}$  at  $Q = 7.0 \text{ m}^3 \text{ s}^{-1}$ ) at certain discharges.

Further highlighting the irregularity of the reduced models, the correlation coefficients for all reduced (1A, 2A and 3A) scenarios with the ‘Best-Practices’ model were below 0.40 (Figures 4.22, 4.24 and 4.26, Table 4.12). In the cases of individual models, some were observed to produce better replications of the Scenario 0 habitat estimates with  $0.5 < R^2 < 0.6$  (e.g., Models 1Ai, 2Aii and 3Ai,3Aii) (Figures 4.22, 4.24 and 4.24, Table 4.13). However, these models were in the minority, and when these scenarios were taken as a whole, minimal resemblances to the ‘Best-Practices’ model were observed. Observations of these few moderately accurate models were largely offset by a greater number of models that were substantively different from the ‘Best-Practices’ model (e.g., Models 1Ai and 3Aiv). The most extreme example of this was Scenario 3A (only 5-6 transects), which produced seemingly accurate estimates of flow depth and velocity at the calibration discharges (Tables 4.10-4.11) but, at discharges outside the calibration range, reach-averaged WUW estimates were quite distinct from the ‘Best-Practices’ scenario (Figures 4.19 and 4.26) with the correlation coefficient plummeting to 0.073 (Table 4.13).

Model 3Aiv, which performed the poorest of all models by severely overestimating habitat values, had only five transects incorporated but three of them (4, 18, and 23) were high-value transects (Figure 5.5). With roughly 60% (3/5) of the reach modelled being a high-value habitat, it was surprising that values contributed to significant overestimates compared to Scenario 0 of which only 37% or 10 of 27 transects were high value. The removal of surrounding transects seems to have reduced the local slope at these transects, thereby also decreasing the flow

velocities and increasing the modelled habitat for juvenile RBT. In a similar vein, and highlighting the significance of key transects, Model 1Ai which included every odd-numbered transect, had a significantly close fit to Scenario 0 versus Model 1Aii which included every even-numbered transect. Model 1Ai's close fit to Scenario 0 is suspected to be a result of the total combination of transects being a close representation of the habitat units present, including several high habitats transects, such as transects 5, 17, 19 and 23. Likewise, Model 1Aii was shown to have reduced flow velocities across the reach (Table 4.11) likely because of the unique slope profile, and this factor increases the habitat available, hence leading to a large overestimate of habitat availability.

It is possible for surveys with a limited number of transects to adequately estimate instream hydraulic habitat, but the chances are reduced considerably for mountain streams when the number of transects is limited. For example, in Scenario 1A, when the total number of transects ( $16.7 \text{ transects km}^{-1}$ ) exceeded the recommended standard of 15 transects per kilometre (Williams 1996) correlation with the 'Best-Practices' scenario (0) was below 0.4 (Figure 4.22, Table 4.13). When transect sampling density was reduced to every fourth one (Scenario 3A,  $6.4 \text{ transects km}^{-1}$ ) the chances of replicating the outputs of the 'Best-Practices' case are extremely poor (Figures 4.19, 4.21 and 4.26; Table 4.13) and there is minimal confidence that the outputs can be representative of the true situation. This is critical because practitioners are always faced with logistical challenges that limit the number of transects that can be surveyed and often base their decisions on the existing literature, which has traditionally utilized guidance from the bootstrapping approach (Williams, 1996; Payne *et al.* 2004; Gard, 2005; Williams, 2010; Alleyon *et al.*, 2012; Railsback, 2016). The minimum transect density (Scenario 3A,  $6.4 \text{ transects km}^{-1}$ ) in this study roughly matched the median number of transects that Payne *et al.* (2004) found for detailed project evaluations at  $6.71 \text{ transects km}^{-1}$ . Compared to an average of  $2.09 \text{ transects km}^{-1}$  for most water licencing assessments (Payne *et al.*, 2004), the minimum sampling density for the UMC study was three times greater.

The UMC results support those of Inoue (2019), as the spacing between transects increases above 1.5 times the channel width, the estimates of channel hydraulics become significantly less reliable. Sampling a transect at each distance interval between 0.5-1.0 times the channel width, as recommended in Inoue (2019), leads to a greater degree of confidence in the hydraulic

models. However, for UMC this would've required 45-90 transects to be established for the 780 m long study reach. Accomplishing these gains in transects surveyed has already been discussed as extremely challenging with traditional techniques because of the environmental conditions and the resources required. To produce a reliable habitat model for a mountainous stream the previous recommendations of Bovee and Milhous (1978), Navarro *et al.*, (1994) and Lewis *et al.* (2004) currently stands as the most pragmatic set of guidelines, with at least one of every habitat unit being sampled and ensuring that total combination of these units is representative of the general character of the reach morphology.

While a portion of this departure from the existing literature is likely due to the increased heterogeneity of mountainous streams, a significant portion comes from this study taking a different approach from the traditional bootstrapping methodology of resampling transects (Williams, 1996; Gard, 2005; Williams, 2010; Alleyon *et al.*, 2012). For all these studies, the primary or 'Best-Practices' HSC would be plotted and for each modelled scenario with a reduced number of transects, the confidence intervals would spread farther apart (Williams, 1996; Payne *et al.*, 2004; Gard, 2005; Williams, 2010; Alleyon *et al.*, 2012). The overall shape of the HSC should remain about the same, suggesting a degree of regularity despite increasing uncertainty. Contrary to the results from these bootstrapping studies, the habitat response curves modelled in the UMC study demonstrated no regularity of form as transect numbers were decreased (Figure 4.17-4.26).

Key assumptions underlying the bootstrapping approach are likely not applicable to mountainous environments and recommendations of transect density that are based on bootstrapping exercises are therefore inapplicable. The bootstrapping approach assumes that the hydraulic outputs at each transect across the range of modelled discharges are fixed on the basis of the primary hydraulic model using all transects, regardless of the combination of transects incorporated into the habitat assessment model. This means that for resampling with a reduced subset of transects, transect-specific WUW values are simply extracted in a random draw from the complete results of the original 'Best-Practices' model (e.g., WUWs from 40 of 107 transects) to generate a new estimate of WUA or reach averaged WUW without changing the basic hydraulic model. By automating this procedure, it is possible to resample the reach average WUW for each subset up to 2000 times to ensure a full range of possible combinations were accounted for. However, the

basic hydraulic model remains unchanged, thereby ignoring any alterations to the energy slope between transects as the number of transects is reduced. Statistically, the method works to evaluate how uncertainty in WUW estimates increases with a smaller number of transects relative to the full survey of transects, but practically this ignores the fact that those additional transects would not be available to the modeller to simulate the flow hydraulics.

To adequately predict how estimates of habitat would differ if a limited number of transects were surveyed in the field, a separate hydraulic model needs to be constructed for each unique combination of transects to account for the complex hydraulic and hydrological interactions between transects. This allows for more robust modelling of the flow conditions that can be realistically simulated given varying logistical constraints leading to smaller numbers of transects available to be incorporated into the hydraulic model. The limitation of this approach is that the creation of a unique model for each iteration prevents automation for rapid sampling and effectively limits sample size to a much smaller number (e.g., 20 models versus 2000 bootstrapped samples). It was this independent modelling approach which was adopted for this study, and it is argued to be more robust than a bootstrapping exercise for environments such as UMC, which provides useful but different information about predictive uncertainty.

It does bear noting that the argument against the bootstrapping approach is specifically for mountainous streams such as UMC, which has a steep average gradient with rapid slope changes, very coarse channel beds, complex morphology and braided reaches. A cursory review of the most cited studies that evaluated the impacts of transect density for this thesis found that none of the published studies were conducted on streams of high gradient (Williams, 1996; Payne, 2004; Gard, 2005; Williams, 2010; Alleyon *et al.* 2012). It could be argued that on streams with: 1) a gentle gradient; 2) regular riffle-pool sequences; 3) a well-defined channel with no side channels and limited hyporheic exchange, the changes in energy gradient and discharge might not be drastic enough to yield different estimates of habitat value at a transect. However, if any of the previous three criteria are not met, it stands to reason that the assumption of transect-specific WUW estimates remaining constant cannot be made.

In contrast to the findings for reductions in transect sampling density, the supplementation of photogrammetric transects was observed to largely negate reductions in surveyed transects,

thereby stabilizing the habitat estimates close to the ‘Best-Practices’ scenario (Figures 4.17-4.26, Table 4.12). Models supplemented with photogrammetric transects significantly outperformed the models with a limited number of surveyed transects across all comparisons. As long as twenty-seven transects were incorporated into a model, the specific combination of photogrammetric and surveyed transects proved to be largely irrelevant. While there remain minor deviations between the photogrammetric and traditional surveys, these discrepancies appear to be inconsequential relative to the uncertainty introduced by using a limited number of transects in the hydraulic model. The likely reason is that a discrepancy of only a few centimetres between photogrammetric and traditional estimates of bathymetry are inconsequential compared to alterations in slope that come with removing transects from the simulations. Additionally, while a not-perfect replication, the supplementation with photogrammetric transects ensures that all habitat units in the reach are still represented, and habitat values are not assigned weighting that is distinct from reality, as was seen in models 1Aii and 3Aiv previously.

In each of the HSC pairings plotted in Figures 4.17 – 4.20, not only was the spread between the upper and lower WUW bounds for the supplemented scenario (e.g., 1B) significantly smaller than in the matched reduced scenario (e.g., 1A) but there were only slight deviations from the ‘Best-Practices’ profile. The clearest demonstration of this can be found in Figure 4.19, where scenario 3B (supplemented) closely parallels Scenario 0, with the upper and lower bounds on either side and centred on the primary HSC, yet the upper habitat bounds for scenario 3A (reduced) are often two-four times greater.

Perhaps the most positive results came from the regression analyses. After supplementation with photogrammetric transects, not only was the error reduced for each pairing (e.g., 1A-1B), but it remained consistent across all supplemented scenarios with a mean error between 0.19-0.20 m s<sup>-1</sup>, median error of 0.13-0.14 m s<sup>-1</sup>, standard deviation around 0.19-0.20 m s<sup>-1</sup>, and root-mean-squared error 0.24-0.26 m s<sup>-1</sup> (Table 4.11). Where the reduced scenarios were observed to have no significant correlation to the ‘Best-Practices’ scenario ( $R^2 < 0.4$ ), the worst correlation observed for the supplemented was Scenario 3B at 0.72. This result though was dragged down by model 3Bi which had an  $R^2$  of 0.58. Out of ten models supplemented with photogrammetric transects, nine had correlation coefficients greater than 0.82. In stark contrast to reduced models, 1Ai and 1Aii (Figures 4.17 and 4.21, Table 4.12), both models 1Bi and 1Bii were observed to be

very similar to each other and Scenario 0 (Figures 4.17 and 4.22, Table 4.12), in a dramatic example of the photogrammetric supplementation stabilizing WUW estimates around the ‘Best-Practices’ case. Likewise, when the confidence intervals of each scenario are assessed, the CIs for the supplemented scenarios were significantly tighter and more uniform in spread than reduced scenarios.

Finally, there is evidence to suggest that the photogrammetric dataset may provide a more functional representation of real-world conditions, with the entirely photogrammetric model (Scenario 4) having simulated flow velocities with the least error among all scenarios, by virtually all metrics (Table 4.11). The most likely hypothesis for the more accurate simulations of flow velocities is that the ten-fold increase in the number of survey points per transect is critically important when modelling complex channel bathymetry. Small errors in the accuracy of the photogrammetric method with respect to mean depth are outweighed by the resolution of channel configuration. Alternatively, or in conjunction, it could be that the photogrammetric DEM is more accurate than either the wading rod or the engineer’s level surveys, thereby allowing the HEC-RAS model to simulate flow conditions more accurately. The former point seems more plausible given that both the wading rod and engineer’s surveys were in close agreement with each other, however, the latter cannot be discounted without further data collection efforts. A complete series of surveys using all three methods completed on the same day at constant discharge would help to resolve this issue.

## Chapter 6 . Summary and Conclusions

This chapter summarizes the key findings of the study and addresses the research objectives and questions laid out in section 1.3. Recommendations are made for future research and practical improvements to IFIM assessments.

### 6.1 Key Findings

The vast majority of instream habitat assessments in North America have followed the Incremental Flow Instream Methodology (Ahmadi-Nedushan *et al.*, 2006; Booth *et al.*, 2016), utilizing standard surveying protocols and wading rod surveys to sample topographic and hydrometric data. The IFIM approach has been evaluated repeatedly since its formal inception in the 1970s (Bovee and Milhous, 1978), and while it has been criticized due to its limitations (Lancaster and Downes, 2011; Railsback, 2016), it has been judged to serve as an invaluable tool for assessing instream habitat (Booth *et al.*, 2016; Stalnaker *et al.*, 2017; Reiser and Hilgert, 2018; Nester *et al.*, 2019). Nevertheless, the need for further refinement has been highlighted (Shintani and Fonstad, 2017). Specifically, the rugged terrain and complex channel morphologies inherent to steep mountain streams pose challenges to conducting topographic and bathymetric surveys using an engineer's level, total station, or RTK-DGPS. In addition, there are pervasive constraints based on limited time and resources (human as well as financial). In the Western Cordillera of North America, this has been especially problematic due to the number of watersheds with high fisheries value that are difficult to access.

A potential solution to overcome these limitations is the use of remote-sensing technologies to conduct aerial surveys of stream channel morphology and bathymetry. The use of drones to enable airborne LiDAR scans or Structure-from-Motion (SfM) photogrammetry are particularly attractive options because data can be acquired rapidly over large areas with greater precision, in theory, than traditional surveying techniques. The SfM approach has been of particular interest because it is more cost-effective and within reach of most assessment projects requiring only a standard UAV with a high-quality camera. An RTK-DGPS system, for georeferencing, can be rented, borrowed, or purchased, and increasingly, more sophisticated UAVs are RTK-DGPS enabled directly onboard.

The research question that motivated this thesis research was:

*Does the use of UAVs to obtain photogrammetric data on reach-scale channel morphology and hydraulics lead to statistically significant improvements over traditional field surveying methods for assessing salmonid habitat in small mountain streams?*

Previous research has demonstrated that the SfM-UAV was a feasible and cost-effective approach to surveying channel topography for the purposes of hydraulic modelling on low-gradient streams with clear water (Biron *et al.*, 2013; Woodget *et al.*, 2014; Tamminga, 2016; Dietrich, 2016; Shintani and Fonstad, 2017; Bennett *et al.*, 2016; Wheaton *et al.*, 2017; Lane *et al.* 2020). However, none of these prior studies addressed the applicability of the method to high-gradient streams with heterogenous channel morphology and tannin-rich water—the very type of stream that is prevalent throughout the PNW and often providing valuable fish habitat.

To address the primary research question, an extensive field campaign was undertaken in 2019, yielding a total of thirty transects over ~780 m. This exceeds the best practices protocols for IFIM assessments (Lewis *et al.* 2004) with more than double the recommended transect density of fifteen transects per km (Williams, 1996; Payne *et al.*, 2004). Each transect was surveyed a minimum of three times during the study period, once each with the standard surveying convention (engineer's level and stadia rod), again with a flow meter and wading rod (as part of discharge measurements), and finally using the photogrammetric approach based on imagery acquired with a drone.

Following extensive quality control evaluations of the data set, HEC-RAS 1D hydraulic modelling was conducted using both the measured transects and photogrammetrically extracted transects in different combinations to test whether habitat assessments could be improved with the incorporation of the photogrammetric data. The results lead to the following key observations:

For high-gradient streams dominated by very coarse substrate, the sampling error with traditional surveying methodologies was slightly greater than reported by previous studies, due in large part to the size of the substrate (i.e., cobbles and boulders rather than sand and gravel). This increase in sampling error was consistent for the engineer's level, wading rod, and GPS surveys, pointing

to the importance of measurement redundancy in assessing quality control.

Photogrammetric sampling of the channel bathymetry replicated the results from repeat surveys with traditional techniques within a small margin of error. There were slight deviations between the methodologies, but the average differences in topographic accuracy (mean error) and precision (standard deviation) were less than 5 cm, which is deemed acceptable for purposes of hydraulic modelling.

The use of photogrammetrically derived transects in the hydraulic models yielded mean flow velocities that replicated instream measurement with greater accuracy and precision than the models based on transects measured with the engineer's level. It is believed that the increased number of sampling points per transect from the photogrammetric survey produced a hydraulic model with enhanced spatial fidelity than one based on traditional surveying techniques for which there are far fewer sampling points across the transect.

Reducing the number of transects incorporated into a hydraulic model had severe consequences for estimates of habitat availability, greatly increasing the uncertainty associated with values of WUA. For example, reducing the number of transects by one-half relative to the best practices model resulted in habitat areas not correlating well with the best practices estimates, despite transect density being equivalent to the minimum recommendation of fifteen per kilometre. When the number of transects incorporated into the model was reduced to six, which is common practice for mountainous streams such as UMC, the correlation in habitat outputs is essentially nil. Thus, there can be no confidence in the results from such a sparse sampling design.

Supplementation of transects using photogrammetric methods was found to be very effective, largely negating the impacts of a small number of measured transects based on standard surveying methods. Somewhat surprisingly, building a model based entirely on photogrammetric transects produced results that were at least as good as, if not better than, the best practices model.

It remains challenging to survey a large number of transects in mountainous environments while ensuring quality control. Initial concerns that the environmental conditions would negatively impact the photogrammetric surveys were proven to be valid in the preliminary test runs.

However, with due diligence, designed redundancies and in-field adjustments such as the use of the high contrast control markers, the quality of the photogrammetric dataset cannot be statistically differentiated from the data collected with the engineer's level or wading rod survey. To do so would require more duplication of all three surveys at all twenty-seven transects, completed within a much shorter period. This though could only be expected to reduce the measured error by a few centimetres (i.e., less than 5 cm), which is a minor and likely insignificant gain when compared to the variability in substrate size, the dynamic nature of the channel bed, and the significant increases in cost for each survey duplicated.

The results of resampling habitat values with a reduced number of transects demonstrated that utilizing a small number of transects has severe consequences for the assessment of instream habitat, more so than simple sampling error due to logistical challenges in the field. While error in transect bathymetry based on photogrammetric sampling can be expected to be slightly greater than those with traditional techniques, the increased number of sampling points for each transect appears to improve the precision and accuracy of modelled flow velocities. Moreover, by supplementing the model with photogrammetric transects, the gains made in the accuracy, precision, and confidence in the habitat assessment were significant. **Thus, the null hypothesis that “there is no net improvement in the accuracy of habitat assessments based on traditional field methods following the BCIFM if photogrammetric data from UAVs are incorporated into the assessment” is rejected. Instead, the evidence supports the alternative hypothesis that “the inclusion of photogrammetric data from UAVs significantly improves the accuracy of the habitat assessments above what can be attained following the BCIFM”.**

The UAV survey was completed in one afternoon, compared to eight days of fieldwork to acquire the just engineer's level and wading rod surveys, and therefore the photogrammetric approach has great potential for expanding both the detail and areal reach of IFIM surveys. Within a larger study reach, the ability to extract a virtually unlimited number of transects from the photogrammetric DEM for one-dimensional modelling or using the complete DEM to populate a 2D hydraulic model is expected to offer significant gains in the accuracy of the hydraulic models to simulate real-world conditions. This would be an invaluable improvement over traditional practices in mountain streams, especially for reaches with multiple channels

spread out over a horizontal distance too wide for traditional techniques. Without the use of aerial surveys, sampling transects for purposes of robust IFIM assessments becomes largely unfeasible in these inaccessible habitats.

## 6.2 Future Recommendations

Upon the successful completion of this project fourteen recommendations for those interested in supplementing IFIM with UAV-SfM techniques are provided below:

1. Assessing the pre-existing visual challenges of the site using existing maps and aerial imagery is essential. As a minimum requirement for sampling high-quality data with the UAV-SfM approach, the majority of areas that will be sampled (preferably the entirety) must have a top-down (i.e., drone-to-channel bed) line of sight that is clear of obstructions.
  - For surveying transect profiles only, each transect needs to have a band that spans the length of the desired transect (e.g., bankfull width), and is ~0.5 m wide, without any obstructions or strong shadows. A minimum spacing of only 0.1-0.2 m of spacing from the riparian zone was found to be sufficient at times for this study, however, it would be risky to assume this in most situations.
  - If the plan is to perform a 2D hydraulic modelling exercise, the entirety of the study channel must be clearly visible UAV. Otherwise, there is a serious risk that artifacts in the DEM from obstructions such as overhead cover or channel spanning debris could generate major inaccuracies in the 2D model with flow being directed overland.
2. Study reach length is limited by both the ability of field crews and equipment (e.g., RTK-DGPS or UAV) to maintain clear lines of communication with the base station. For this study the ~800 m long reach was found to be the maximum length that could be sampled for the following reasons:
  - If either the drone spotter losses sight of the drone or is unable to communicate with the pilot, the drone must be recalled to the base station as a safety precaution.

The more rugged and steeper the terrain, the slower the spotter can manoeuvre to follow the drone and the sooner it passes out of sight.

- Communication between the RTK rover and base station can become unreliable towards the extremities of the study reach if there are obstructions in the line of communication between rover and base station such as dense thickets of riparian vegetation.
3. The location of each base station should be as close as possible to the centre of the areal survey to avoid multiple re-positioning of the base station, thereby saving significant amounts of time.
    - For sites that require more than one base-station location because lines of communication are restricted and project objectives require an extended the reach, the additional base stations should be established so the flight paths out of each location overlap for ~ 50-100 m, with at least one surveyed transect and two or more ground control points incorporated in overlap zone for redundancy.
  4. When planning where the traditional field surveys are required, the minimum number of surveyed transects should be established in advance. As previously discussed in Section 5.4, the uncertainty around habitat estimates becomes quite large if any of the areas where changes in slope, discharge or key morphological and habitat units are located, end up excluded from the hydraulic models. Therefore, surveyed transects will need to be established at:
    - The upstream and downstream boundaries of the study reach.
    - Any location where there is a noticeable change in discharge (e.g., the confluence with a tributary or side channel).
    - All locations where there is a change in slope (e.g., transition from glide to riffle) or major habitat unit and visual obstructions prohibit photogrammetric sampling.
  5. Expand and combine the RTK-GPS and wading rod surveys, replacing the engineer's

level surveys to save on time and resources.

- Specifically, utilize the RTK-DGPS rover to measure the elevation of the rebar markers (top and bottom), the general topography above the waterline and the elevation of the water surface on each bank.
  - The tape measure, wading rod and flow meter can be used to sample the flow depth and velocity for each wetted point along the transect, with depth, estimates being subtracted from the elevation of the water survey to get estimates of channel bathymetry in place of the engineer's level, tripod, and stadia rod.
6. A circular polarized lens (CPL) filter should be utilized at all times when sampling aerial images for two reasons:
- The development of site-specific refraction indexes is a complex and resource extensive exercise that most assessments won't have access to.
  - The application of a CPL largely achieved the same effect of improving the exposure of the image and with it the photogrammetric estimates of channel bathymetry, without additional processing.
7. To improve upon the confidence of the photogrammetric data further, utilize lightweight, packable, and high-contrast markers such as those used on the final Sept. 30<sup>th</sup> flight (Figure 3.8) in even greater numbers than used in this study (e.g., 30 vs 15).
- This would increase the redundancy in data to overcome unforeseen optical challenges (e.g., high albedo substrate) or errors in the GPS survey that might limit the number of usable ground control points.
  - Additionally, a large number of markers will improve confidence in the dataset by reducing the interpolation between points, thereby significantly reducing the chances of 'warping' entering the DEM in visually challenging areas, or towards the edges of the DEM away from the channel.
8. Consideration must be given to the selection of the camera and drone system employed,

within the context of the assessment's objectives.

- The DJI Phantom 4 RTK-DGPS drone utilized in this study was highly effective and not too costly; however, there are increasingly numerous UAV setups on the market that come with or can be equipped with significantly better-performing cameras. Specifically, the camera on the DJI Phantom 4 was only a 1-inch sensor with 8-bit colour recording, 20 effective megapixels, 12.8 stops of dynamic range and limited low-light performance at an effective ISO score of 466 (DXOMARK 2022).
- For stream reaches of particular high habitat value, but with challenging light conditions, upgrading the drone and camera setup to one with a larger sensor should significantly improve the success and confidence of photogrammetric surveys. An example of one such set-up, if maximum dynamic range, resolution and low light performance are required, would be the Sony ARS-S1 UAV (SONY 2022<sup>1</sup>) equipped with a Sony A7R iv full-frame camera (SONY 2022<sup>2</sup>). The camera sensor on this would not only have less distortion utilizing a full-frame sensor and lenses, but it also has 26-bit colour recording, 61 effective megapixels, 14.8 stops of dynamic range and an effective ISO score of 3344 for much better low-light performance (DXOMARK 2022).
- As the need for a ground-level RTK-DGPS system with a rover and base station has already been identified as a requirement for georeferencing the transect pins, water surface elevations and ground control points, an additional RTK system for the drone may be redundant in many situations. Therefore, unless features such as assisted landings, real-time terrain tracking and following (i.e., flying height auto-adjusted along the path), fully automated flights off pre-drawn paths are beneficial then considerable costs can be saved by not purchasing an RTK system (~ \$5600 difference between the DJI Phantom 4 PRO vs RTK). These differences in costs though are a one-time payment and might be justified for conducting numerous surveys of this nature, especially if returning to a site and wanting to repeat the same georeferenced flight path as previous surveys.

9. Significantly increase the number of transects extracted from the photogrammetric DEM to improve confidence in the hydraulic modelling exercises.
  - The objective should be to sample at such a density that there is a transect (traditional or photogrammetric) for every 0.5-1.0 times the channel width, per the recommendations from Inoue (2019). This will ensure that there is a high degree of confidence in the resulting hydraulic outputs.
10. To accommodate the greater number of transects, the majority of the water surface elevations for model calibration can be extracted from the photogrammetric dataset.
  - By matching up the location of the waterline in the georeferenced orthographic photo, overlaid with the DEM, it is possible to extract the elevation of the water surface on both the left and right banks for each photogrammetric transect.
  - To validate the photogrammetric dataset, cross-reference photogrammetric estimates of water-surface elevation against infield measurements for the surveyed transects.
  - Likewise, model estimates of flow velocity can also be validated against infield measurements from the flow meter at the surveyed transects.
11. If resources allow for the repeated surveys of the site, the hydraulic model should ideally be calibrated for both small and large discharges.
  - This study focused on calibrating the hydraulic model for low-flow conditions as that is the principal limiter of year-round habitat for most streams in the BC interior; There are exceptions where peak discharge events and the associated greater velocities can be the principal limiting factor.
  - Therefore, it is recommended if time and resources are available the model be calibrated to multiple different discharges to ensure the confidence of habitat estimates across a variety of flow conditions.
12. To improve the calibration of the hydraulic models it is recommended that a formal

procedure be developed to integrate either the Manning-Strickler equation or the dimensionless hydraulic geometry methods proposed in Ferguson (2007), Powell (2014) and Schneider *et al.* (2015) to determine the relative roughness factors.

- In particular, Schneider *et al.* (2015) demonstrated how photogrammetry can be utilized to sample the grain size distribution for a mountain channel and general measures of hydraulic geometry (e.g., channel width, depth, etc..) to determine the values of relative bed roughness utilized, which improved hydraulic modelling predictions.

13. It would be worthwhile conducting a similar study that implements a 2D hydraulic model that is capable of modelling flow conditions continuously in both the downstream and lateral directions of the channel. If there are minimal artifacts in the DEM, it is expected that the 2D estimates of hydraulic habitat will be a significantly more accurate representation of the real-world conditions for channels with complex flow morphology.

14. Further improvements are expected if a habitat suitability index (HSI) for adjacent lateral flow velocities was incorporated with the conventional indexes as was done in Naman *et al.* (2020). The additional HSI accounts for the fish's feeding habits of moving in and out of areas of calm water for resting and adjacent high velocity flows to catch drifting invertebrate prey. This has been found to significantly increase modelled estimates of habitat available for salmonids in cobble-dominated streams, such as UMC (Naman *et al.*, 2020).

## References

- Ahmadi-Nedushan, B., St-Hilaire, A., Bérubé, M., Robichaud, É., Thiémonge, N., and Bobée, B. (2006). A Review of Statistical Methods for the Evaluation of Aquatic Habitat Suitability for Instream Flow Assessment. *River Research and Applications*, 22(5), 503–523. DOI: 10.1002/rra.918
- Ayllón, D., Almodóvar, A., Nicola, G. G., and Elvira, B. (2011). The Influence of Variable Habitat Suitability Criteria on PHABSIM Habitat index results. *River Research and Applications*, 28(8), 1179–1188. <https://doi.org/10.1002/rra.1496>
- Backes, D., Smigaj, M., Schimka, M., Zahs, V., Grznárová, A., & Scaioni, M. (2020). River Morphology Monitoring of a Small-Scale Alpine Riverbed using Drone Photogrammetry and LiDAR. *The International Archives of the Photogrammetry, Remote Sensing and Spatial Information Sciences*, XLIII-B2-2020, 1017–1024. <https://doi.org/10.5194/isprs-archives-xliii-b2-2020-1017-2020>
- Barnes, H. H. (1967). *Roughness Characteristics of Natural Channels*. Washington, D.C, United States Geological Survey, Dept. of the Interior.
- Bear, E., McMahon, T. and Zale, A. (2007). Comparative Thermal Requirements of Westslope Cutthroat Trout and Rainbow Trout: Implications for Species Interactions and Development of Thermal Protection Standards. *Transactions of the American Fisheries Society*. 136:4, 1113–1121, DOI: 10.1577/T06-072.1
- Beecher, H. A., Caldwell, B. A., DeMond, S. B., Seiler, D., and Boessow, S. N. (2010). An Empirical Assessment of PHABSIM using Long-term Monitoring of Coho Salmon Smolt production in Bingham Creek, Washington. *North American Journal of Fisheries Management*, 30(6), 1529–1543. <https://doi.org/10.1577/m10-020.1>
- Belletti, B., Rinaldi, M., Bussetini, M., Comiti, F., Gurnell, A. M., Mao, L., and Vezza, P. (2017). Characterizing Physical Habitats and Fluvial Hydromorphology: A New System for the Survey and Classification of River Geomorphic Units. *Geomorphology*, 283, 143–157. DOI: 10.1016/j.geomorph.2017.01.032
- Benjankar, R., Tonina, D., McKean, J. A., Sohrabi, M. M., Chen, Q., and Vidergar, D. (2018). An Ecohydraulics Virtual Watershed: Integrating Physical and Biological Variables to Quantify Aquatic Habitat Quality. *Ecohydrology*, 12(2). DOI: 10.1002/eco.2062
- Biron PM, Choné G, Buffin-Bélanger T, Demers S, Olsen T. (2013). Improvement of Streams Hydro-Geomorphological Assessment using LiDAR DEMs. *Earth Surface Processes and Landforms*. DOI:10.1002/esp.3425
- Blue Marble Geographics. (2022, February 23). *Global mapper*. Blue Marble Geographics. Retrieved March 12, 2022, from <https://www.bluemarblegeo.com/global-mapper/>

Booth, D., Scholz, J., Beechie, T., and Ralph, S. (2016). Integrating Limiting-Factors Analysis with Process-Based Restoration to Improve Recovery of Endangered Salmonids in the Pacific Northwest, USA. *Water*, 8(5), 174. <https://doi.org/10.3390/w8050174>

Bovee, K. D. and R. Milhous. (1978). Hydraulic Simulation in Instream Flow Studies: Theory and Techniques. *U.S. Fish and Wildlife Service, Instream Flow Paper 5*, FWS/OBS-78/33, Washington, D.C.

Bovee, K. D. (1982). A Guide to Stream Habitat Analysis Using the Instream Flow Incremental Methodology. *U. S. Fish and Wildlife Service, Office of Biological Services, Instream Flow Information Paper 12*, FWS/OBS-82/26, Washington, D.C.

Bovee, K. D. (1986). Development and Evaluation of Habitat Suitability Criteria for use in the Instream Flow Incremental Methodology. *U.S. Fish and Wildlife Service, National Ecology Center, Instream Flow Information Paper 21*, FWS/OBS-86/7, Washington, D.C.

Brown, R. A. and Pasternack, G. B. (2008). Engineered Channel Controls Limiting Spawning Habitat Rehabilitation Success on Regulated Gravel-Bed Rivers. *Geomorphology*, 97(3-4), 631-654. DOI: 10.1016/J.Gemorph.2007.09.012

Bennett, S., Pess, G., Bouwes, N., Roni, P., Bilby, R. E., Gallagher, S., and Greene, C. (2016). Progress and Challenges of Testing the Effectiveness of Stream Restoration in The Pacific Northwest Using Intensively Monitored Watersheds. *Fisheries*, 41(2), 92-103. DOI:10.1080/03632415.2015.1127805

Bovee, K.D. and Milhous R.T. (1978). Hydraulic Simulation in Instream Flow Studies: Theory and Techniques. Instream Flow Paper No.5, *U.S. Fish and Wildlife Service*, FWS/OBS-78/33

Carrivick, J. L., Smith, M. W. and Quincey, D. J. (2016). Structure from Motion in the Geosciences. Chichester, West Sussex: *Wiley Blackwell*.

Cienciala, P. and Hassan, M. A. (2016). Sampling Variability in Estimates of Flow Characteristics in Coarse-Bed Channels: Effects of sample size. *Water Resources Research*, 52(3), 1899–1922. DOI: 10.1002/2015wr017259

Courtney R.F., Walder G.L., and Vadas R.L. (1998). Instream flow requirements for fish in the Kananaskis River. Fisheries and Recreation Enhancement Working Group: Calgary, AB; 1–164.

Cram, J. M., Torgersen, C. E., Klett, R. S., Pess, G. R., May, D., Pearsons, T. N., and Dittman, A. H. (2017). Spatial Variability of Chinook Salmon Spawning Distribution and Habitat Preferences. *Transactions of the American Fisheries Society*, 146(2), 206–221. DOI: 10.1080/00028487.2016.1254112

Department of Fisheries and Oceans Canada, Communications Branch. (2019, August 27). Summary of Pacific salmon outlook units for 2019. Retrieved November 9, 2019, from

Dietrich, J. T. (2016). Bathymetric Structure-from-Motion: Extracting Shallow Stream Bathymetry from Multi-View Stereo Photogrammetry. *Earth Surface Processes and Landforms*, 42(2), 355 – 364. <https://doi.org/10.1002/esp.4060>

Dorava, J. M. (2001). *Geomorphic Processes and Riverine Habitat* (Vol. 4). Washington, D.C.: *American Geophysical Union*

DJI Phantom4 Pro. DXOMARK. (n.d.). Retrieved March 10, 2022, from <https://www.dxomark.com/Cameras/DJI/Phantom4-Pro>

Mavic 2 enterprise series - DJI. DJI Official. (n.d.). Retrieved May 21, 2022, from <https://www.dji.com/ca/mavic-2-enterprise>

Carter, K. (2019, November 27). Sony A7R IV Sensor Review. DXOMARK. Retrieved May 18, 2022, from <https://www.dxomark.com/sony-a7r-iv-sensor-review/>

Eaton B.C. and Church M. (2007). Predicting Downstream Hydraulic Geometry: A Test of Rational Regime Theory. *Journal of Geophysical Research: Earth Surface*, (2003–2012) 112(F03025): DOI:10.1029/2006JF000734.

Flener, C., Vaaja, M., Jaakkola, A., Krooks, A., Kaartinen, H., Kukko, A., Kasvi, E., Hyypä, H., Hyypä, J., and Alho, P. (2013). Seamless mapping of river channels at High Resolution Using Mobile Lidar and UAV-Photography. *Remote Sensing*, 5(12), 6382–6407. <https://doi.org/10.3390/rs5126382>

Ferguson, R. (2007). Flow Resistance Equations for Gravel and Boulder-Bed Streams. *Water Resources Research*, 43(5). <https://doi.org/10.1029/2006wr005422>

Grant, G., O'Connor, J., and Wolman, M. (2013). A River Runs Through It: Conceptual Models in Fluvial Geomorphology. *Treatise on Geomorphology*, 6-21. DOI:10.1016/b978-0-12-374739-6.00227-x

Gibson S. (2013). Comparing Depth and Velocity Grids Computed with One and Two-Dimensional Models at Ecohydraulic scales. *M.S. Thesis, University of California at Davis, Davis, CA.*

Gibson, S. A. and Pasternack, G. B. (2015). Selecting Between One-Dimensional and Two-Dimensional Hydrodynamic Models for Ecohydraulic Analysis. *River Research and Applications*, 32(6), 1365–1381. DOI: 10.1002/rra.2972

Gore, J. A. (2001). Models of Habitat Use and Availability to Evaluate Anthropogenic Changes in channel geometry. *Geomorphic Processes and Riverine Habitat Water Science and Application*, 27–36. DOI: 10.1029/ws004p0027

Hatfield T. and Bruce J. (2000). Predicting Salmonid Habitat–Flow Relationships for Streams from Western North America. *North American Journal of Fisheries Management* 20 (4): 1005–1015

- HEC-RAS (5.0) [Software]. (2019). U.S. Army Corps of Engineers. Retrieved April 2, 2019, from <http://www.hec.usace.army.mil/software/hec-ras/downloads.aspx>
- James, M. R., Chandler, J. H., Eltner, A., Fraser, C., Miller, P. E., Mills, J. P., and Lane, S. N. (2019). Guidelines on the Use of Structure from Motion Photogrammetry in Geomorphic Research. *Earth Surface Processes and Landforms*, 44(10), 2081–2084. DOI: 10.1002/esp.4637
- Jarrett, R. D. (1990), Hydrologic and Hydraulic Research in Mountain Rivers, *Water Resour. Bull.*, 26(3), 419–429.
- Jerlov, N. G. (1976). *Marine optics*. Elsevier Scientific Publishing.
- Jowett, I.J. and Davey, A.J.H. (2007). A Comparison of Composite Habitat Suitability Indices and Generalized Additive Models of Invertebrate Abundance and Fish Presence-Habitat Availability. *Transactions of the American Fisheries Society* 136: 428–444.
- Kondolf, G. M. (2000). Assessing Salmonid Spawning Gravel Quality. *Transactions of the American Fisheries Society*, 129(1), 262-281. DOI:10.1577/1548-8659(2000)129.0.co;2
- Kondolf, G. M. (2013). Setting Goals in River Restoration: When and Where Can the River "Heal Itself"? *Stream Restoration in Dynamic Fluvial Systems Geophysical Monograph Series*, 29-43. DOI:10.1029/2010gm001020
- Laliberte, J. J., Post, J. R., and Rosenfeld, J. S. (2013). Hydraulic Geometry and Longitudinal Patterns of Habitat Quantity and Quality for Rainbow Trout (*Oncorhynchus Mykiss*). *River Research and Applications*, 30(5), 593-601. DOI:10.1002/Rra.2666
- Lancaster, J. and Downes, B. J. (2010). Linking the Hydraulic World of Individual Organisms to Ecological Processes: Putting Ecology into Ecohydraulics. *River Research and Applications*, 26(4), 385–403. DOI: 10.1002/rra.1274
- Lichatowich, J. (1999). *Salmon Without Rivers: A History of the Pacific Salmon Crisis*. Washington, D.C.: *Island Press*.
- Legleiter, C. J. and Fonstad, M. A. (2012). An Introduction to the Physical Basis for Deriving River Information by Optical Remote Sensing. In *Fluvial remote sensing for science and Management*. Chichester, West Sussex: Wiley-Blackwell.
- MacDuff, A., McRae, G., St-Pierre, C., and Whitehouse, C. (2019) An Evaluation of Temperature Sensitive Streams in the Thompson-Okanagan region. *BC Ministry of Forests, Land, Natural Resources Operations and Rural Development*.
- Meuse, M. (2017, August 22). DFO Does Not Adequately Monitor B.C. Salmon Spawning Streams, Study Suggests | *CBC News*. Retrieved November 16, 2019, from <https://www.cbc.ca/news/canada/british-columbia/sfu-salmon-study-1.4256265>
- McParland, D., Eaton, B., and Rosenfeld, J. (2014). At-A-Station Hydraulic Geometry Simulator. *River Research and Applications*, 32(3), 399–410. DOI: 10.1002/rra.2851

- McCrae, C., Warren, K., and Shrimpton, J. (2012). Spawning Site Selection in Interior Fraser River Coho Salmon *Oncorhynchus kisutch*: An Imperiled Population of Anadromous Salmon from a Snow-Dominated Watershed. *Endangered Species Research*, 16(3), 249-260. DOI:10.3354/esr00401
- McCleary, R. J., and Hassan, M. A. (2008). Predictive Modeling and Spatial Mapping of Fish Distributions in Small Streams of the Canadian Rocky Mountain foothills. *Canadian Journal of Fisheries and Aquatic Sciences*, 65(2), 319–333. DOI: 10.1139/f07-161
- Montgomery, D. and Buffington, J. (1998). Channel Processes, Classification, and Response. *River Ecology and Management: Lessons from the Pacific Coastal Ecoregion*. Springer-Verlag, New York, New York, 13-42.
- Montgomery, D. and Buffington J. (1997). Channel-Reach Morphology in Mountain Drainage Basins. *Geological Society of America Bulletin*, 109(5): 596–611.
- Moir, H. J. and Pasternack, G. B. (2008). Relationships Between Mesoscale Morphological Units, Stream Hydraulics and Chinook Salmon (*Oncorhynchus tshawytscha*) Spawning Habitat on The Lower Yuba River, California. *Geomorphology*, 100(3-4), 527-548. DOI: 10.1016/J.Geomorph.2008.02.001
- Nahorniak, M., Wheaton, J., Volk, C., Bailey, P., Reimer, M., Wall, E., and Jordan, C. (2018). How Do We Efficiently Generate High-Resolution Hydraulic Models At Large Numbers of Riverine Reaches? *Computers & Geosciences*, 119, 80-91. DOI: 10.1016/j.cageo.2018.07.001
- Naman, S. M., Rosenfeld, J. S., Jordison, E., Kuzyk, M., & Eaton, B. C. (2020). Exploitation of Velocity Gradients by Sympatric Stream Salmonids: Basic Insights and Implications for Instream Flow Management. *North American Journal of Fisheries Management*, 40(2), 320–329. <https://doi.org/10.1002/nafm.10411>
- Navarro, J. E., McCauley, D. J., and Blystra, A. R. (1994). Instream Flow Incremental Methodology (IFIM) for Modelling Fish Habitat. *Journal of Water Management Modeling*. DOI: 10.14796/jwmm.r176-01
- Nestler J. M., Milhous, R. T., Payne, T. R., and Smith, D. L. (2019, August 28). *History and review of the habitat suitability criteria curve in applied aquatic ecology*. Wiley Online Library. <https://onlinelibrary.wiley.com/doi/full/10.1002/rra.3509>.
- Newbury, R. (2010). Stream Restoration Hydraulics. *Newbury Hydraulics*
- NRCAN. (n.d.). *Precise point positioning - NRCAN*. Precise Point Positioning. Retrieved December 19, 2019, from <https://webapp.geod.nrcan.gc.ca/geod/tools-outils/ppp.php?locale=en>
- PHABSIM: Physical Habitat Simulation Software [Software]. (2019). U.S. Geological Society. Retrieved December 11, 2019, from <https://www.usgs.gov/software/physical-habitat-simulation-phabsim-software-windows>

- Parkinson, E. A., Lea, E. V., Nelitz, M. A., Knudson, J. M., and Moore, R. D. (2015). Identifying Temperature Thresholds Associated with Fish Community Changes in British Columbia, Canada, to Support Identification of Temperature Sensitive Streams. *River Research and Applications*, 32(3), 330–347. DOI: 10.1002/rra.2867
- Pasternack, G. B., Bounrisavong, M. K., and Parikh, K. K. (2008). Backwater Control on Riffle–Pool Hydraulics, Fish Habitat Quality, and Sediment Transport Regime in Gravel-Bed Rivers. *Journal of Hydrology*, 357(1-2), 125-139. DOI: 10.1016/J.Jhydrol.2008.05.014
- Payne T.R., Eggers S.D., and Parkinson D.B. (2004). The Number of Transects Required to Compute a Robust PHABSIM Habitat Index. *Hydroe' cologie Applique 'e*, 14,27–53.
- Pike, R.G., T.E. Redding, R.D. Moore, R.D. Winker and K.D. Bladon (editors). 2010. Compendium of forest hydrology and geomorphology in British Columbia. *B.C. Min. For. Range, For. Sci. og.*, Victoria, B.C. and FORREX Forum for Research and Extension in Natural Resources, Kamloops, BC Land Management.  
Handb.66. [www.for.gov.bc.ca/hfd/pubs/Docs/Lmh/Lmh66.htm](http://www.for.gov.bc.ca/hfd/pubs/Docs/Lmh/Lmh66.htm)
- Powell, D. M. (2014). Flow Resistance in Gravel-Bed Rivers: Progress in research. *Earth-Science Reviews*, 136, 301 – 338. <https://doi.org/10.1016/j.earscirev.2014.06.001>
- Quinn, T. P. (2004). The Behaviour and Ecology of Pacific Salmon and Trout. Vancouver: *UBC Press*.
- Railsback, S. F. (2016). Why it is Time to put PHABSIM out to Pasture. *Fisheries*, 41(12), 720–725. <https://doi.org/10.1080/03632415.2016.1245991>
- Reiser, D. W. and Hilgert, P. J. (2018). A Practitioner's Perspective on the Continuing Technical Merits of PHABSIM. *Fisheries*, 43(6), 278–283. <https://doi.org/10.1002/fsh.10082>
- Rumps, J. M., Katz, S. L., Barnas, K., Morehead, M. D., Jenkinson, R., Clayton, S. R., and Goodwin, P. (2007). Stream Restoration in the Pacific Northwest: Analysis of Interviews with Project Managers. *Restoration Ecology*, 15(3), 506-515. DOI:10.1111/J.1526-100x.2007.00246.X
- River2D [Software]. (2019). The University of Alberta. Retrieved December 11, 2019, from <http://www.river2d.ualberta.ca> RStudio [Software]. (2020).
- Rosenfeld J., Beecher H., and Ptolemy R. (2016). Developing Bioenergetic-Based Habitat Suitability Curves for Instream Flow Models. *North American Journal of Fisheries Management* 36 (5): 1205–1219
- Rosenfeld J.S., Campbell K., Leung E.S., Bernhardt J.R., and Post J.R. (2011). Habitat Effects on Depth and Velocity Distributions: Implications for Modeling Hydraulic Variation and Fish Habitat Suitability in Streams. *Geomorphology*. 130: 127–135.

- Rosenfeld J.S. and Ptolemy, R. (2012). Modelling Available Habitat versus Available Energy Flux: Do PHABSIM Applications that Neglect Prey Abundance Underestimate Optimal Flows for Juvenile Salmonids? *Canadian Journal of Fisheries and Aquatic Sciences* 69 (12): 1920–1934
- Schneider, J. M., Rickenmann, D., Turowski, J. M., & Kirchner, J. W. (2015). Self Adjustment of Stream Bed Roughness and Flow Velocity in a Steep Mountain Channel. *Water Resources Research*, 51(10), 7838 – 7859. <https://doi.org/10.1002/2015wr016934>
- Slaney, P. and Zaldokas, D. (1997). Fish Habitat Rehabilitation Procedures. B.C. Ministry of Environment. Watershed Restoration Program. <[Http://Www.Env.Gov.Bc.Ca/Wld/Documents/Wrp/Wrtc\\_9.Pdf](http://Www.Env.Gov.Bc.Ca/Wld/Documents/Wrp/Wrtc_9.Pdf)> (Accessed 15.10.12)
- SEFA: Systems for Environmental Flow Analysis [Software]. (2019). Aquatic Habitat Analysts, Inc. Retrieved December 11, 2019, from <http://sefa.co.nz>
- Selong, J., McMahon, T., Zale, A., and Barrows, F. (2001). Effect of Temperature on Growth and Survival of Bull Trout, with Application of an Improved Method for Determining Thermal Tolerance in Fishes. *Transactions of the American Fisheries Society*, 130(6), 1026–1037. DOI: 10.1577/1548-8659(2001)130<1026:eotoga>2.0.co;2
- Shintani, C. and Fonstad, M. A. (2017). Comparing remote-sensing techniques collecting bathymetric data from a gravel-bed river. *International Journal of Remote Sensing*, 38(8-10), 2883–2902. <https://doi.org/10.1080/01431161.2017.1280636>
- SONY. (n.d.). *Ars-S1*. Airpeak S1. Retrieved March 10, 2022, from <https://electronics.sony.com/more/airpeak/p/arss1>
- SONY. (n.d.). *Sony A7R IV 35 mm full-frame camera with 61.0 MP*. Sony. Retrieved March 10, 2022, from <https://www.sony.ca/en/electronics/interchangeable-lens-cameras/ilce-7rm4>
- Stalnaker, C. B., Chisholm, I., and Paul, A. (2017). Comment 2: Don't throw out the BABY (PHABSIM) with the Bathwater: Bringing scientific credibility to the use of HYDRAULIC Habitat models, specifically PHABSIM. *Fisheries*, 42(10), 510–516. <https://doi.org/10.1080/03632415.2017.1380986>
- Steffler, P. and Blackburn, J. (2002). Two-Dimensional Depth Averaged Model of River Hydrodynamics and Fish Habitat. River2D User's Manual, *University of Alberta*, Canada.
- Tamminga, A. (2016). UAV-Based Remote Sensing of Fluvial Hydro geomorphology and Aquatic Habitat Dynamics. Ph.D. Thesis. Geography. The University of British Columbia.
- Tomlinson, M. J., Gergel, S. E., Beechie, T. J., and McClure, M. M. (2011). Long-Term Changes in River–Floodplain Dynamics: Implications for Salmonid Habitat in the Interior Columbia Basin, USA. *Ecological Applications*, 21(5), 1643–1658. DOI: 10.1890/10-1238.1

- Wheaton, J., Bouwes, N., McHugh, P., Saunders, C., Bangen, S., Bailey, P., and Jordan, C. (2017). Upscaling Site-Scale Ecohydraulic Models to Inform Salmonid Population-Level Life-Cycle Modeling and Restoration Actions - Lessons from The Columbia River Basin. *Earth Surface Processes and Landforms*, 43(1), 21-44. DOI:10.1002/Esp.4137
- Wheaton, J., Fryirs, K., Brierley, G.J., Bangen, S.G., Bouwes, N., and O'Brien, G. (2015) Geomorphic Mapping and Taxonomy of Fluvial Landforms. *Geomorphology* 248: 273–295. <https://doi.org/10.1016/j.geomorph.2015.07.010>.
- Wilding, T. K., Bledsoe, B., Poff, N. L., and Sanderson, J. (2013). Predicting Habitat Response to Flow using Generalized Habitat Models for Trout in Rocky Mountain Streams. *River Research and Applications*, 30(7), 805–824. <https://doi.org/10.1002/rra.2678>
- Wirth, L., Rosenberger, A., Prakash, A., Gens, R., Margraf, F. J., and Hamazaki, T. (2012). A Remote-Sensing, GIS-Based Approach to Identify, Characterize, and Model Spawning Habitat for Fall-Run Chum Salmon in a Sub-Arctic, Glacially Fed River. *Transactions of The American Fisheries Society*, 141(5), 1349-1363. DOI:10.1080/00028487.2012.692348
- Winterhalt, L.M. (2015). Physical Habitat Below a Hydropeaking Dam: Examining Progressive Downstream Change. MSc. Thesis. Geography. The University of British Columbia.
- Williams, R. D., Rennie, C. D., Brasington, J., Hicks, D. M., and Vericat, D. (2015). Linking the Spatial Distribution of Bed Load Transport to Morphological Change During High-flow Events in a Shallow Braided River. *Journal of Geophysical Research: Earth Surface*, 120(3), 604-622. DOI:10.1002/2014jf003346
- Williams, J.G. (1996) Lost in Space: Minimum Confidence Intervals for Idealized PHABSIM Studies. *Transactions of the American Fisheries Society* 125 (3): 458–465
- Williams, J. G. (2009). Lost in Space, the Sequel: Spatial Sampling Issues with 1-D PHABSIM. *River Research and Applications*. DOI: 10.1002/rra.1258
- Wohl, E. and Merritt, D.M. (2008) Reach-Scale Channel Geometry of Mountain Streams. *Geomorphology*, 93, 168–185.
- Wolman, M. G. (1954). A method of sampling coarse river-bed material. *Transactions, American Geophysical Union*, 35(6), 951. <https://doi.org/10.1029/tr035i006p00951>
- Woodget, A. S., Carbonneau, P. E., Visser, F., and Maddock, I. P. (2014). Quantifying submerged fluvial topography using hyperspatial resolution UAS imagery and structure from motion photogrammetry. *Earth Surface Processes and Landforms*, 40(1), 47–64. <https://doi.org/10.1002/esp.3613>
- Wyrick, J., Senter, A., and Pasternack, G. (2014). Revealing the Natural Complexity of Fluvial Morphology Through 2D Hydrodynamic Delineation of River Landforms. *Geomorphology*, 210, 14-22. DOI: 10.1016/j.geomorph.2013.12.013

## Appendices

### Appendix A. Field Survey Discrepancies by Transect

Comparisons are only between Engineer's level surveys and the RTK-DGPS surveys.

<u>Horizontal Distance</u>				<u>Elevation</u>		
Transect	GPS Distance (m)	Difference vs Tape Measure (m)	Difference vs Tape Measure (%)	Left Pin – Right Pin Difference (m)	Difference in Waterline Elv. (m)	Difference in Waterline Elv. (%)
1	19.79	0.07	0.36	0.02	0.28	2.28
2	19.17	0.50	2.59	0.50	0.21	1.74
3	17.97	0.24	1.35	0.09	0.20	1.59
4	16.46	0.02	0.11	0.09	0.22	1.82
5	12.53	-0.02	-0.19	-0.04	0.04	0.36
6	15.23	0.05	0.30	-0.09	0.09	0.77
7	15.69	0.23	1.45	-0.11	0.14	1.17
8	22.85	0.09	0.41	0.03	0.11	0.89
9	21.78	0.01	0.05	-0.18	0.27	2.16
10	14.28	0.04	0.31	-0.02	0.10	0.81
11	13.15	-0.12	-0.91	0.03	0.08	0.64
12	11.04	0.00	-0.04	0.00	0.06	0.52
13	12.16	-0.23	-1.89	-0.04	0.03	0.22
14	15.47	0.01	0.07	-0.04	0.02	0.20
15	9.90	-0.26	-2.71	0.00	0.01	0.06
16	10.34	0.01	0.10	0.03	0.01	0.08
17	32.39	-0.02	-0.07	0.05	-0.09	-0.69
18	32.64	0.18	0.55	-0.05	0.07	0.58
19	N/A	N/A	N/A	0.00	0.09	0.74
20	26.27	0.00	-0.01	-0.01	0.10	0.80
21	16.96	0.09	0.52	-0.03	0.01	0.07
22	15.98	0.21	1.32	0.02	-0.13	-1.10
23	24.15	0.13	0.53	0.01	0.12	0.95
24	20.93	0.02	0.08	-0.04	0.15	1.26
25	15.37	0.23	1.51	-0.03	0.16	1.29
26	12.46	0.03	0.21	0.03	0.12	0.98
27	16.41	0.09	0.54	-0.01	0.13	1.07

## Appendix B. GPS Survey Data

A comparison of GPS coordinates discrepancies between the Sept. 30<sup>th</sup> and Nov. 11<sup>th</sup>, 2019, surveys.

Transect	Easting (m)	Northing (m)	Elevation (m)
1	0.06	-0.08	-0.50
2	0.04	0.06	-0.51
3	-0.02	-0.04	-0.56
4	-0.06	0.05	-0.58
5	0.10	-0.34	-0.51
6	4.53	9.91	0.09
7	0.10	-0.11	-0.51
8	0.05	-0.08	-0.54
9	0.07	0.08	-0.54
10	-0.03	-0.04	-0.56
11	0.00	-0.06	-0.53
12	0.04	0.01	-0.53
13	-0.19	-0.02	-0.58
14	-14.11	-6.51	-0.63
15	-8.59	5.01	-0.08
16	-0.01	-0.01	-0.53
17	-0.28	0.07	-0.56
18	0.04	-0.12	-0.51
19	0.11	0.04	-0.53
20	0.14	0.06	-0.54
21	0.08	-0.02	-0.55
22	-0.01	-0.07	-0.54
23	-0.09	-0.05	-0.56
24	-0.08	-0.18	-0.60
25			
26	0.02	-0.07	-0.56
27	0.07	0.02	-0.59
<b>Mean</b>	-0.69	0.29	-0.51
<b>Median</b>	0.03	-0.03	-0.54

## Appendix C. Photogrammetric Survey Error by Transect

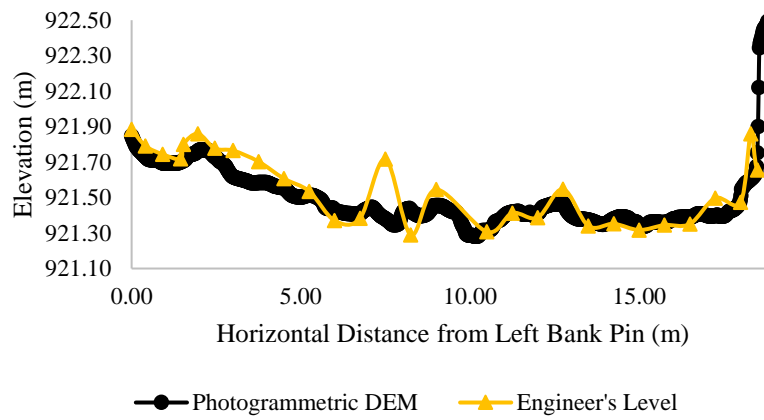
Transect	Photogrammetric Discrepancies				Wading Rod Discrepancies		
	Mean (m)	Median (m)	SDE (M)	Max Depth Recorded (m)	Mean (m)	Median (m)	SDE (M)
1	-0.01	0.01	0.10	0.29	0.03	0.03	0.12
2	-0.03	-0.05	0.11	0.33	N/A	N/A	N/A
3	0.05	0.06	0.04	0.34	0.05	0.01	0.09
4	0.09	0.12	0.07	0.44	0.00	0.03	0.08
5	0.07	0.05	0.09	0.54	0.00	0.01	0.06
6	-0.03	0.00	0.11	0.31	0.00	-0.01	0.08
7	0.00	0.00	0.09	0.39	0.00	0.00	0.05
8	0.09	0.09	0.07	0.44	0.03	0.04	0.05
9	-0.12	-0.12	0.03	0.33	0.00	0.03	0.06
10	0.03	0.03	0.05	0.23	0.00	0.00	0.04
11	0.04	0.06	0.07	0.26	0.00	0.00	0.08
12	0.00	0.00	0.06	0.32	0.00	0.01	0.06
13	0.00	-0.02	0.08	0.29	0.00	-0.01	0.04
14	0.00	-0.02	0.07	0.27	0.00	0.00	0.06
15	0.10	0.09	0.13	0.41	0.00	0.03	0.06
16	0.07	0.11	0.10	0.32	0.00	0.00	0.05
17	0.04	0.03	0.07	0.27	0.09	0.13	0.10
18	-0.04	-0.07	0.10	0.51	0.00	0.03	0.07
19	-0.02	0.00	0.25	1.54	0.00	0.01	0.08
20	0.02	0.03	0.07	0.25	0.00	0.00	0.08
21	0.03	0.05	0.07	0.30	0.00	0.01	0.08
22	0.09	0.08	0.10	0.28	0.00	0.00	0.04
23	0.01	0.02	0.05	0.24	0.00	-0.01	0.06
24	0.0	0.05	0.09	0.30	0.00	-0.01	0.08
25	0.08	0.11	0.05	0.45	0.00	-0.02	0.10
26	0.13	0.15	0.12	0.50	0.03	0.01	0.13
27	0.08	0.10	0.10	0.28	0.00	-0.01	0.09
<b>Reach Average</b>	0.03	0.04	0.09	0.39	0.01	0.01	0.07

## Appendix D. Hydraulic Calibration Data

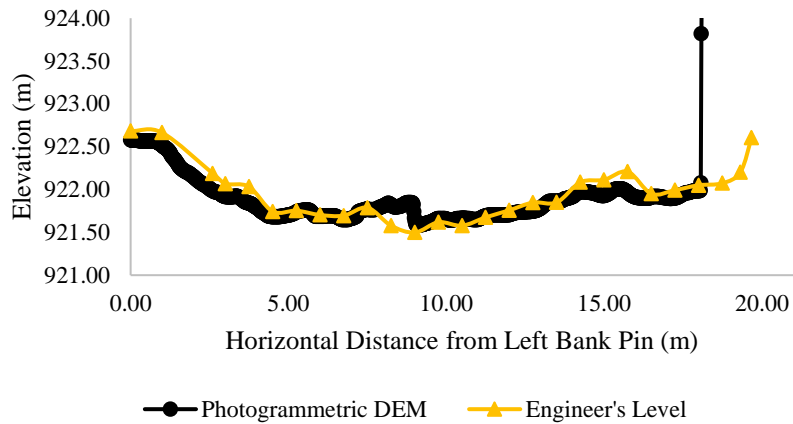
Transect	Modelled Discharge (m <sup>3</sup> s <sup>-1</sup> )	Measured Discharge (m <sup>3</sup> s <sup>-1</sup> )	Measured Mean Waterline (m)	Modelled Mean Waterline (m)	Difference in Waterline (m)	Mannings n	Froude Number	Headloss (m)
1	1.51	1.52	921.63	921.63	0.00	0.11	0.38	
2	1.51	1.79	921.96	921.98	-0.02	0.07	0.36	0.35
3	1.51	1.50	922.71	922.69	0.02	0.13	0.41	0.71
4	1.51	1.61	922.72	922.76	-0.04	0.06	0.24	0.06
5	1.51	1.25	922.84	922.84	0.00	0.09	0.23	0.08
6	1.51	1.77	923.57	923.51	0.06	0.19	0.5	0.68
7	1.51	1.28	924.41	924.4	0.01	0.06	0.35	0.88
8	1.51	1.46	926.03	925.93	0.10	0.18	0.96	1.56
9	1.51	1.43	926.56	926.58	-0.02	0.065	0.36	0.61
10	1.09	1.09	926.67	926.72	-0.05	0.07	0.22	0.13
11	0.49	0.44	926.70	926.76	-0.06	0.03	0.19	0.04
12	0.49	0.41	927.10	927.06	0.04	0.09	1.03	0.07
13	0.49	0.47	927.81	927.83	-0.02	0.06	0.35	0.74
14	0.49	0.52	928.48	928.42	0.06	0.08	0.63	0.6
15	0.49	0.58	928.55	928.54	0.01	0.035	0.29	0.11
16	0.49	0.55	928.86	928.73	0.13	0.17	0.99	0.24
17	0.31	0.31	929.77	929.77	0.00	0.06	0.3	0.99
18	0.31	0.31	930.42	930.18	0.24	0.15	0.23	0.41
19	0.66	0.67	930.33	930.2	0.13	0.15	0.06	0.02
20	0.66	0.70	931.11	930.92	0.19	0.18	1	0.22
21	0.66	0.81	931.25	931.22	0.03	0.06	0.24	0.27
22	0.66	0.48	931.46	931.33	0.13	0.14	0.16	0.11
23	0.66	0.60	932.90	932.84	0.06	0.13	0.38	1.52
24	0.66	0.64	933.03	933.03	0.00	0.05	0.22	0.18
25	0.66	0.63	933.07	933.05	0.02	0.06	0.17	0.02
26	0.66	0.82	933.12	933.08	0.04	0.1	0.13	0.03
27	0.66	0.63	933.82	933.67	0.15	0.15	1.01	0.27

## Appendix F. Transect Profiles

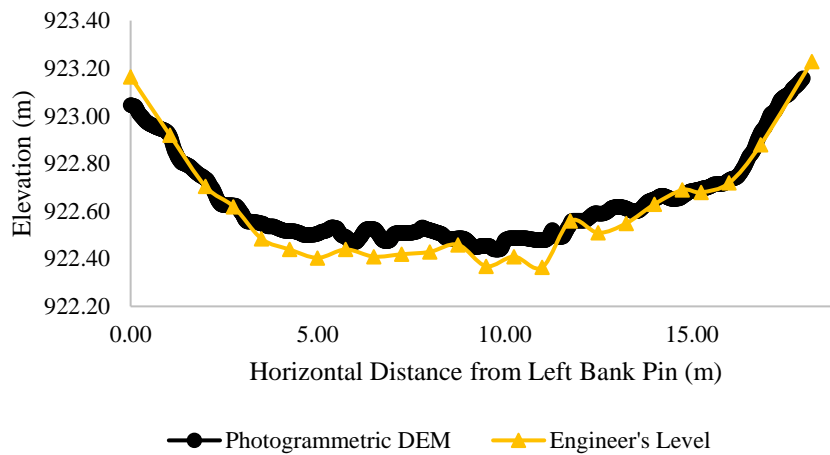
### Transect 1



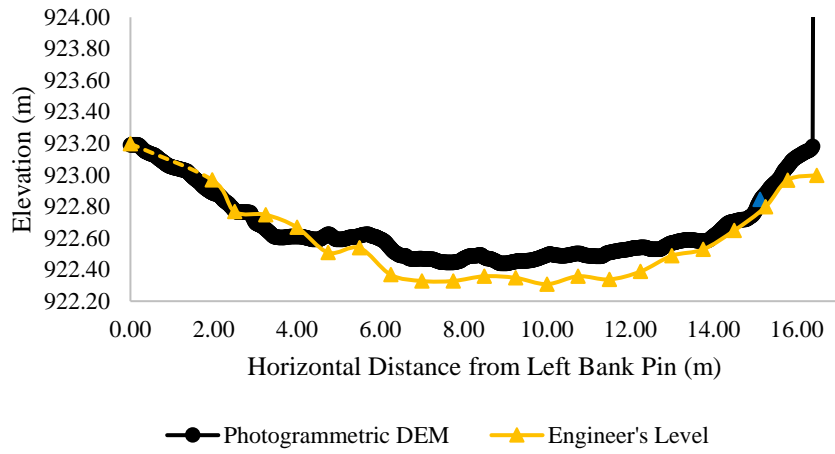
### Transect 2



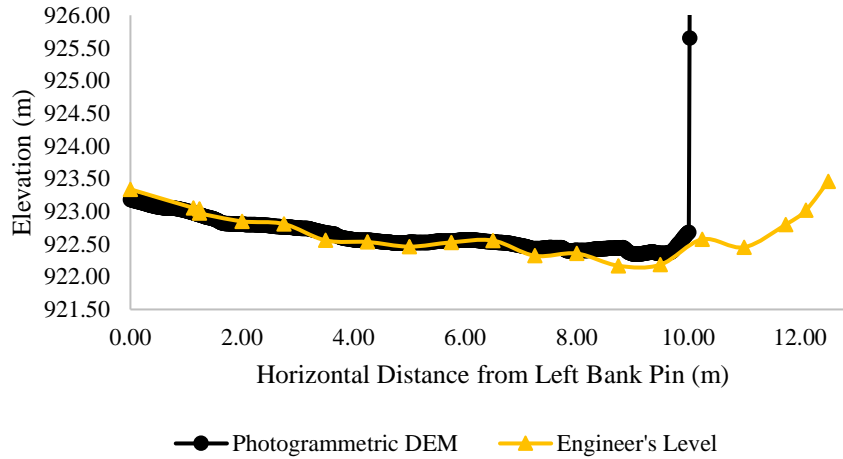
### Transect 3



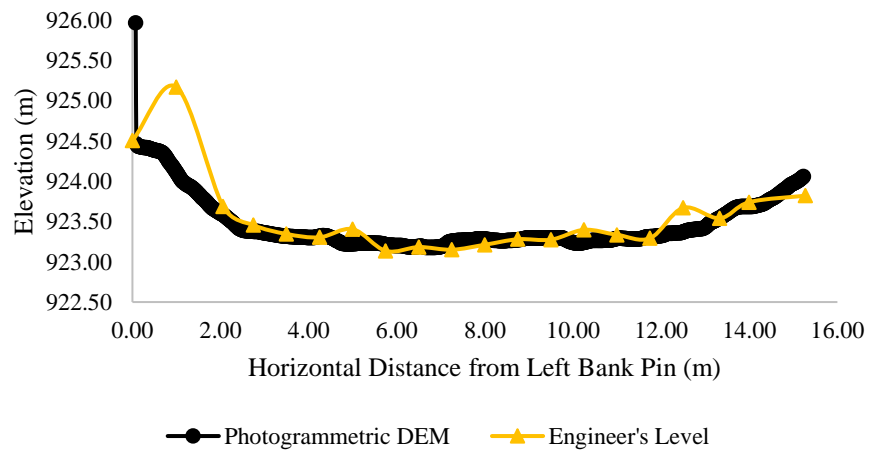
### Transect 4



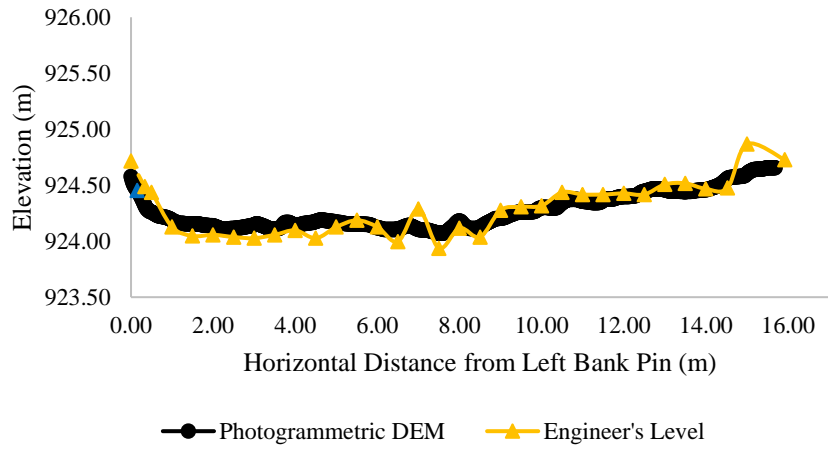
### Transect 5



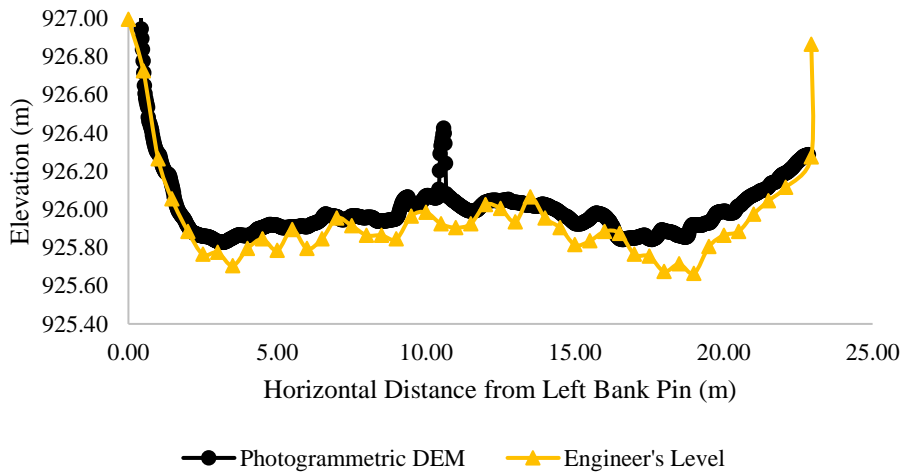
### Transect 6



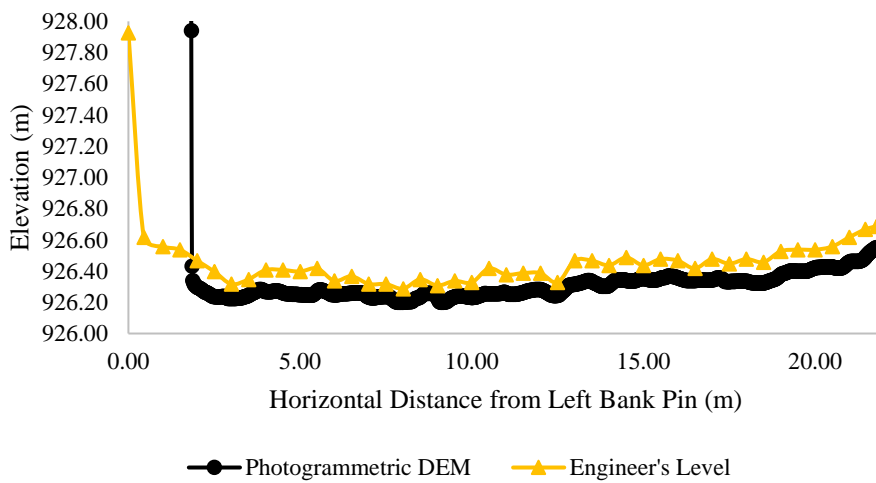
### Transect 7



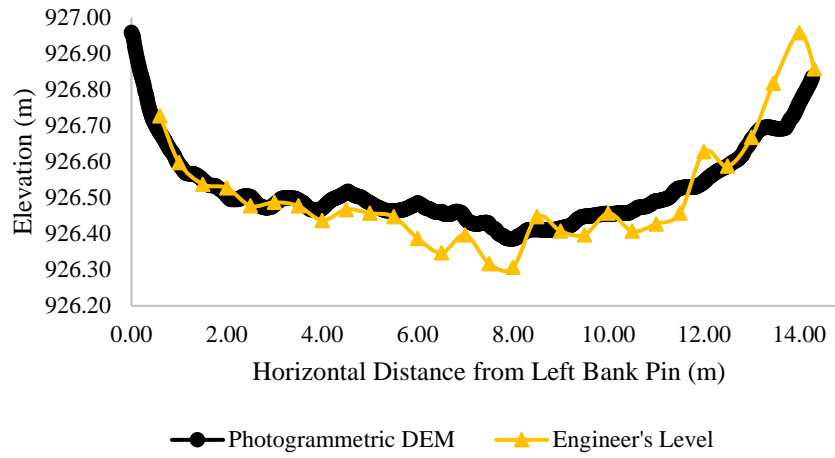
### Transect 8



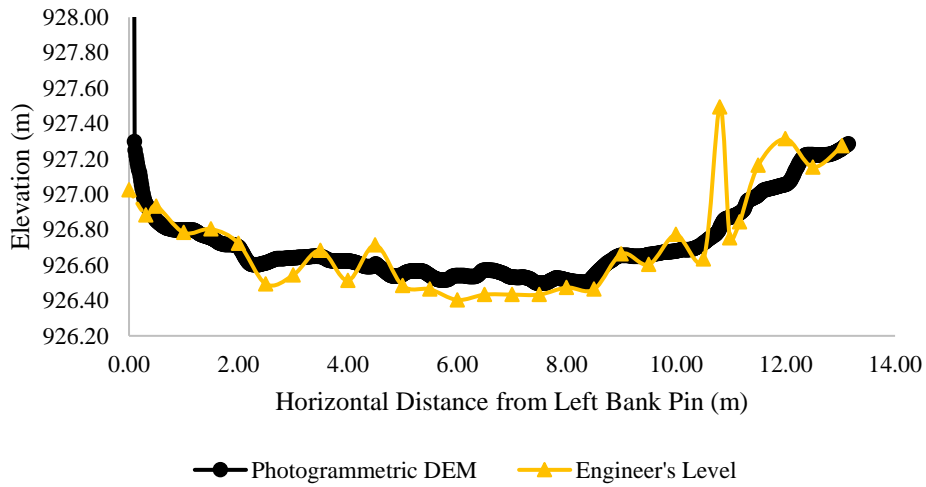
### Transect 9



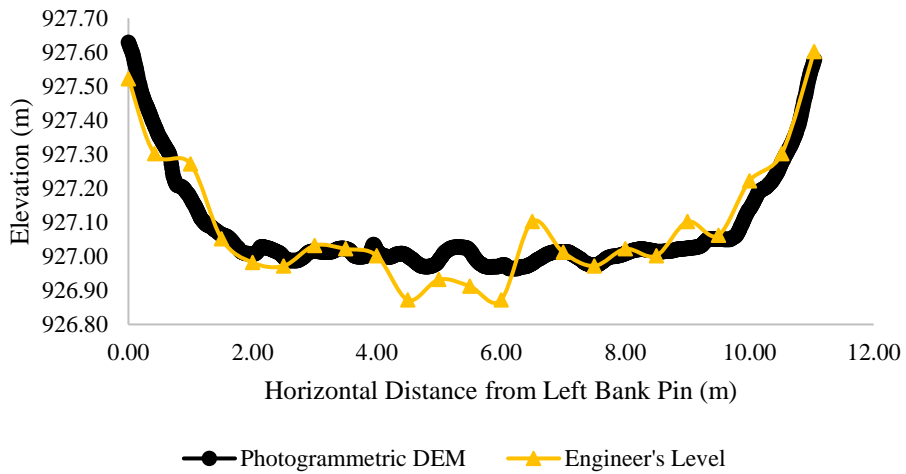
Transect 10



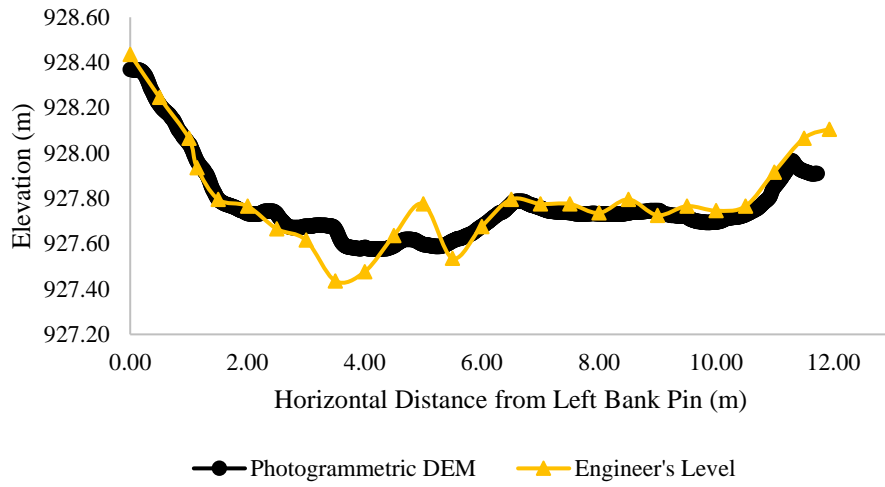
Transect 11



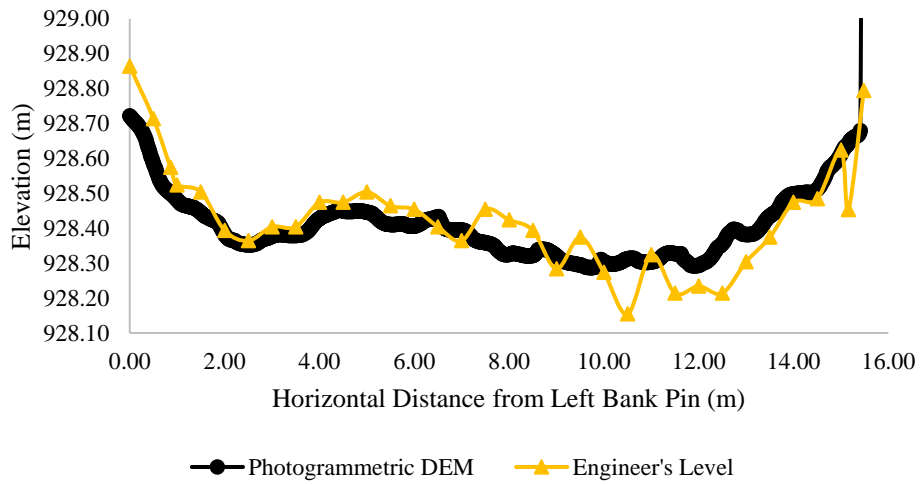
Transect 12



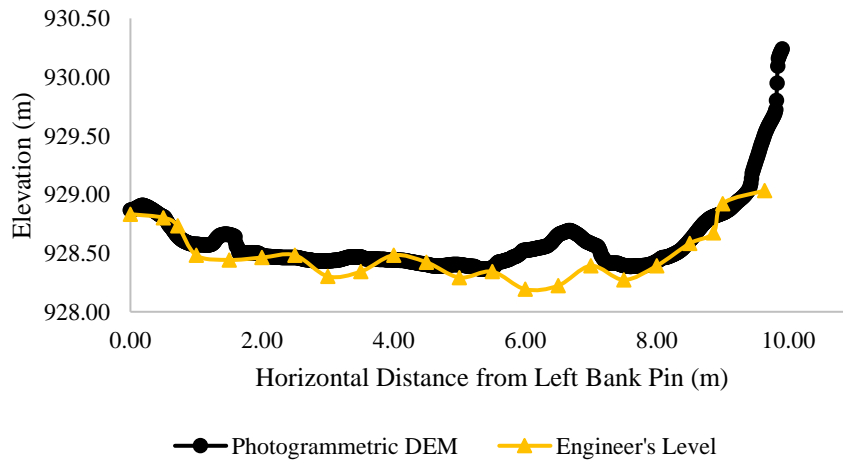
Transect 13



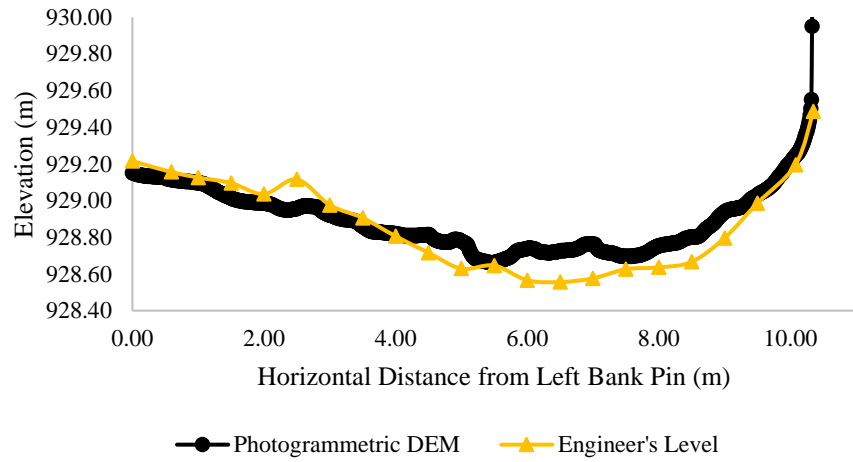
Transect 14



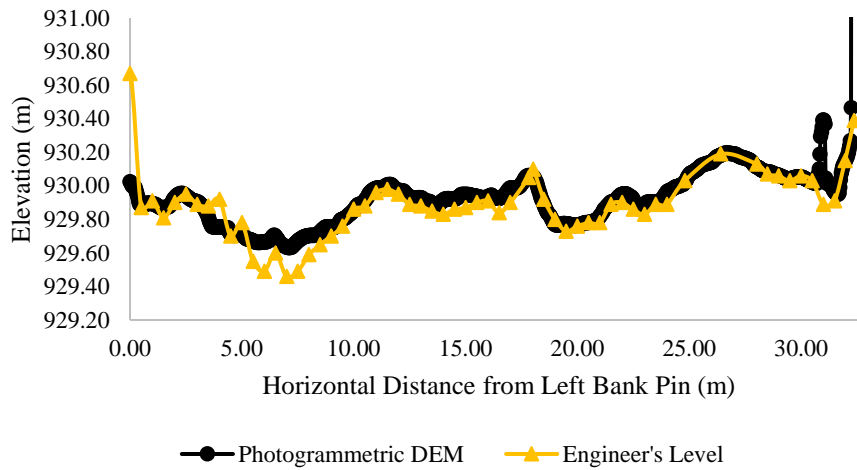
Transect 15



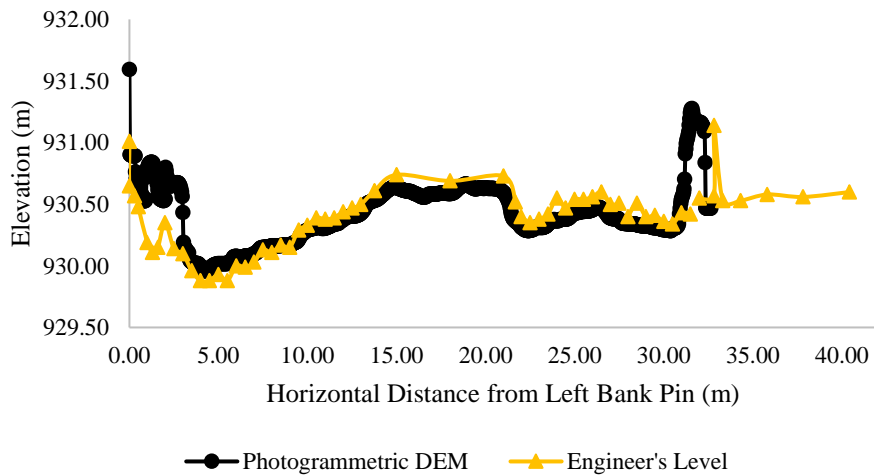
Transect 16



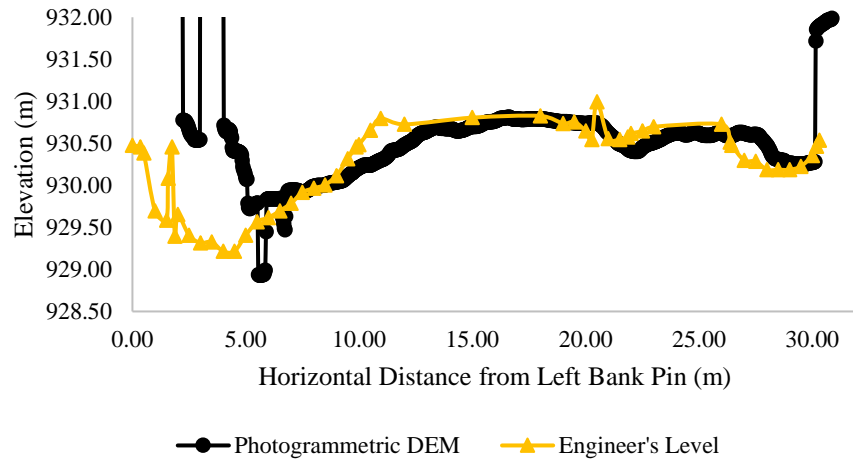
Transect 17



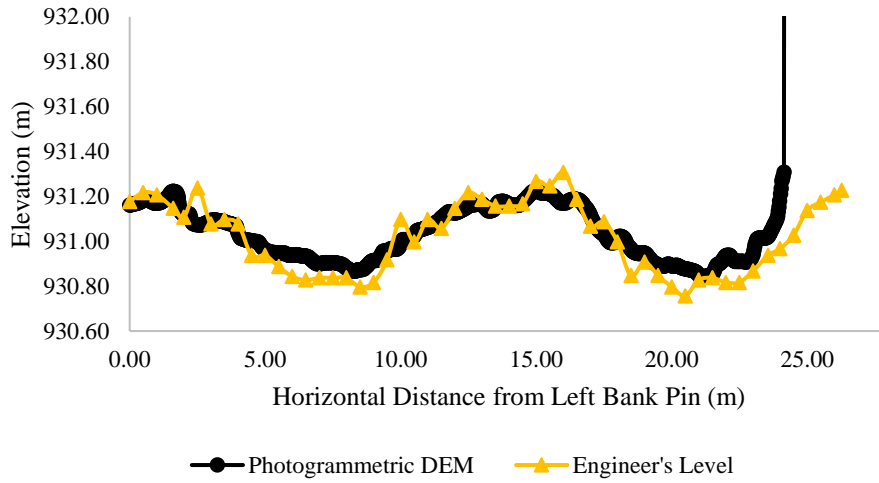
Transect 18



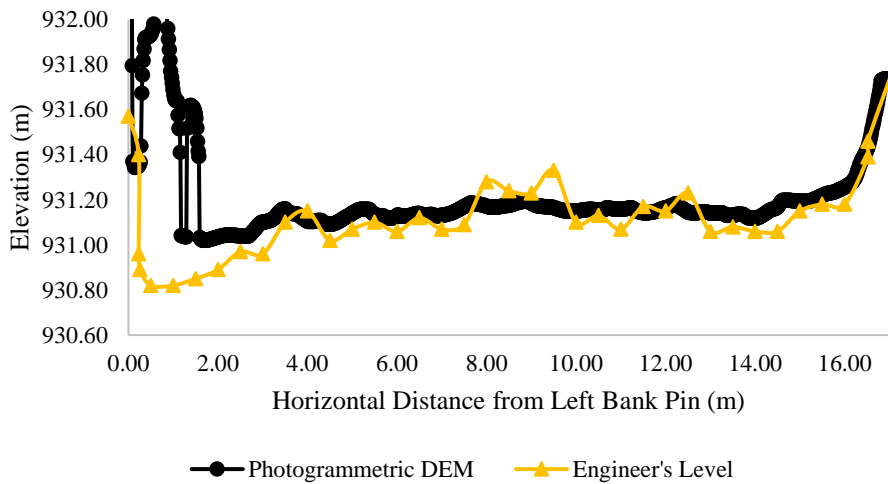
Transect 19



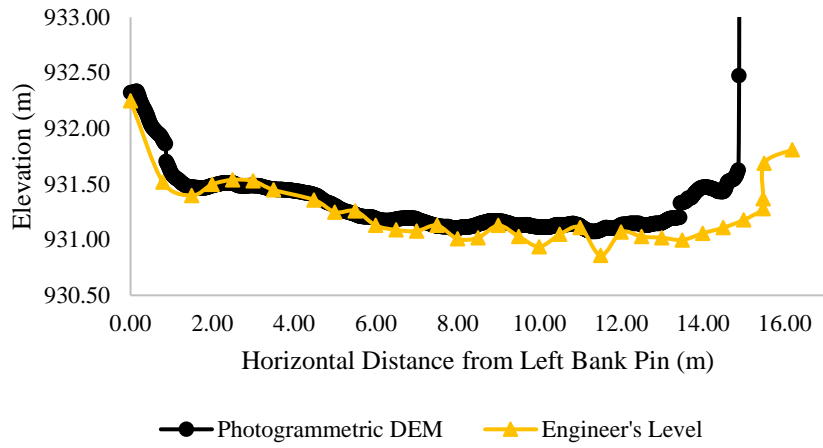
Transect 20



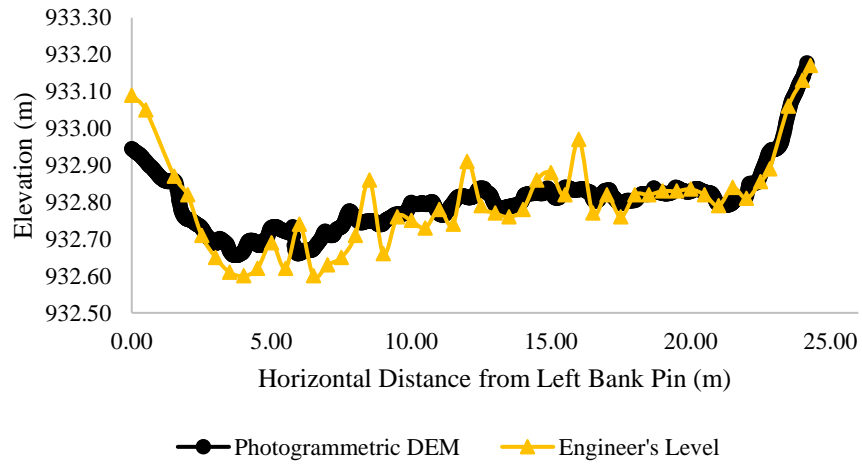
Transect 21



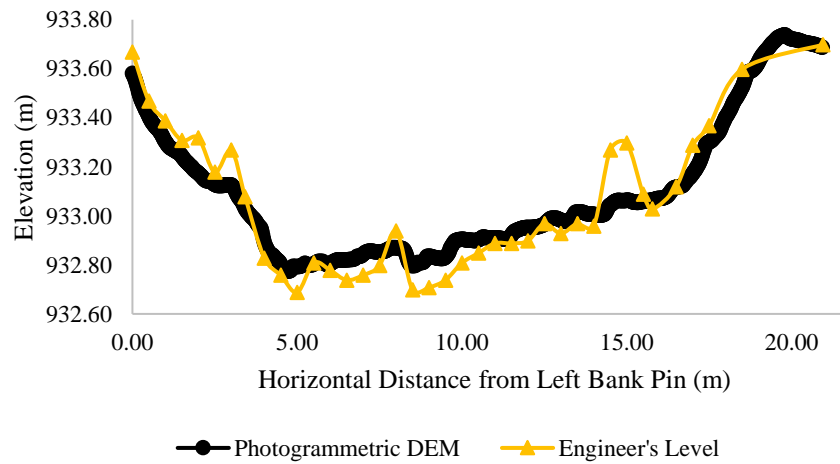
Transect 22



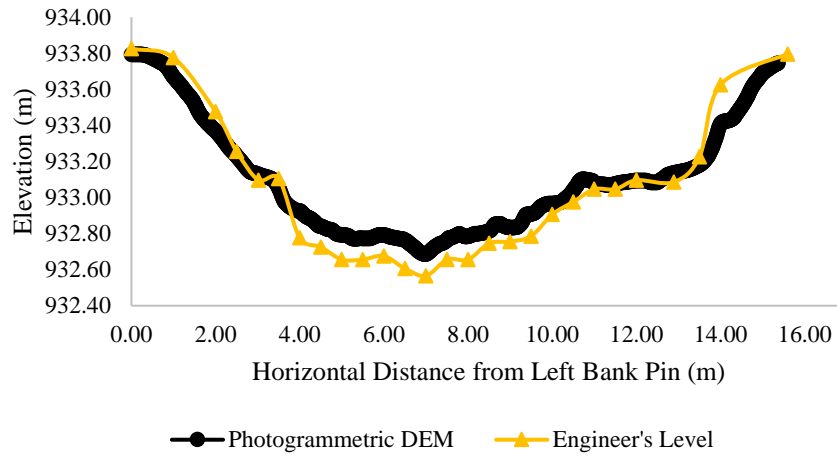
Transect 23



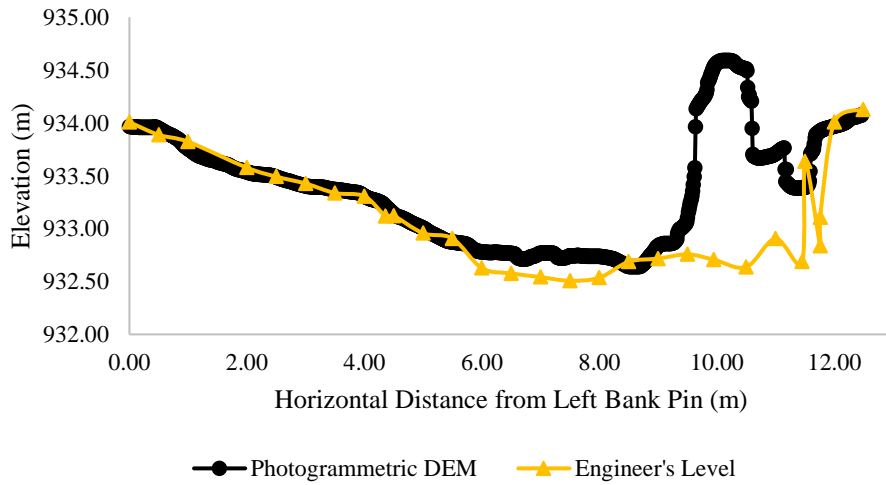
Transect 24



Transect 25



Transect 26



Transect 27

